University of Bath

PHD

An invermectin sensitive ion channel from haemonchus contortus

Mccavera, Samantha

Award date:
2008

Awarding institution:
University of Bath

Link to publication

Alternative formats
If you require this document in an alternative format, please contact:
openaccess@bath.ac.uk

Copyright of this thesis rests with the author. Access is subject to the above licence, if given. If no licence is specified above, original content in this thesis is licensed under the terms of the Creative Commons Attribution-NonCommercial 4.0 International (CC BY-NC-ND 4.0) Licence (https://creativecommons.org/licenses/by-nc-nd/4.0/). Any third-party copyright material present remains the property of its respective owner(s) and is licensed under its existing terms.

Take down policy
If you consider content within Bath's Research Portal to be in breach of UK law, please contact: openaccess@bath.ac.uk with the details. Your claim will be investigated and, where appropriate, the item will be removed from public view as soon as possible.

Download date: 05. May. 2023

AN IVERMECTIN SENSITIVE ION CHANNEL FROM *HAEMONCHUS CONTORTUS*

Samantha J. C. McCavera

A thesis submitted for the degree of Doctor of Philosophy
University of Bath
Department of Biology and Biochemistry
July 2008

COPYRIGHT

Attention is drawn to the fact that copyright of this thesis rest with its author. This copy of the thesis has been supplied on condition that anyone who consults it is understood to recognise that its copyright rests with its author and that no quotation from the thesis and no information derived from it may be published without the prior written consent of the author.

This thesis may be made available for consultation within the University Library and may be photocopied or lent to other libraries for the purposes of consultation.

.....

Summary

The avermectins (ivermectin, doramectin etc) and milbemycins are effective anthelmintics used widely in animal and human medicine for the past twenty years. The actual site of action of the avermectins on the GluCl is unclear, but binding studies have concluded that it does not share a binding site with glutamate. The GluCl channels have been well characterised in *Caenorhabditis elegans* and are beginning to be characterised in parasitic nematode species such as *Haemonchus contortus, Dirofilaria immitis* and *Cooperia oncophora.*

The aim of this project was to characterise the *H. contortus* GluClα3B subunit and its interactions with agonists, glutamate and ivermectin using electrophysiology to study *Xenopus* oocytes expressing GluClα3B homomeric channels and ligand binding studies on COS-7 cells expressing the subunits. Site–directed mutagenesis was used to introduce resistance associated candidate polymorphisms into the *H. contortus* GluClα3B subunit. The effects of these changes on the response to glutamate and ivermectin were assessed. One mutation found in IVR *C. oncophora,* L256F, confers a 3-fold loss of sensitivity to glutamate and a 6.5 fold loss of sensitivity to IVM. This mutation is found in the C-terminal area of the extracellular region of the channel and, from homology modelling, we know it lies in close proximity and possibly interferes with another candidate mutation V235A, and the Cysteine residue at position 192 which forms one side of the structurally significant disulphide bridge. Further introduction of different mutations at this position showed the larger the substituted amino acid, the greater the effect on IVM sensitivity.

Another amino acid substitution (T300S) results in the prohibition of a functional channel. The protein is produced and is able to bind IVM with high affinity but does not create a functional channel.

These data show that polymorphisms found in field isolates of parasites can have a significant effect on GluCl channels and may contribute to drug resistance.

Acknowledgements

I would like to thank my Supervisor Dr Adrian Wolstenholme for his tireless help and support throughout my PhD. I would also like to thank my industrial supervisor Dr Debra Woods at Pfizer animal health for her assistance and hospitality.

I would also like to extend my thanks to Dr Adrian Rogers for all his preliminary work on GluClα3B pharmacology and his help during the first few months in Bath. Also huge thanks to Dr Tom Walsh for his company, sense of humour and his ability to put lab-based disasters into perspective. I am also grateful to all members of the lab and write-up room (past and present) who have made my time in the lab thoroughly enjoyable.

I would also like to thank Allan, who has always been there, through the ups and downs, supplying me with endless cups of tea, chocolate, a calming influence and infinite support.

Finally I would like to thank my parents, Peter and Trish McCavera and my sister Fiona, who, without a doubt, are my greatest source of strength and inspiration. It was their belief that I could achieve anything that made this PhD possible.

This research was funded by a BBSRC-CASE award with Pfizer Animal Health.

List of Abbreviations

5-HT	5-hydroxytryptamine
ACh	Acetylcholine
AM	Avermectins/ Milbemycins
AVM	Avermectin
B.C	Biological Control
bp	base pairs
BSA	Bovine Serum Albumin
cDNA	complementary Deoxyribonucleic acid
CMV	Cytomegalovirus
ddH_20	distilled deionised water
DEPC	Diethyl pyrocarbonate
DMEM	Dulbecco's Modified Essential Medium
DNA	Deoxyribonucleic acid
DNase	Deoxyribonuclease
dNTP	Deoxyribonucleoside triphosphate
dsDNA	double strand DNA
DYT	Double Yeast Tryptone
EC	Effective concentration
EDTA	ethylenediaminetetraacetic acid
EMBL	European Molecular Biology Laboratory
FBS	Foetal bovine serum
GABA	γ- aminobutyric acid
GFP	Green Fluorescent Protein
GluCl	Glutamate gated chloride channel receptor
Hc	Haemonchus contortus
HEPES	4-(2-hydroxyethyl)-1-piperazineethanesulfonic acid
IPTG	Isopropyl β-D-1-thiogalactopyranoside
IVM	Ivermectin

IVR	Ivermectin Resistant
IVS	Ivermectin Sensitive
Kb	Kilobase pairs
K_D	Dissociation constant
kDa	Kilo Daltons
LB	Luria Broth
LGIC	Ligand gated ion channel
L_x	Larval stage x
MEM	Minimal Essential Medium
MOPS	3-(N-morpholino)propanesulfonic acid
mRNA	messenger Ribonucleic acid
nAChR	Nicotinic acetylcholine receptor
NMJ	Neuromuscular junction
NZY buffer	NZ amine yeast buffer
O.D	Optical Density
PBS	Phosphate Buffered Saline
PCR	Polymerase Chain Reaction
PEI	Polyethyleneimine
P-gp	P-glycoprotein
PMSF	(4- bromo) phenylmethylsulphonyl fluoride
PTX	Picrotoxin
RE	Restriction Endonuclease
RNA	Ribonucleic Acid
RNase	Ribonuclease
rol	Rolling phenotype
Rpm	Revolutions per minute
RT	Room Temperature
SDS	Sodium Dodecyl Sulphate
TAE	Tris Acetate EDTA
Taq	*Thermus aquaticus*
TBE	Tris Borate EDTA
TE	Tris EDTA
TEMED	N, N, N' Tetramethylethylenediamine

TM	Transmembrane domain
Unc	Uncoordinated
UV	Ultraviolet
X-gal	5-bromo-4-chloro-3-indolyl- beta-D-galactopyranoside

Contents

Figures

Tables

Chapter 1: General Introduction

1.1 Phylum Nematoda.

The body of a nematode is long and threadlike and it is from this that the phylum gets its name-from the Greek *Nema* for Thread and *Eidos* for form. They make up a large, successful and fascinating phylum.

Nematodes are almost unbelievably abundant; within the animal kingdom they are second only to arthropods in the number of both species and individuals (Wharton 1986), with over 20,000 described nematode species in the world with an estimated 20,000 to 10 million yet to be discovered (Blaxter 1998).

The nematodes or roundworms are an extremely diverse family that has adapted to survive and thrive in a wide range of habitats from compost heaps to desert, salt and fresh water and even the permafrost soils of the Arctic and Antarctic tundra. Nematode species can feed on a wide range of foodstuffs such as bacteria, fungus and algae; they can be omnivores, herbivores, parasites or predators (Wharton 1986). Many species live in a number of different environments, whereas others are extremely specific about their habitat, a famous example being a nematode only found living under the beer soaked felt beer-mats of a few towns in Germany. The diversity within the phylum extends to more that just the range of habitats. Different nematode species can display a wide array of life cycles from the simple and direct to complex parasitic multi-host lifecycles involving different animal hosts and even different tissues within those hosts. Nematodes can vary in size from just 0.3mm in the length to over 8 metres like *Placentonema gigantisma*, a nematode discovered in in 1950 in the placenta of a sperm whale and noted to have 32 ovaries (Gubanov 1951).

Approximately half of the known nematode species are free living and carry out essential roles in the ecosystem such as contributing to the decomposition of vegetation. The remaining nematodes are classed as parasitic and inhabit a wide range of hosts. Some prey on plants, others fish, reptiles, birds, insects and mammals. There are few species in the world completely free from parasitic nematodes (Blaxter 1998).

1.1.1 Nematode anatomy

Despite adaptations to their individual environments, all nematodes are built around similar, characteristic anatomical structures which are conserved through out the phylum. The body of the typical nematode is a flexible cylinder which tapers at each end, with a pointed tail and a blunt head (White et al. 1986).

Nematode anatomy has been most closely studied in the free living nematode *Caenorhabditis elegans* which is widely used a model organism and the large- easily dissected parasitic nematode *Ascaris suum.* The nematode anatomy is generated by conserved developmental patterns, which have been well characterized using *C. elegans*

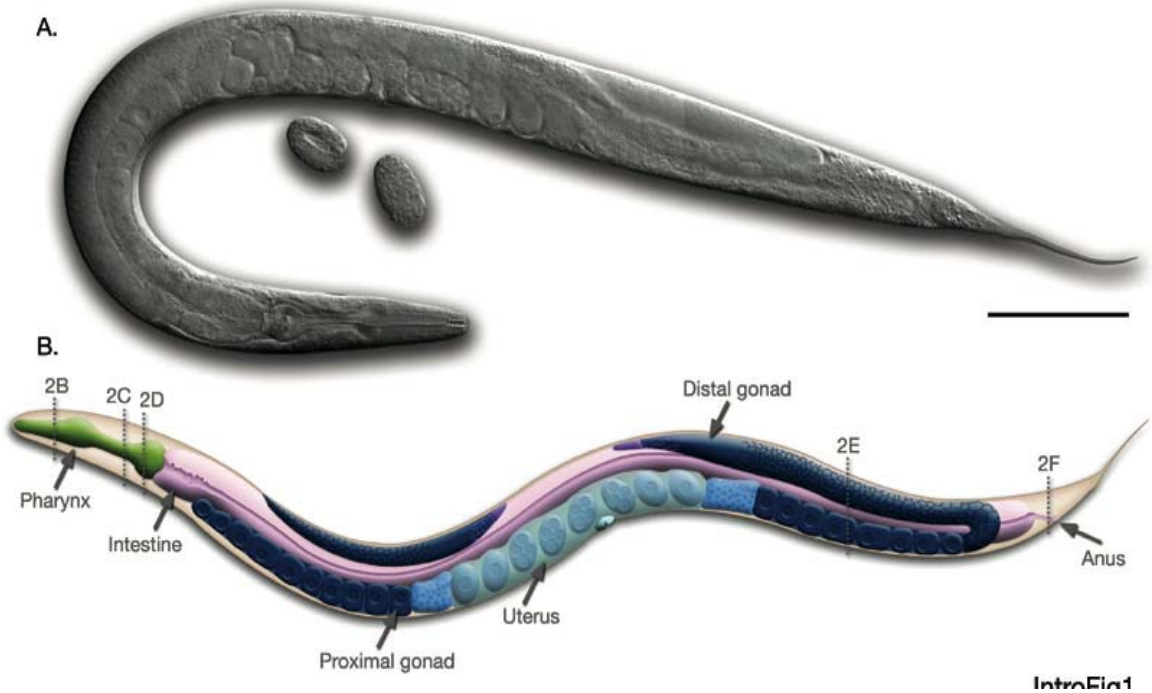

Figure 1: Anatomy of an adult hermaphrodite.

A. DIC image of an adult hermaphrodite on left lateral side. Scale bar 0.1 mm.
B. Schematic drawing of anatomical structures on left lateral side. Dotted lines and annotations labelled 2B to 2F mark the level of each section in Figure 2. Taken from (Altun et al. 2005)

Nematodes are bounded by the strong but flexible collagenous extracellular cuticle which lines the animal completely including any invaginations and which is shed at the end of each larval stage. Beneath the cuticle is a hypodermis which may be either cellular or syncytial (White et al. 1986). The basic plan of the internal nematode body has been described as “a tube within a tube” and consists of two concentric tubes separated by a fluid-filled space which maintains the shape of the nematode using internal hydrostatic pressure known as the pseudocoelom (see Figure 2) (Riddle et al. 1997) although there are a few exceptions such as the monohysterid marine nematode, *Theristis,* which lacks a pseudocoelom. The outer tube contains the secretory/excretory components, nervous system, the gonad and the coelomocytes. The excretory/secretory system is involved in osmoregulation which is essential to the maintenance of the structural integrity of the nematode. The excretory cell is the largest cell in the animal, with excretory canals running the length of the body that are connected to an excretory/secretory pore on the ventral side of the head, which is responsible for the secretion of glycoproteins thought to make up a surface coat over the cuticle. This coat acts as a protective barrier, protecting the nematode from infection and, in the case of parasites, protects from invasion by a host immune system. The layers of body wall musculature are attached to the cuticle via a thin layer of hypodermis. The nematode muscle is similar in structure to vertebrate striated muscle and insect flight muscle but Z bands are not present. The musculature is arranged in four longitudinal strips, and it is contraction of the two subventral muscle strips with relaxation of the corresponding subdorsal strips, and vice versa that generates the characteristic sinusoidal movement in the dorsal-ventral plane (Sulston et al. 1988). The inner tube primarily comprises of the digestive system. Nematodes have a complete digestive system. The nematode digestive system is generally divided into three parts, the stomodeum, intestine, and proctodeum. The stomodeum consists of the “mouth and lips”, buccal cavity, and the pharynx (oesophagus).

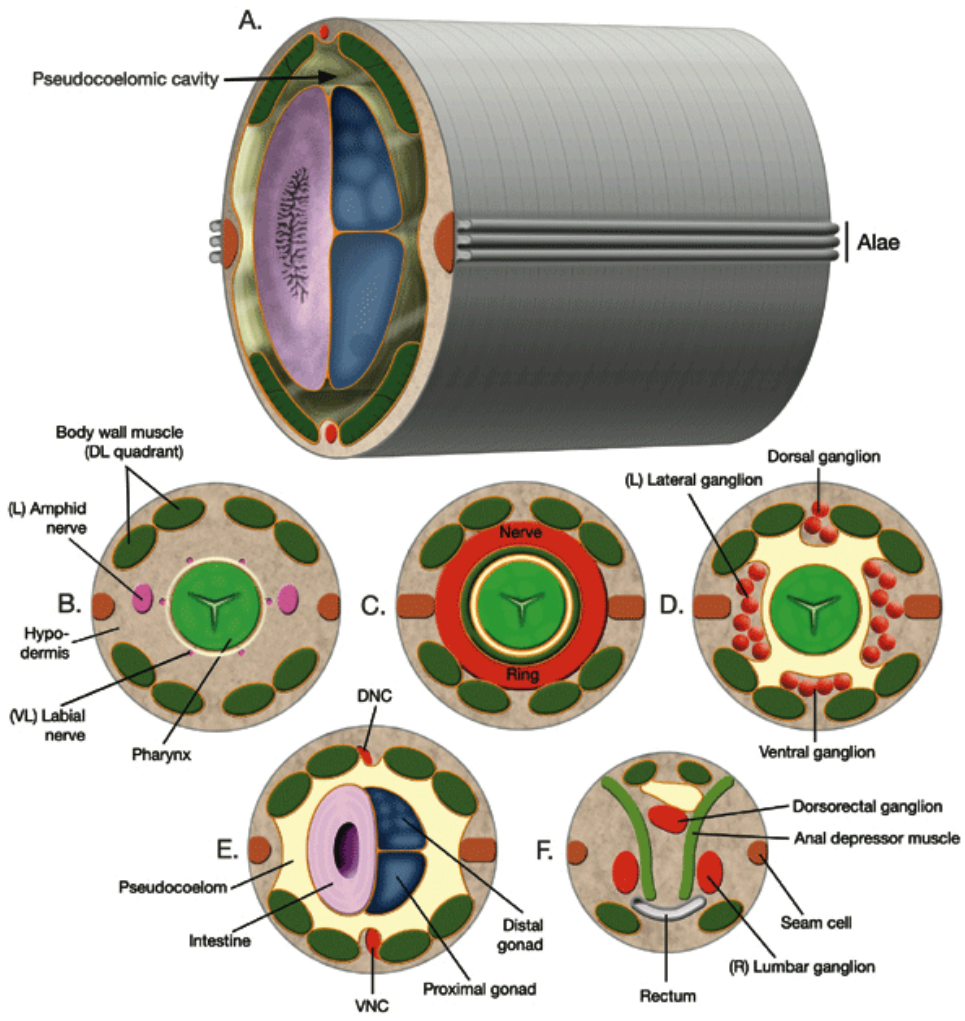

Figure 2: Nematode body plan with cross sections from head to tail.

Approximate level of each cross section is labelled in Figure 1. taken from (Altun et al. 2005)
A. Posterior body region. Body wall (outer tube) is separated from the inner tube (alimentary system, gonad) by a pseudocoelom. Orange lines indicate basal laminae.
B. Section through anterior head. The narrow space between the pharynx and the surrounding tissues anterior to the NR can be considered an accessory pseudocoelom since the main pseudocoelom is sealed off by the GLRs at the NR level.
C. Section through the middle of head.
D. Section through posterior head.
E. Section through posterior body. DNC: Dorsal nerve cord; VNC: Ventral nerve cord.
F. Section through tail, rectum area

The pharynx is a variable and highly muscular organ that usually contains several enlargements (bulbs) and lies posterior to the mouth behind the buccal cavity, which is highly variable in size and structure between nematode species to the extent that the buccal cavity and pharynx are used extensively in taxonomy and classification of nematodes, as well as providing as indication of feeding habit or trophic group, for example, the buccal cavity of plant parasitic nematodes (and some insect parasites) is modified in the form of a hollow spear, adapted to penetrate and withdraw the contents of host cells. Predaceous nematodes often have a buccal cavity characterized by teeth or hook-like projections. The pharynx is primarily a pumping organ and acts by contraction of the buccal and anterior pharyngeal muscles which force the mouth open and cause dilation of the anterior of the pharynx. This produces a negative pressure gradient causing food and outside material into the mouth. Then the high hydrostatic pressure applied from the pseudocoelom acts to close the mouth and the oesophageal lumen when the muscles relax creating the characteristic sucking/pumping action. The food passes through a second bulb which grinds it, breaking up the food source e.g. opening blood cells or rupturing bacterial cell walls etc to create a directly digestible pulp. The intestinal cells surround a central lumen which connects to the anus (Riddle et al. 1997) These intestinal cells are not muscular and food debris is forced through the intestine and toward the rectum by the pharyngeal pumping, The anus is opened via contraction of anal dilator muscles and closed by the turgor of the internal hydrostatic pressure.

1.1.2 The nematode life cycle

The typical life cycle of the nematode is made up of six distinct stages, the egg followed by four larval stages known as L1-L4, and the adult stage (see figure 3). Some species undergo their first moult while still in the egg and hatch as second-stage larvae (Bird et al. 1991). The process and purpose of moulting is an area of conflict. Moulting has been proven to have little effect on the gro*wt*h curve (Wharton 1986; White et al. 1986). The large intestinal parasite *Ascaris* is only slightly larger than *C. elegans* at its final molt, but it undergoes a massive increase in size as an adult. The act of moulting allows the nematode the opportunity to replace and modify

the cuticle and this necessity to change surface composition to survive changing environments is one explanation for moulting in the parasitic nematodes (Blaxter et al. 1992). For free-living nematodes the moulting cycle has been proven to trigger basic developmental cues controlling postembryonic cell lineages, and developmental plasticity in cell morphology and function (Singh et al. 1978; Riddle et al. 1997).

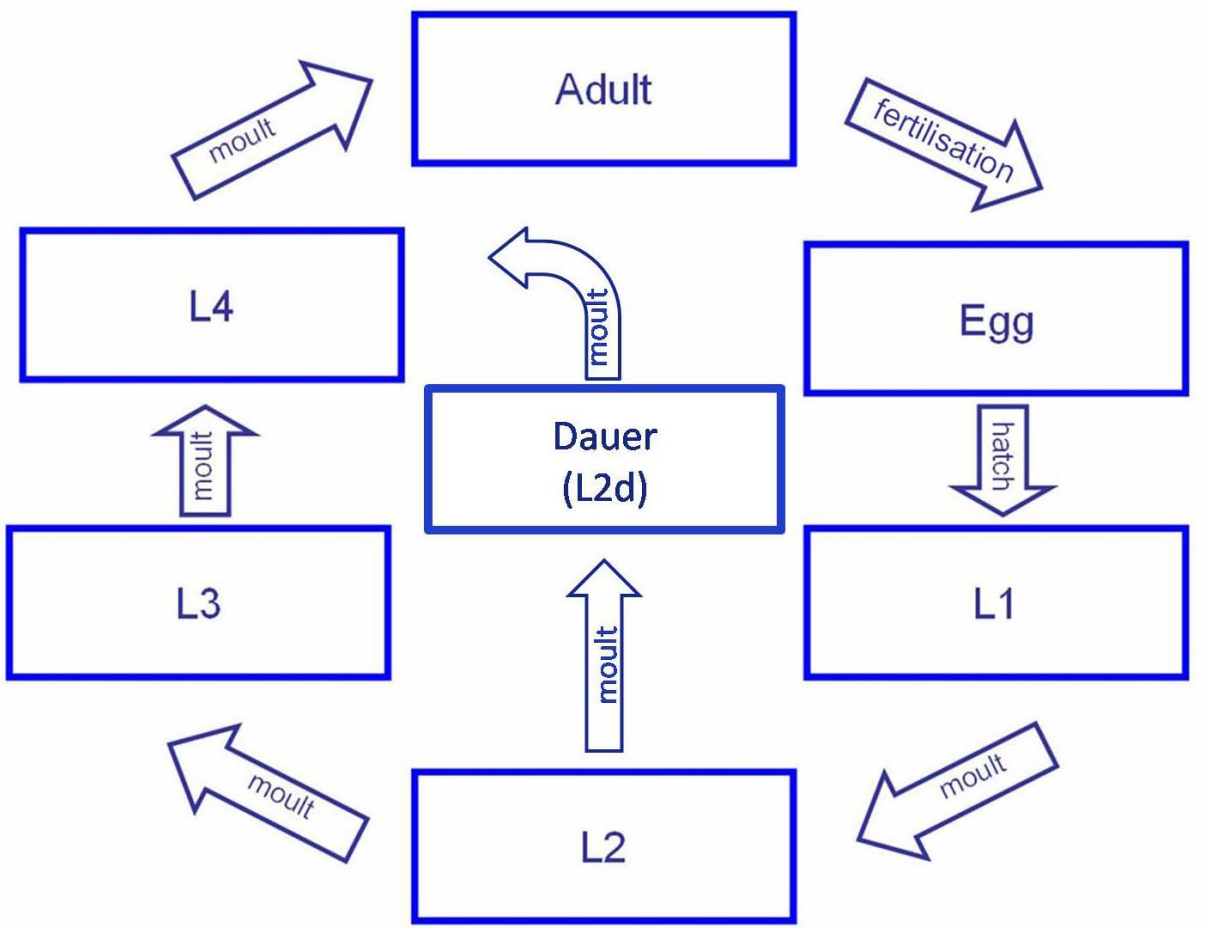

Figure 3: Basic life cycle pattern of nematodes.

1.1.3 The nematode nervous system

Most of our understanding of the nematode nervous system and neurobiology stems from the extensive study of the tiny free living *C. elegans* and the much larger parasitic nematode *Ascaris suum*. The striking similarities between the nervous systems of these two very different nematodes suggest there is a high level of continuity within the phylum.

The nematode nervous system consists of a set of parallel interconnected neuronal processes that run the length of the nematode body, or circle the nematode body adjacent to the hypodermis. The nerve bundles in the nematode body run through the ventral cord (part of the hypodermis), but nematodes also have nerves in the dorsal cord, the two lateral cords and the nerve ring. The nervous system can be split into two near autonomous units, the pharyngeal and somatic nervous systems. (Chalfie et al. 1988). The pharyngeal nervous systems contains about 20 neurons and is responsible for control of pharyngeal pumping, in experiments when the pharynx is removed from the rest of they body or destroyed it will continue pump demonstrating it's myogenic nature (Avery et al. 1989). There is a level of communication between the somatic and pharyngeal nervous systems via by a pair of neurons known in *C. elegans* as RIP cells.

The cell bodies of most neurons are positioned around the pharynx, along the ventral midline and in the tail. Most of their cell processes form a ring around the basement membrane that surrounds the pharynx, or they join the dorsal or ventral nerve cords as in the somatic nervous system. Most chemosensory and mechanosensory neurons extend afferent processes from the region of the nerve ring to sensory organs near the tip of the head. Other sensory neurons extend their processes along the body or to the tail. The nerve ring receives and integrates sensory information and connects to motor neurons in the head or along the nerve cords (Riddle et al. 1997).

The first complete study of the nematode nervous system was published in 1986 in a massive 340 page paper. The study of the *C. elegans* nervous system involved the painstaking reconstruction of thousands of electron micrographs of serial sections.

This showed the presence of 302 component neurones (*A. suum* has 298). The neurones could then be classed into 118 groups with similar morphologies and connectivities (White et al. 1986).
The basic neuron structure proved to be very simple with few branches that often made up nerve processes that run in bundles (like the nerve ring) following defined routes in defined positions, the bundles often run adjacent to the ridges of hypodermis (as in the dorsal and ventral nerve cords). The 1986 reconstruction yielded not only a connectivity pattern, but also an excellent understanding of the structure of synapses in *C. elegans*. It described most of the morphologically identifiable synaptic connections in a typical animal. These consist of about 5000 chemical synapses, 2000 neuromuscular junctions and 600 gap junctions (White et al. 1986; Rand et al. 1997).

The neuromuscular processes in the nematode are unique in that instead of the nerves forming processes and reaching out to the muscles the opposite is true with the muscle fibres producing muscle arms which grow to meet the neurons (White et al. 1986). Neurons are generally highly locally connected, making synaptic connections with many of their neighbours. It has also been showed that the specificity of synaptic contacts made by individual neurons was relatively conserved from nematode to nematode (White et al. 1986; Hall et al. 1991).

1.1.4 Parasitic nematodes.

Half of all known nematode species are parasitic, infecting and living off plants, animals (invertebrates, vertebrates, terrestrial and aquatic) and, of course, humans.
In plants parasitic nematodes have a catastrophic effect on the crop harvests around the world The cost of the loss of crops due to nematodes has been put at £100 billion per year (Amoussou et al. 2004). Nematodes, in particular *Meloidogyne* spp and *Globodera* spp*,* cause 12% reduction in the world potato harvest. This represents the loss of 35 million tonnes world-wide, of which 13 million tonnes are lost in the developing world, particularly in poor areas of South America where potato

is a primary source of carbohydrate. Nematode infestations vary in severity and Individual losses can be higher than this average both nationally and locally, Higher infestations occur particularly in poorer areas due to the lack of access to the necessary pesticides or land for crop rotation (Lilley et al. 1999; Amoussou et al. 2004).

Of those parasitic nematodes that infect vertebrates, the vast majority are the soil-transmitted nematode parasites, or geohelminths, so called because they have a direct life cycle, which involves no intermediate hosts or vectors, and are transmitted by faecal contamination of soil, foodstuffs and water supplies (Holland et al. 2002). The primary members of this group are the Ascaris, Trichus and hookworm species. The adult geohelminths inhabit the intestine or the stomach of the host, where they compete with the host for nutrients. Infection causes anaemia, malnutrition which leads to further complications such as stunted gro*wt*h, physical weakness and a weakened immune system. Most species also have tissue-migratory juvenile stages, so the disease manifestations they cause can therefore be both local and systemic, and often causing serious complications due to ectopic establishment of nematodes.
A second, important group of parasitic nematodes that cause infection in vertebrates are the filaria, a group of closely related nematodes that are tissue dwelling and long lived; transmission of filaria requires an intermediate host, usually a biting arthropod. The human diseases caused by filarial nematodes include Onchocerciasis caused by *Onchocerca volvulus* and Lyphantic filariasis caused by *Wucheria bancrofti* and *Brugia spp.*

1.1.5 Parasitic nematodes and human infection

Over 342 species of helminths have been found in association with humans, of which 138 are nematodes (Crompton 1999). Of all the helminths 197 would be considered as primarily inhabitants of the gastrointestinal (GI) tract. Many are harmless and are likely to be due to accidental infections from other species that are normal hosts or perhaps, in some communities, even commensal in the GI tract.
Around 20 species are considered to cause disease, of which six (*Enterobius*, *Ascaris*, *Necator*, *Ancylostoma*, *Trichuris* and *Strongyloides*) together affect over half of the world's population (Horton 2003).

It has been reported that 1.3 billion people in the world are infected with hookworms (either *Ancylostoma duodenale* and *Necator americanus)* (Pawlowski et al. 1991; Chan et al. 1994; Crompton 1999). Although hookworm is rarely fatal it is still a leading cause of maternal and child morbidity in the developing countries of the tropics and subtropics. In susceptible children hookworms cause anemia and malnutrition causing retardation of intellectual and cognitive development and stunted gro*wt*h. Poor iron status and iron deficiency anaemia are the hallmarks of hookworm disease. In the developing foetus of an infected mother often suffers intrauterine gro*wt*h retardation, premature birth, and low birth weight. Hookworm infection is rarely fatal when looked at as a percentage of people infected, but due to the number of people infected it still accounts for the deaths of 65,000 people per annum, usually due to significant anemia in the heavily infected individual (Crompton 1999).
Ascaris lumbricoides, the most frequent human intestinal nematode, is the causative agent of ascariasis, with an estimated worldwide prevalence of over 1472 million people (~25% of the world's population) (Crompton 1988; Chan et al. 1994; Peng et al. 1998; Crompton 1999), It is primarily found in moist tropical and subtropical regions, but is also found in cooler climates. Reduced food intake, impaired digestion, malabsorption, and poor gro*wt*h rate are frequently observed in children suffering from ascariasis and trichuriasis (Crompton et al. 2002). Although characterised with proportionally low mortality rates, the global prevalence of ascariasis still results in approximately 60,000- 100,000 deaths annually (Crompton 1999), primarily as a consequence of intestinal obstruction. In humans, transmission of infective eggs usually occurs by hand-to-mouth route by way of faecal

contamination through agricultural products and food, or from dirty hands due to poor sanitation. Three phases of ascariasis may be present, pulmonary, intestinal and complications stages (Georgiev 2001). Pulmonary disease is caused by the migration of the juvenile nematodes through tissues to the lungs causing haemorrhage and oedema. The resulting accumulation of fluids in the lungs results in "ascaris pneumonia", and along with the partial or complete obstruction of biliary or intestinal tracts can, in rare cases, cause death.

Another problematic parasitic nematode of humans is the filarial nematode *Onchocerca volvulus*. Transmission occurs through bites of vector blackflies in the family *Simuliidae*. Although a few vector species breed in slow-moving streams, most require fast-flowing, highly oxygenated streams or rivers leading to high prevalence of disease in these areas. For this reason, ocular onchocerciasis is often called "river blindness." The most serious clinical manifestation of onchocerciasis is blindness, caused by microfilariae that wander into the eye. In endemic areas, corneal opacities resulting from the reaction to dying microfilariae often suggest onchocercal infection. Alternatively, active living microfilariae may be seen when the eye is examined with a slit lamp (Baron et al. 1996). Onchocerciasis is prevalent in many parts of tropical Africa and has been reported in a few places in the Middle East. In the Americas, it is an important and widespread infection in Guatemala and the southern states of Mexico. It also appears in other areas of Central America, and a few foci have been found in Venezuela, Colombia, Surinam, Brazil, and Ecuador. In addition to visual impairment, onchocerciasis is associated with serious pathological changes of skin. There is a great deal of discrepancy over levels of infection worldwide. According to some sources total of 18 million people are infected with the disease and have dermal microfilariae, of which 99% are in Africa. 45,000 fatalities per year are attributed to onchocerciasis and over 500,000 are thought to be blind or severely visually impaired (Molyneux et al. 1997; Crompton 1999; Basanez et al. 2006). Other surveys show that the WHO figures are an underestimate of the extent of disease—37 million people are now thought to be infected, with 90 million at risk in Africa and more than 400 000 infected in Central and South America (Basanez et al. 2006; Osei-Atweneboana et al. 2007).

In lymphatic filariasis, disease is caused by the presence of one of several types of nematode in the regional lymphatic vessels and, particularly, by the host response to the nematode and nematode products. The microfilariae are released into the blood. Infections involving small numbers of worms are often asymptomatic. Early symptoms of lymphatic filariasis consist of intermittent fever and enlarged, tender lymph nodes. The inguinal lymph nodes are very often involved. The lymphatic vessels that drain into the lymph nodes and that harbour the developing and adult worms also become inflamed and painful. In more chronic infections, there may be pain also in the epididymis and testes. Swollen lymphatics may burst and drain into the genitourinary system resulting in chyluria (milky urine) (Baron et al. 1996) In a small number of chronic cases, permanent lymphatic dysfunction caused by repeated exposure to infection over a number of years results in the massive lymphedema and accumulation of excess tissue known as elephantiasis). Lymphatic filariasis is most commonly caused by the nematodes *Wuchereria bancrofti* and *Brugia malayi*, amongst others, depending on geographical origin and is transmitted by a feeding vector mosquito. It is one of the world's most disfiguring and debilitating parasitic diseases. Over 120 million people are afflicted in 83 countries (WHO 2000).

1.1.6 Parasitic nematode infection in animals.

Nematodes are also important parasites of livestock and companion animals. *A. suum* is a large intestinal worm very similar to the human parasite *A. lumbricoides* described above, and it is the causative nematode of ascariasis in swine. Like *A. lumbricoides, A. suum* has a direct life cycle with the primary infection caused by ingestion of viable fertilised eggs in food or water.

As with *A. lumbricoides, A. suum* larvae hatch in the small intestine and the juveniles can migrate through the tissue of the intestinal wall and through to the heart; lungs to the trachea and larynx where they are often re-swallowed and return to the intestine (Campbell 1981; Baron et al. 1996). The female produces between 200- 200,000 eggs per day which are released from the animal in faeces. The eggs alone can survive for up to seven years (Smyth 1994) and the longevity and the sheer number of the eggs means that the level of re-infection of both *A. lumbricoides* and *A. suum*

is very high. Although the mortality rate for pigs with *A. suum* infections is relatively low, the morbidity is high with the animals losing condition due to diarrhoea, malnutrition and intestinal blockage. Re-infection of juveniles in the porcine lungs can result in allergic broncho-pneumonia. As the aim of pig farming is to gain the largest muscle mass per animal possible, the competition for nutrients is financially damaging to the farmer.

D. immitis is a filarial worm known as the dog heartworm and is found in the right hand chambers of the heart and the adjacent blood vessels, particularly the pulmonary arteries. In chronic infections it results in pulmonary hypertension leading to right sided heart failure (Knight 1987). It primarily affects domesticated dogs and sometimes cats; other wild carnivores such as ferrets, dogs and foxes may act as reservoirs for potential infection.

Microfilariae are carried from the heart through the lungs and into the systemic bloodstream, from where a mosquito can take a blood meal. Within the mosquito digestive system the microfilariae moult and develop into infective L3-stage larvae which are passed into a new carnivorous host with a second blood meal by the mosquito. Zoonosis is rare but can occur with *D. immitis* if the second blood meal is from a human.

1.1.7 *Haemonchus contortus*

The members of the family Tristrongylidae are parasites of the mammalian small intestine. Such nematodes include *Ostertagia spp.* and *Haemonchus contortus* commonly known as the “barber pole” worm. The common name originates from the characteristic red and white stripes of the female formed as the ovaries wrap around the intestines which are red from blood feeding.

H. contortus is a parasite of the digestive tract of ruminants and as a result costs the grazing livestock industry hundreds of millions of dollars worldwide in production losses and treatments and accounts for the vast majority of Australia’s 1994 expenditure of AUS$ 222 million on sheep nematodes (McLeod 1995).

As with all geohelminths no intermediate host is required. Adult male and female worms live in the abomasum (or true stomach) of ruminant animals. The female

deposits 5,000 to 10,000 eggs per day which pass out of the host with the faeces. First stage (L-1) juveniles hatch from the eggs in the warm moist conditions of the animal faeces. First and second stage juveniles feed on soil dwelling bacteria. By the time the L-3 stage they are infective for the vertebrate host, cannot feed and retain the second stage cuticle as a sheath. The ruminant becomes infected while grazing by eating the L-3 juveniles which migrate up blades of grass and other vegetation is order to be ingested. Ex-sheathment occurs in the rumen, anterior to the abomasum, and the young fourth-stage (L-4) worms pass into the abomasum where they burrow into the mucosa. Here they undergo another moult, and the juveniles come back into the paramucosal lumen of the abomasum. They begin to feed on the blood vessel rich area of the stomach epithelia and undergo another moult before reaching adulthood (Georgi et al. 1990) (See figure 4).

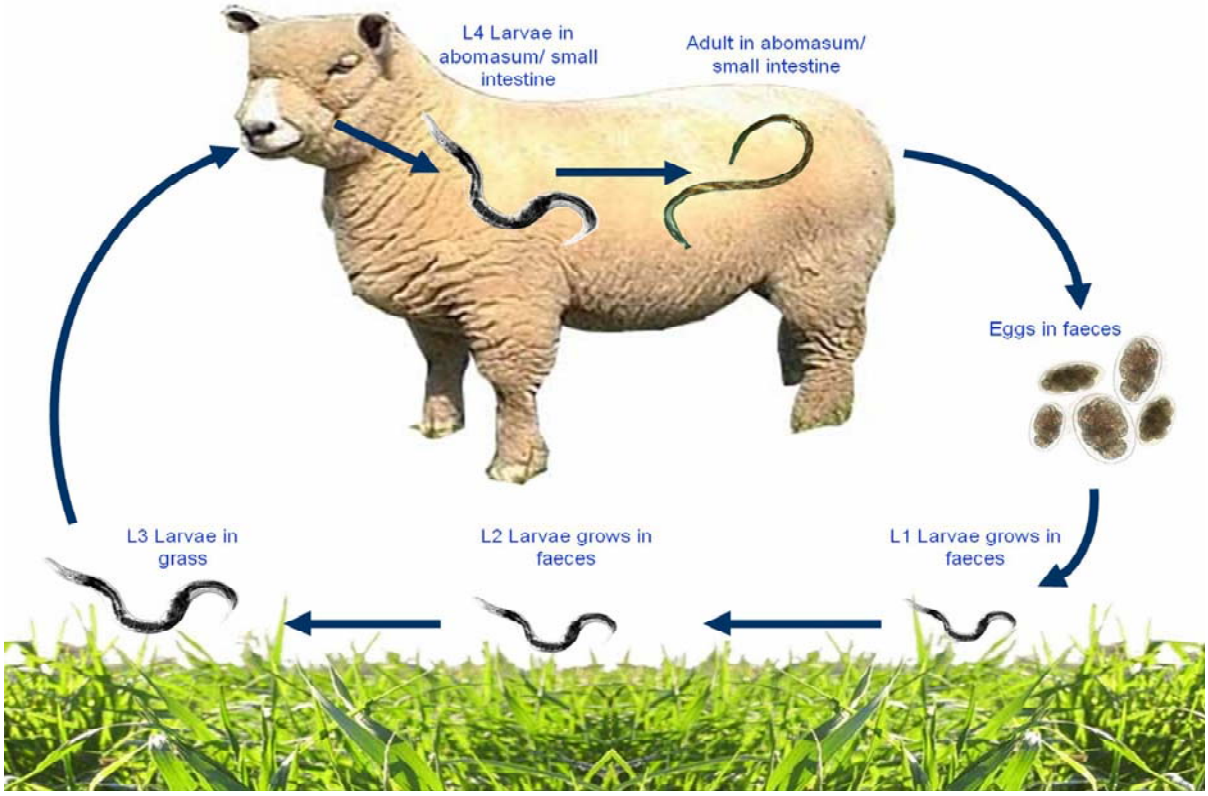

Figure 4: *Haemonchus contortus* life cycle

Each worm is relatively small (The males are 10 to 20 mm and the females 18 to 30 mm long) but can consume up to 15 µl of blood per day and with a single infestation

carrying thousands of worms, this blood loss is significant. In a sudden acute infestation in smaller ruminants such as young lambs that are most susceptible, the blood loss can be fatal. In rare cases of hyperacute haemonchosis, sudden deaths in a flock of previously healthy sheep are seen. This syndrome results from ingestion of large numbers of infective larvae by sheep grazing on a heavily contaminated pasture. It often follows a period of warm, wet weather during which massive numbers of Haemonchus eggs develop rapidly to infective stages. Post mortem examination shows large numbers of worms in the abomasum - anywhere from 20,000 to as many as 50,000 have been reported (Johnstone 1998)

In chronic infestations the animals suffer from anaemia, weight loss and loss of condition resulting in loss of milk productivity in dairy cows, lower quality wool in sheep and goats and smaller malnourished animals for slaughter, consequentially there is a monetary loss to the farmer. Animals can fight back against a *H. contortus* infection by a phenomenon known as “self cure” which is common in sheep in endemic areas. Significant acquired immunity to *H. contortus* can be seen in sheep older than 6 months, but this immunity is not absolute, and sheep in endemic areas may remain susceptible throughout their lives. "Self-cure" is the periodic natural expulsion of adult *H. contortus* from sheep and appears to have an immunological basis; there is a steep increase in the level of the serum antibodies IgG and IgA. A response to excretory secretory antigens resulting in an increase of the specific antibody IgE (Newton et al. 1999). The elimination of L3 worms from immune sheep is now thought to be as a result of eosinophils (Meeusen 1999). A type 1 immediate hypersensitivity response such as an mild allergic reaction provoked by antigens secreted by developing larvae has been credited with causing nematode expulsion (Miller 1984; Miller 1996). However, self-cure induced by a challenge infection is not always followed by protection since larvae in the challenge infection may develop to maturity (Johnstone 1998).

1.2 Chemical control of nematodes

Since the discovery of the first of the three major classes of anthelmintics there have been significant advances in the treatment of helminth infections in humans and in domesticated animals rendering the vast majority of infections fully treatable. Human helminth control programmes have also been shown to have important impacts on measures such as nutrition and cognition at the population level (Reynoldson et al. 1997; Sacko et al. 1999; Horton 2003). Chemotherapy is the most commonly used form of nematocidal control. Discovery of drug-target sites that are pharmacologically distinct from those of the host have been fundamental in the in the production of high potency, broad spectrum drugs that are up to 100% effective at removing worm burdens. In 1994 it cost the British farming industry £1 billion to treat parasitic gastroenteritis caused by parasites such as *H. contortus* (Newton et al. 1999). The vast majority of this money went on anthelmintics. Treatment of animals with parasitic infections can be highly successful. There are several types of drug on the market for the treatment of nematode infections, one of the most important are the avermectins, which are used with great success to treat all of the nematodes discussed thus far in both humans and animals. In 1999 anti-parasitic drugs accounted for 13% and 39% of expenditure in the world livestock and companion animal product sales respectively (Witty 1999).

There are three major classes of drugs that take over 90% share of the anthelmintic market: the benzimidazoles (BZ) make US$ 365 million per year (1999 figures) the imidazothiazoles US$ 260 million, but, the avermectins/milbemycins (AM) command the greatest market share bringing in US$ 995 million per year (Witty 1999). More recently, the BZ, albendazole (ABZ) is being administered widely in combination with either diethylcarbamazine (DEC) or ivermectin (IVM) as part of the Global Program to Eliminate Lymphatic Filariasis (GPELF). Many hundreds of millions of doses of ABZ have been administered to people worldwide since its development. (Prichard 2007)

1.2.1 The Benzimidazoles

Thiabendazole was discovered in 1964, and proven to have a highly effective antifungal activity in addition to being a highly potent broad spectrum anthelmintic (Conway 1964). Over time thiabendazole was modified and improved upon to create a whole class of drugs called then benzimidazoles (BZ) that included other, more potent compounds such as albendazole, mebendazole, fenbendazole and triclabendazole amongst others They all composed of a bicyclic ring system containing a benzene fused to the 4- and 5- position of a heterocyclic compound (de Silva et al. 1997). (See figure 5).

The mode of action of the benzimidazoles has been investigated and well characterised. Initally it was reported that treatment with the BZs resulted in damage to the intestinal walls of the nematodes, a loss of cytoplasmic tubules, prevention of secretory vesicle transportation and inhibition of glucose uptake. As a result the nematodes die of starvation (Lacey 1990; Lubega et al. 1991; Lubega et al. 1991; Beugnet et al. 1996). This is because the benzimidazoles bind directly to the β-tubulin monomer of nematodes, causing inhibition of the proliferation of polymeric microtubules by addition of α-/β-tubulin heterodimers and interfering with microtubule dynamics and consequently disturbing the essential microtubule-based processes in these helminths (Enos et al. 1990; Lacey 1990; Lubega et al. 1991; Lubega et al. 1991; Beugnet et al. 1996; Jasmer et al. 2000; Robinson et al. 2004). The helminth intestinal damage that is observed is due to the BZ causing ectopic release of release of digestion enzymes causing damage to the intestine surface and component cells, which, in turn prevents digestion of food, nutrients being absorbed by the gut and results in starvation. Experiments with *C. elegans* has also shown suggests that treatment with BZ also causes retardation in oocyte formation due to the necessity for a competent and complete cytoskeleton in order to complete meiosis (Enos et al. 1990; Beugnet et al. 1996). Effects of BZ can also be found in the mitochondria where an uncoupling of oxidative phosphorylation causes mitochondrial damage (McCracken et al. 1991).

Benzimidazole

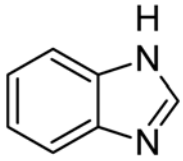

Albendazole

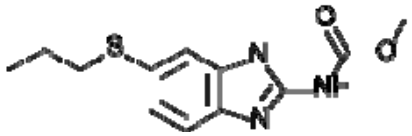

Fenbendazole

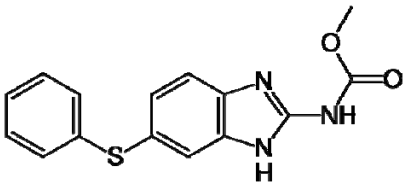

Thiabendazole

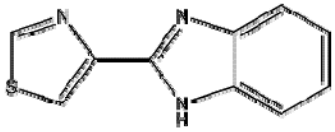

Triclabendazole

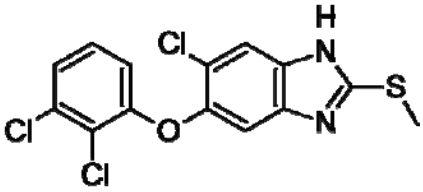

Figure 5: Structure of commonly used Benzimidazoles

1.2.1.1 Benzimidazole resistance

Benzimidazole (BZ) resistance started to appear in veterinary nematode parasites soon after the introduction of thiabendazole, the first BZ. Veterinary resistance has become such a large problem that several recent field studies have demonstrated that the extent of BZ resistance in cyathostomins has reached drastic levels, with at

least 50%, and in some countries >90%, of tested farms showing signs of resistance (Bauer et al. 1986; Varady et al. 2000; Çirak et al. 2004; Wirtherle et al. 2004; Von Samson-Himmelstjerna et al. 2007).

Much work has been done to understand the mechanism of BZ resistance. It has been observed that a number of naturally occurring β-tubulin mutations have been shown to be associated with BZ resistance in parasitic nematodes. It has been discovered that point mutations in the β-tubulin isotype 1 gene leading to amino acid substitutions at codons 167, 198, and 200 confer resistance. The best documented of these is the phenylalanine-to-tyrosine substitution at position 200 on the β-tubulin isotype-I and β-tubulin isotype-II molecule of Haemonchus contortus (Kwa et al. 1994; Prichard 2001). Similarly, a phenylalanine-to-tyrosine or histidine substitution at position 167 is also found in BZM-resistant trichostrongylid nematodes (Prichard 2001; Silvestre et al. 2002). Finally, recent evidence suggests that a third mutation in isotype 1 can also contribute to BZ resistance in *H. contortus* (Ghisi et al. 2007) an adenine-to-cytosine transversion has been identified that leads to a glutamate-to-alanine polymorphism at codon 198 in BZ-resistant populations from Australia and South Africa (Ghisi et al. 2007; Von Samson-Himmelstjerna et al. 2007).

1.2.2 Imidazothiazoles and anthelmintics that act on nicotinic acetylcholine receptors

The Imidazothiazoles (levamisole) and tetrahydropyridines (pyrantel and morantel) (see figure 6) are two classes of highly effective broad spectrum anthelmintics, first used in livestock in the mid to late 1960s (Guilhon 1966; Brimblecombe et al. 1969; Turton 1969). These compounds all act on the nicotinic acetylcholine receptors found in nematode muscle with high affinity, but only have a low level of activity at the vertebrate nAChRs making them an ideal drug with a high efficacy against nematodes but low toxicity to the host. In the nematode addition of Imidazothiazoles and tetrahydropyridines opens ACh-gated cation-selective ion channels, which constitute the nAChRs, on nematode muscle membranes, producing a depolarization and causing muscle contraction and spastic paralysis in treated

nematodes. This was discovered in experiments using pyrantel carried out on *Ascaris suum.* The large size of this particular nematode is convenient allowing dissection of large, individual, muscle strips or cells to carry out contractile assays on (Aubry et al. 1970). This effect was later confirmed in other nematode species *H. contortus* (Sangster et al. 1991) and *C. elegans* (Lewis et al. 1980). Pyrantel and its analogues (including morantel) caused a slowly developing contracture of strip preparations of *Ascaris*, being more than 100 times more potent than acetylcholine. Pyrantel also caused depolarization and increased spike discharge frequency in single muscle cells, these changes being accompanied by increase in tension (Aubry et al. 1970). Later electrophysiological readings showed an increase in the input conductance of the membrane to potassium and sodium has also been shown on addition of pyrantel or levamisole. This effect is also seen with application of acetylcholine, although, the anthelmintics had a more potent effect (Harrow et al. 1985).

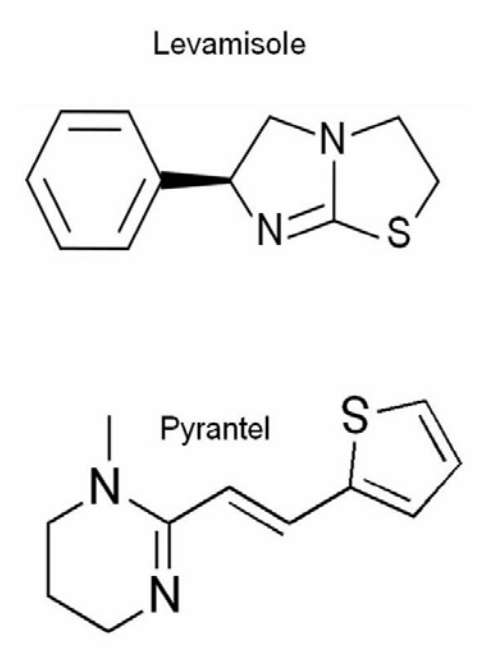

Figure 6: Chemical structure of the two major nicotinic anthelmintics

1.2.2.1 Resistance to Imidazothiazoles and tetrahydropyridines

As with the BZ family resistance to the Imidazothiazoles and tetrahydropyridines is becoming a more common occurrence (Sangster et al. 2002; Martin R et al. 2007) and is now recognized in parasites of both humans and domesticated animals. Unlike BZ resistance to cholinergic agonists is not caused by a few amino acid substitutions. It seems the mechanism for resistance is more complex and may be produced by a combination of four general mechanisms, increased metabolism or excretion of the drug, a reduced number of susceptible receptors, post-receptor modification or a change in receptor binding sites due to amino acid substitution. Some amino acid substitutions have been implicated in resistance to the nicotinic agonists such as E153G mutations in UNC-38 and Q57G mutations in UNC-63 (both proteins are nAChR α-subunits) from *C. elegans* (Rayes et al. 2004; Bartos et al. 2006; Martin R et al. 2007). All of these mechanisms could play a role in resistance to levamisole and pyrantel and so it is anticipated that resistance to these drugs is polygenic (Sangster et al. 2002).

A new class of broad spectrum anthelmintics that act on nematode nAChRs has been described. The amino-acetonitrile derivatives (AADs) are a class of low molecular mass compounds that are easily accessible by alkylation of phenols with chloroacetone, Strecker reaction and acylation of the amine with aroyl chlorides (see figure 7) (Kaminsky et al. 2008). The AADs act on nematode specific nAChR subunits including DEG-3, and is effective in nematodes resistant to levamisole and pyrantel and other multidrug-resistant parasites. This is claimed to be due to a presumed activation of signalling via nematode-specific DEG-3 subtype nAChRs (Kaminsky et al. 2008). Commercial use of AADs is still some years off and if it is successfully brought to market there is little doubt that resistance to AADs will emerge in the future, but proper management of the drug and its distribution and use can go a long way to slowing down the emergence of resistance.

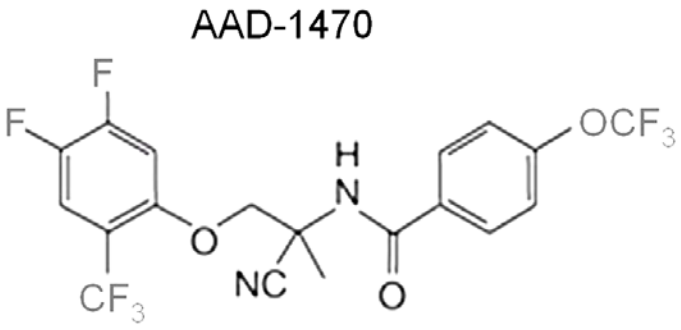

Figure 7: Structure of amino-acetonitrile derivative- 1470

Modified from figure (Kaminsky et al. 2008)

1.2.3 Emodepside

Emodepside is a relatively new anthelmintic on the market. Developed in the 1990's, it is a derivative of a fermentation product of *Mycelia sterilia,* a fungus found on the shrub *Camelia japonica* (Holden-Dye et al. 2007). The effects on *C. elegans* include inhibition of pharyngeal pumping, decreased locomotion general retardation of development and inhibition of egg-laying resulting in "bagging" in adult hermaphrodites. Emodepside acts through latrophillins, in particular the LAT-1 gene, which mediates the inhibitory effects on feeding and locomotion. RNAi knockout studies (Willson et al. 2004; Bull et al. 2007; Guest et al. 2007) determined that the *lat-1* mutants show a level of reduced sensitivity to emodepside but also exhibit the same locomotor inhibition (Guest et al. 2007). Emodepside has also been linked to the SLO-1 calcium activated potassium channel (Wang et al. 2001). It is thought that emodepside activates a SLO-1-dependent pathway; null mutants of the *slo-1* gene are highly resistant to the emodepside effects on locomotion and feeding. In addition, strains carrying gain-of-function alleles of *slo-1* genes behave in the same way as emodepside treated animals but are not emodepside hypersensitive (Holden-Dye et al. 2007). The fact that emodepside appears to act on novel drug targets shows that it may be an excellent alternative to the classic three drug classes that overwhelm the market. As resistance to the benzimidazoles, nAChRs agonists and the

macrocyclic lactones becomes increasingly widespread, new drugs are needed. Emodepside has proven effective on nematodes from populations resistant to benzimidazole, levamisole and ivermectin (Harder et al. 2002) indicating that it will play an important role in veterinary and human medicine in the future.

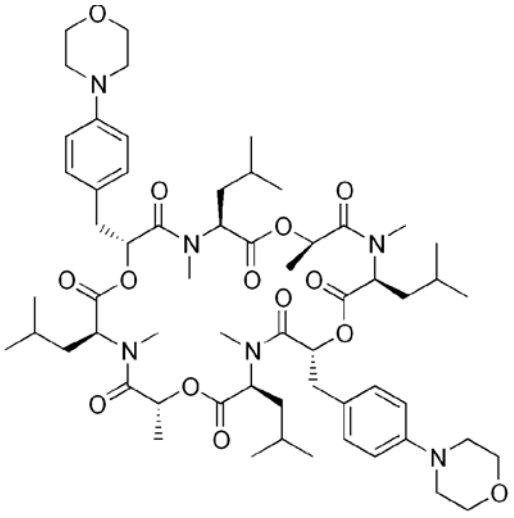

Figure 8: Structure of emodepside

1.2.4 The Macrocyclic lactones

The avermectins (AVMs) and the milbemycins are two structurally related drug classes' macrocyclic lactones that possess potent anthelmintic, insecticide and acaricide properties.

Both the AVMs and milbemycins (AM) were discovered due to a large scale screening program at Merck in the mid 1970's (Vercruysse et al. 2002), by which bacterial and fungal fermentations were sequentially tested for any antihelmintic properties. The avermectins were famously derived from the microorganism *Streptomyces avermitilis* isolated from a soil sample taken from a bunker on a Japanese golf course in 1976. Once proven to have antiparasitic properties several synthetic derivates with enhanced therapeutic properties were produced and are

known collectively as “The Avermectins”. The first commercial use of these compounds came in 1981 when ivermectin was cleared for use in animals. Ivermectin (a mixture of two compounds, 22, 23 di-hydroavermectin B_{1a} and 22,23-dihydroavermectin B1b) are semi-synthetic derivatives of avermectin B_{1a}, which of the 8 originally isolated avermectin had proved to have the most potent antihelmintic properties (Chabala et al. 1980; Egerton et al. 1980). Other avermectins have been introduced over the years, all contain the same basic structure such as doramectin from Pfizer, abermectin designed as an injectable agent in cattle and eprinomectin for use in lactating dairy cows (Vercruysse et al. 2002) and Moxidectin, a milbemycin produced by Fort Dodge.

The AVMs are characterised by their broad spectrum activity and are used to combat nematode infections in humans, animals and crops. Avermectins are used as an insecticide, the most common being abermectin (Ali et al. 1985), although in the last three years new synthetic avermectin derivatives have also been created for the insecticide market, as endectocides against ticks and fleas (Wei et al. 2005).

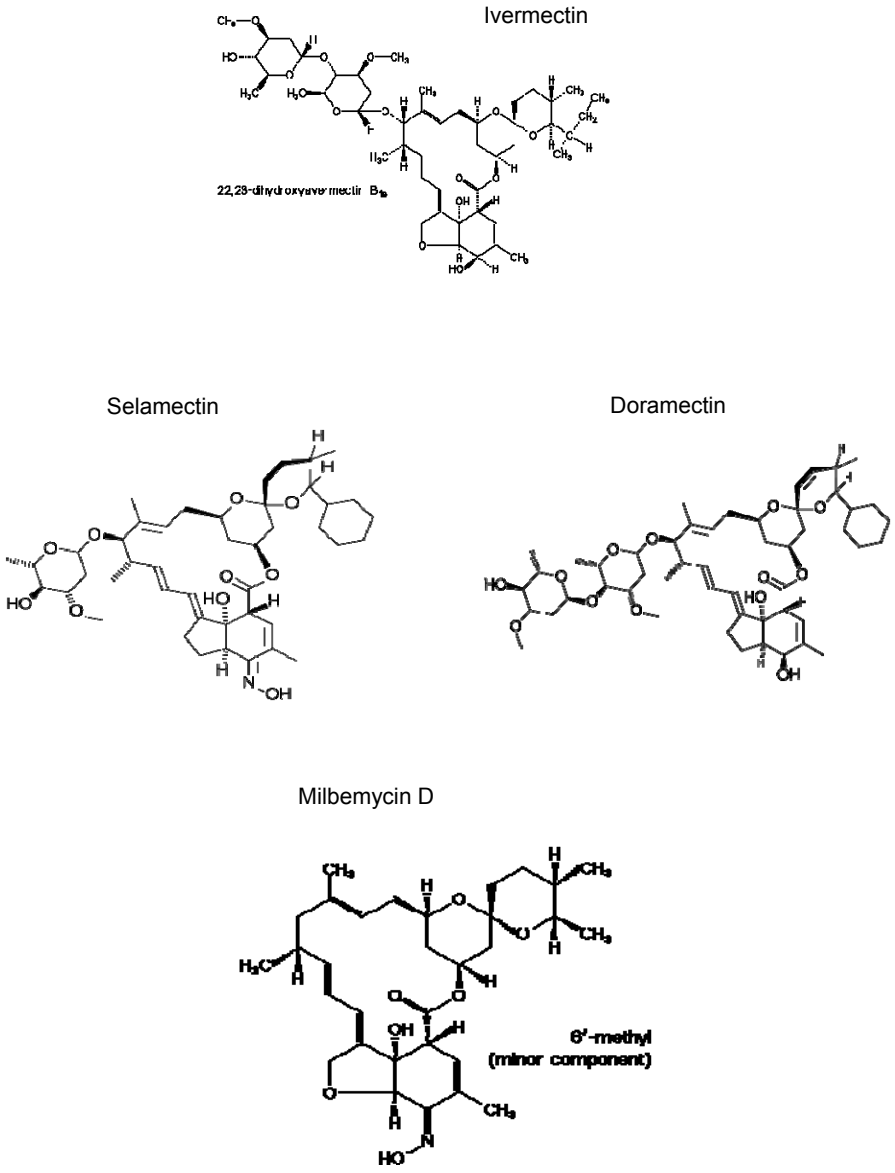

Figure 9: Structure of some avermectins and milbemycins

1.2.4.1 Biological effects of AMs

The AMs can have an effect on several different sites, but it is widely believed that the major effective site of action is the glutamate-gated chloride channel (GluCl). Although the AMs are also known to act of GABA-gated ion channels, they were

seen to non-competitivley block GABA receptors in *Ascaris* muscle at micromolar concentrations (Holden-Dye et al. 1988; Holden-Dye et al. 1990), but the relatively high concentrations of IVM required to elicit a reposnse on GABA receptors indicate that they were not the primary drug target in nematodes (Martin et al. 1989; Schaeffer et al. 1989). IVM has been also reported to act as an allosteric modulator of nicotinic α7 subunits. It was shown that preapplication of IVM, in the micromolar range, strongly enhances the subsequent acetylcholine-evoked current of the neuronal chick or human α7 nicotinic acetylcholine receptors expressed in *Xenopus* oocytes and K-28 cells (Krause et al. 1998), it was later shown to have the same effect on the *C. elegans* nAChR subunit UNC-16 (Raymond et al. 2000). However, it was investigations into the site of action of a the AMs on *C. elegans* membranes and rat brain and the discovery of high affinity binding sites that first lead to the suggestion that GluCls were present and IVM sensitive (Schaeffer et al. 1989).

A number of *in vitro* studies have shown that AMs inhibit motility, fecundity and pharyngeal pumping in nematodes (therefore halting feeding) (Pemberton et al. 2001). Inhibition of pharyngeal feeding is the most sensitive of the AM sensitive processes (Gill et al. 1991; Geary et al. 1993; Gill et al. 1995; Paiement et al. 1999) with a concentration of ≥ 0.1nM IVM causing complete paralysis of the pharynx in an adult *H, contortus* whereas complete paralysis (defined as loss of motility) requires a concentration of ≥ 10nM IVM (Geary et al. 1993), studies in larval *H. contortus* and in *C. elegans* show similar effective concentrations (Kass et al. 1980; Avery et al. 1990; Arena et al. 1995). But even at these concentrations the head and tail can still move and paralysis is contained to the mid section (Geary et al. 1993). It has been noted that the different effects of the AMs differ between nematodes and even life stages within these nematodes (Gill et al. 1998). In the filarial nematodes AMs are highly effective at killing the larval stages but fail to kill the adults, although they still suppress fecundity in the adult (Awadzi et al. 1985; Lok et al. 1995). This effect on fecundity has also been described in adult *H. contortus* and *C. elegans* (Le Jambre et al. 1995; Grant 2000). The failure of the AMs to kill adult filarial nematodes has maintained a market for alternative anthelmintics (Campbell et al. 1984; Grant 2000).

1.2.4.2 Human antiparasitic chemotherapy

Avermectins were introduced into human medicine in the 1980s. As for animals the avermectins are primarily used to fight parasitic nematode infections such as *O. volvulus*. Merck, the company who discovered the avermectins and produced ivermectin, donated it to 30 countries in Africa and Central and South America in order to combat river blindness and other debilitating parasitic diseases. Annually more than 25 million people are treated with a single dose of ivermectin which acts to clear any young nematodes of all types out of the system and halting the life cycle. In some species, particularly the filaria, the most important effect on the adult worm is to suppress new microfilariae production; similar effects on fecundity are seen in *H. contortus* and *C. elegans* (Vercruysse et al. 2002).

Recently new non anthelmintic applications for the avermectins in human medicine have been discovered. For example some avermectins create a modification of the sensitivity of Hep-2 and P388 tumour cells to taxol and vincristine, substrates of multidrug resistance proteins (Korystov et al. 2004). This property of the naturally occurring avermectins can be used in tumour therapy by combining application of avermectins with anti-tumour preparations. Interestingly it is the synthetic derivatives of the avermectins that are least effective (Korystov et al. 2004).

1.2.4.3 Avermectin Resistance

The avermectins are extremely profitable drugs, but over the past few years an increasing number of instances of resistance have been reported.

Ivermectin resistance involving *Haemonchus* species has been reported by several authors in the southern hemisphere, and is becoming a serious threat to the sheep industry (J.A. Van Wyk et al. 1997). Cases have also been reported from the northern hemisphere in *Teladorsagia circumcincta* and *H. contortus* (Jackson et al.

1992; Maingi et al. 1996; Yue et al. 2003; Schnyder et al. 2005). It appears that the most important issue in the rate at which resistance emerges is the number of worms that are left untreated (J.A. Van Wyk et al. 1997).

At the moment current literature is unclear on the basis of resistance to the avermectins. There is still some debate on the role of GluCls in avermectin resistance with P-glycoproteins also being implicated. Some P-glycoproteins and multidrug resistance proteins act as membrane transporters which pump drugs from the cell. It has been suggested that a disruption of the *mdrla* gene, which encodes a P-glycoprotein in some species of dog, especially the collie, results in hypersensitivity to ivermectin. Genes encoding members of the P-glycoprotein family are known to exist in nematodes but the involvement of P-glycoprotein in nematode ivermectin-resistance has not been described. Some data suggests that a P-glycoprotein may play a role in ivermectin resistance in *H. contortus, C. oncophora* and other nematodes (Blackhall et al. 1998; Xu et al. 1998; Molento et al. 1999; Sangster et al. 1999; Prichard R et al. 2007).

It is clear that avermectins can interact with a variety of different channels in addition to the GluCls, including nematode and mammalian $GABA_A$ and glycine receptors (Adelsberger 2000; Dawson 2000; Shan 2001), α7 nicotinic acetylcholine receptors and $P2X_4$ receptors (Krause 1998; Khakh 1999). Therefore, if the GluCls are not the only target of the avermectins and milbemycins it is possible that they are also not the only source of resistance.

1.3 Cys-loop ligand gated ion channel superfamily

The ligand-gated ion channel (LGIC) superfamily includes the cationic channels activated by acetylcholine and 5-HT (Forrester et al. 2003), as well as anionic channels activated by GABA, glycine, histamine, and 5-HT (Ranganathan et al. 2000; Zheng et al. 2002). The overall structure differs from the excitatory glutamate receptor family of vertebrates and they do not respond to the classical glutamate

receptor agonists such as kainate, aspartate, or *N*-methyl-D-aspartic acid (NMDA) (Cully et al. 1996).

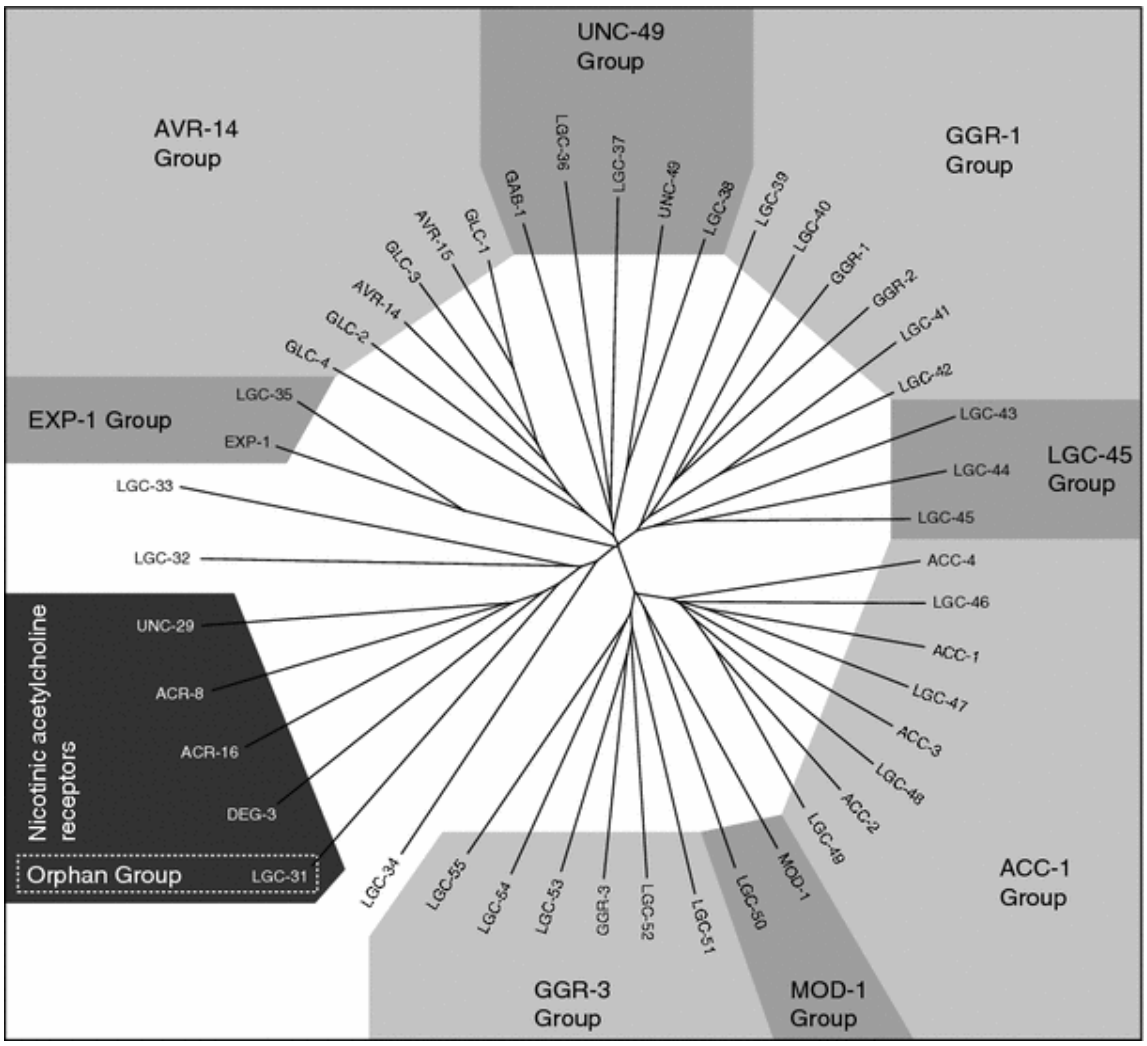

Figure 10: Tree showing the cys-loop LGIC gene superfamily of *C. elegans*.
This figure focuses on cys-loop LGIC subunits other than nAChRs although representative subunits of the nAChR groups are shown (Jones et al. 2008)

1.3.1 Nicotinic Acetylcholine Receptors

The primary member of the LGIC family is the nicotinic acetylcholine receptor family. The nAChR family is by far the most comprehensively studied and characterised.

In nematodes acetylcholine was identified a neurotransmitter in *Ascaris* and other nematodes in 1955 (Mellanby 1955) and was subsequently shown to be an excitatory transmitter at nematode neuromuscular junctions (Del Castillo et al. 1963; Del Castillo et al. 1964; Del Castillo et al. 1967)

The model nematode *C. elegans* has been used as the model organism for understanding the nematode nAChRs and the initial group of *C. elegans* receptor subunits was identified by mutations conferring resistance to levamisole (Lewis et al. 1980; Fleming et al. 1997). Later studies used genomic sequence analysis to elucidate the remaining subunits (Jones et al. 2004). *C. elegans* has 27 genes coding for nAChR subunits; in addition, there are about 20 genes encoding putative ionotropic receptor subunits that have not been fully characterized, but could include additional nAChR subunits, this is an extraordinarily high number when compared to fewer than 20 nAChRs seen in mammals (Rand 2007).

Five classes of protein subunits have been identified, based on sequence similarity- UNC-29, UNC-38, ACR-8, ACR-16, and DEG-3 (Mongan et al. 1998; Mongan et al. 2002; Jones et al. 2004). Each class contains between three and nine subunits, and some of the classes contain both α and non-α type subunits. The UNC-38 class contains three α subunits, and is the most homologous to those found in insects. The ACR-16 class consists of nine members (α and non-α), and its members resemble vertebrate α7 subunits The UNC-29 class contains four non-α subunits; these proteins are similar to vertebrate skeletal muscle non-α and insect non-α subunits. The ACR-8 class is α nematode specific grouping, and contains three α subunits. The DEG-3 class is also nematode specific, and consists of eight verified α and non-α subunits. The best characterized *C. elegans* AChRs, based on electrophysiological recording and reconstitution in heterologous systems, are at neuromuscular junctions (Rand 2007). The muscles of the body wall express two major types of ACh receptors: one type responds to levamisole and the other type to nicotine, but not levamisole (Richmond et al. 1999). The levamisole-sensitive receptors on the body muscles appear to be heteromeric, and contain three essential subunits: UNC-29, UNC-38, and UNC-63 (Fleming et al. 1997; Richmond et al. 1999; Culetto et al. 2004). LEV-1 and LEV-8 are also subunits, but they are either non-essential for the response to levamisole, or else they are only present in a subset of the receptors (Fleming et al. 1997). The nicotine-sensitive receptors appear to be homomeric, containing only the ACR-16 α subunit (Francis et al. 2005; Touroutine et al. 2005).

Characterisation of the nAChR subunits of the parasitic nematodes has only been undertaken in the last few years, with the publishing of the first parasite genomes. The major noticeable fact is that the number of nAChR subunits in the parasites is far lower than in *C. elegans. Brugia malayi* has nine subunits and *Trichinella spiralis* just eight (Williamson et al. 2007). This calls in to question the validity of *C. elegans* as a model nematode for nAChR receptors.

Prior to the structural data becoming available invaluable data on the properties of nAChRs were gathered by the site directed mutagenesis of individual amino acid residues, and the resultant changes in electrophysiological data helped determine the gating, ligand-binding, and cation-conduction properties of the ACh. (Giraudat et al. 1986; Akabas et al. 1994; Labarca et al. 1995; Zhong et al. 1998; Grosman et al. 2000) Subsequent similar experiments, performed on $GABA_A$, glycine, 5-HT3 and neuronal α7 receptors constitute a wealth of complementary information.

1.3.1.1 Nicotinic Acetylcholine Receptor structure

Our understanding of the structure of the ligand gated channels is still far from complete, but great headway has been made in understanding the structure of the primary family member: the nicotinic acetylcholine receptor. Understanding this structure is essential for creating a template for understanding the conserved regions in the ligand gated chloride channels

The extra-cellular portion of the each of the receptor subunits contains the ligand binding domains and is the most variable and characteristic portion of the nAChR subunit. The structure of the N –terminal domain was deduced after the discovery and subsequent crystallization of the closely related soluble protein, Acetylcholine binding protein (AChBP) from the giant pond snail *Lymnaea stagnalis* (Brejc et al. 2001). A series of β- strands form two β-sheets which fold tightly to form a β-sandwich held together by the characteristic disulphide bridge which forms the Cys loop, (Brejc et al. 2001) In the well characterized *Torpedo* pentamer the ACh-binding sites lie at the interface between α–γ and α–δ subunits, and are dominated by interactions on the α subunits between loops A, B and C, which form the strands

connecting β-strands and 6-7, 7-8 and 9-10 respectively (Corringer et al. 2000; Sine 2002; Celie et al. 2004). The intracellular domain of the channel is the smallest part and each subunit contributes one α- helix (part of the M3–M4 loop) which form together to create a cone shaped “vestibule” (Miyazawa et al. 1999; Unwin 2003) See Figure 11.

The membrane spanning domain of the subunit consists of four α-helices M1–M4 (Miyazawa et al. 2003). The M2 regions of each subunit shape and line the pore, the other helices (M1, M3 and M4), coil around each other to create a shield for the inner ring from the lipids. When the channel is closed the M2 helices close and wind together in the middle of the pore space creating a hydrophobic barrier known as a “hydrophobic girdle” tight enough to prevent ion movement (Beckstein et al. 2004; Corry 2004) and it is thought that the opening of this hydrophobic barrier constitutes the gating mechanism of the channel itself (Miyazawa et al. 2003; Unwin 2003).

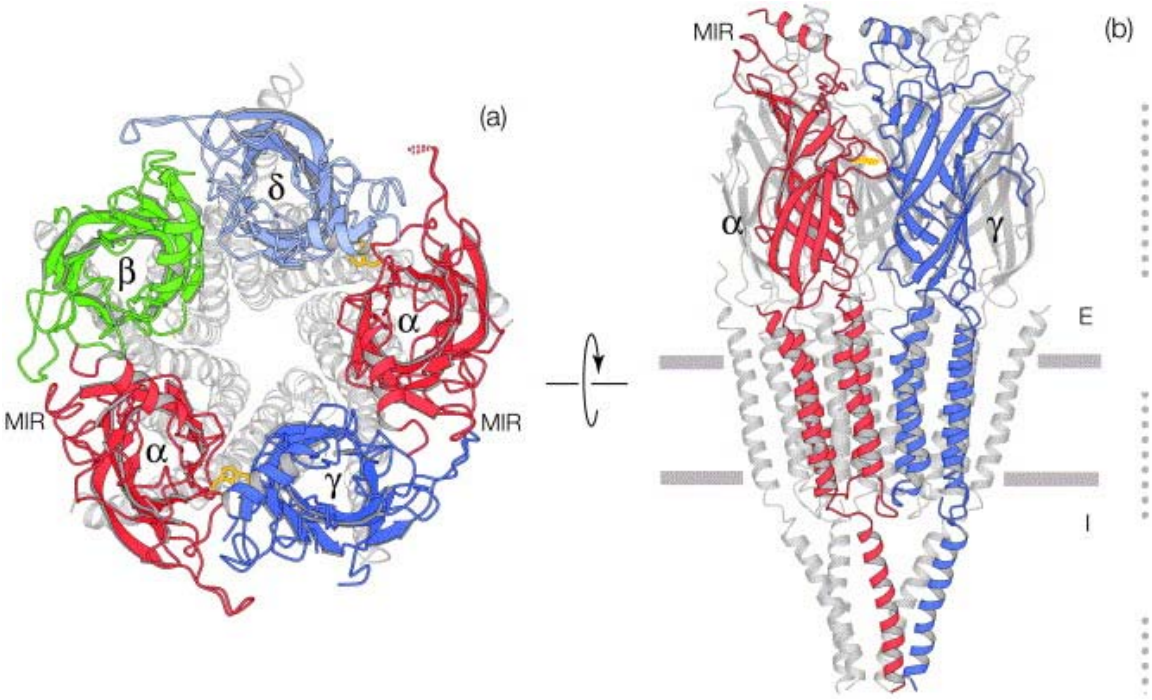

Figure 11: Ribbon diagrams of the nACh receptor
As viewed (a) from the synaptic cleft and (b) parallel with the membrane plane. For clarity, only the ligand-binding domain is highlighted in (a) and only the front two subunits are highlighted in (b), the MIR and the membrane (horizontal bars; E, extracellular; I, intracellular). The dotted lines on the right denote the three main zones of subunit–subunit contacts. (Taken from (Unwin 2005)

Experiments using electron microscopy carried out on cultured *Torpedo* postsynaptic membranes have helped to determine the structure of this channel and how the structure changes upon activation, (Brisson et al. 1984; Toyoshima et al. 1990). These experiments used a rapid spray-freezing technique to mimic the synaptic release of ACh and trap the open-channel form. (Unwin 1995) These experiments showed that binding of ACh initiates two interconnected events in the ligand-binding domain.

The first is a local disturbance in the region of the ACh-binding sites, and the second a larger-scale conformational change, involving rotational movements predominantly in the two α subunits. The inner M2 helices also change their configuration in response to ACh, widening the lumen of the pore at the middle of the membrane. Higher resolution studies of the extended conformational change (Unwin 2002) and of the structure in the membrane suggested a simplified mechanical model for the channel opening mechanism: ACh triggers multiple rotations of the inner β-sheets of the α subunits and instigates the twisting movement in M2 regions which breaks the gate apart (Miyazawa et al. 1999; Miyazawa et al. 2003; Unwin 2005).

1.3.2 GABA receptors

The most abundant synapses in the central nervous system of vertebrates are inhibitory synapses that use the L-glutamine derived neurotransmitter, γ-aminobutyric acid (GABA). GABA was first discovered in 1950 (Awapara 1950; Awapara et al. 1950; Roberts et al. 1950). The electrophysiological studies that followed over the next two decades discovered the role of GABA as a neurotransmitter in the mammalian CNS. Over the years three classes of GABA receptors have been identified $GABA_{A,}$ $GABA_B$ and $GABA_C$ (Schofield et al. 1987). In nematodes the observation of fast hyperpolarisation of muscle on the addition of GABA pointed to the presence of GABA gated ion channels that were chloride dependent but the pharmacological profile of the nematode GABA-mediated

response indicates that it is not directly analogous to either the mammalian $GABA_A$ or $GABA_B$ receptors (Hewitt et al.1986), although nematodes do have distinct GABA receptors that are similar to vertebrate $GABA_A$ or $GABA_B$ based on sequence identity alone. GABA is also an important neurotransmitter in *C. elegans*; however, in contrast to vertebrates where GABA acts at synapses of the CNS, in nematodes GABA acts primarily at the neuromuscular junction (Olsen et al. 1999). GABA acts to relax the body muscles during locomotion and foraging and to contract the enteric muscles during defecation, this was discovered after observation of mutants with GABAergic transmission defects, which although viable, have several severe motor defects. The most obvious phenotype is “shrinker” whereby the nematode has a tendency to contract dorsal and ventral body wall muscle simultaneously in response to touch. This is thought to be as a result of a lack of function of the GABA-containing DD and VD inhibitory motor neurons (McIntire et al. 1993; McIntire et al. 1993)

In *C. elegans* the *unc-49* gene encodes three distinct $GABA_A$ receptor subunits by splicing a common N-terminal ligand-binding domain to one of three alternative C-terminal domains, producing the UNC-49A, UNC-49B, and UNC-49C subunits (Bamber et al. 1999). This gene structure is conserved throughout the phylum and has also been demonstrated in *C. briggsae*. The UNC-49B and UNC-49C subunits are expressed in the muscles and localized to synapses from the D-type GABA motor neurons (Bamber et al. 1999; Gally et al. 2003; Bamber et al. 2005) The GABA receptor localised at neuromuscular junctions is a heteromer composed of the B and C subunits (Bamber et al. 2005). The B subunit has been proven to be required for localization of the receptor to neuromuscular junctions and the C subunit imparts specific pharmacological properties to the heteromeric receptor (Bamber et al. 2003; Bamber et al. 2005). The UNC-49A subunit is barely detectable *in vivo*, and is not found co-localised with UNC-49B or UNC-49C to form a functional receptor *in vitro* (Bamber et al. 1999).

1.3.3 Glutamate-gated chloride channels

The first two glutamate gated chloride channel subunits were discovered by Merck in the early 1990's by isolating mRNAs which elicited an electrophysiological response to IVM-$P0_4$ and glutamate when injected into *Xenopus* oocytes (Arena et al. 1992). The mRNA fragments were then cloned to cDNA (Cully et al. 1994). These subunits were named GluClα and GluClβ and identified as members of the LGIC superfamily from sequence and functional identity with other family members, including the long extracellular domain followed by four transmembrane domains. Throughout the family there is a high degree of amino-acid sequence similarity, and there are some highly characteristic sequence motifs, for example, a 15-residue cys-loop' that is in the N-terminus domain of all members of the family including the GluCls. All the subunits form oligomers, and all of these are pentameric, there is also a great deal of similarity between the individual subunits that make up each different receptor (Ortells et al. 1995). The volume of data that was available on other LGIC family members gave valuable insight into the properties of the GluCls from an early stage. For example the long intracellular loop between TM3 and TM4 has conserved areas with homology to certain protein kinase sequence, which in other family members has been shown to effect channel kinetics, channel function and downstream signaling (Porter et al. 1990; Wafford et al. 1992; Wafford et al. 1992; Leidenheimer et al. 1993; Krishek et al. 1994; McDonald et al. 1994; Macdonald 1995; Moss et al. 1996; McDonald et al. 1997; McDonald et al. 1998; Filippova et al. 2000; McDonald et al. 2001; Song et al. 2005).

The GluCls also had an additional pair of cysteine residues in the extracellular domain, a freature similar to the vertebrate glycine receptor subunits (Cully et al. 1994). The sequence data shows a great deal of homology to the $GABA_A$ and glycine receptors of vertebrates although the GluCls do have their own distict group within the family (Cully et al. 1996; Vassilatis et al. 1997; Jones et al. 2008).

GluCls are found only in invertebrates (Cleland 1996) and therefore make good drug targets. Ivermectin is a widely used anthelmintic which is known to interact with GluCls (Cully et al. 1994; Arena et al. 1995; Cleland 1996; Cully et al. 1996; Vassilatis et al. 1997; Dent et al. 2000). Over the last few years several labs have concentrated on the cloning and expression of GluCls from *C. elegans.* These

studies have revealed that GluCls are closer in structure to vertebrate $GABA_A$ and glycine receptors than the expected nAChRs but this not surprising as both GluCls and $GABA_A$ are anion channels (Cully et al. 1994). Work done on these isolated *C. elegans* GluCl has concluded that they have a unique pharmacological profile by which channel activation occurs on binding with ligands such as L-glutamate and ibotenate (Cully et al. 1994).

GluCls are extremely sensitive to macrocyclic lactone anthelmintics such as ivermectin (IVM) and this interaction contributes to the overall toxic effect of the drug in nematodes. Low nanomolar concentrations of IVM potentiate the glutamate activation of the chloride channel expressed in *Xenopus* oocytes whereas concentrations in the micromolar range directly activate the channel. IVM channel activation is essentially irreversible and this is due to its slow dissociation from the binding site (Schaeffer et al. 1989). This results in cellular inhibition and possible muscle paralysis of parasitic nematodes, which is likely to contribute to their elimination from the host.

GluCls have been cloned from a variety of species including *C. elegans* (Schaeffer et al. 1989; Cully et al. 1994; Dent et al. 1997; Laughton et al. 1997; Vassilatis et al. 1997; Dent et al. 2000), *Drosophila melanogaster* (Cully et al. 1996), and the parasitic nematode, *Haemonchus contortus* (Delany et al. 1998; Forrester et al. 1999; Jagannathan et al. 1999). However, most of our current knowledge regarding the function of GluCls and their interaction with macrocyclic lactones has emerged from the expression of cloned channel subunits from *C. elegans*.

1.3.3.1 Glutamate gated chloride channel pharmacology

GluClα1 and GluClβ were the first GluCls isolated from *C. elegans* in 1994 (Cully et al. 1994) after being discovered as ivermectin sensitive. Analysis of the cDNA sequence showed a high level of sequence homology to both glycine and $GABA_A$ receptor subunits. The GluCls are clearly in the chloride channel branch of the LGIC superfamily alongside muscle nAChR.

C. elegans gene	*C. elegans* subunit	*C. elegans* Expression pattern	*H. contortus* gene	*H. contortus* subunit	*H. contortus* Expression pattern
glc-1	GluCl α1	Unknown	-	-	
glc-2	GluClβ	Pharangeal Muscle (Laughton et al. 1997)	*Hc Glc-2 (HG4)*	Hc GluClβ (HG4)	Unknown
glc-3	GluCl α4	Nerve ring, head muscle[1]	-	-	
glc-4	-	Intestine; anal depressor muscle; head mesodermal cell; Nervous system; nerve ring, head neurons; tail neurons[1]	-	-	
avr-14	GluCl α3A (GBR-2A) GluCl α3B (GBR-2B)	40 extra-pharangeal neurones in the ring ganglia of the head, some motor neurons in the ventral nerve cord and mechanosensory neurons (Dent et al. 2000) M1 and M4 pharyngeal neurones (Franks et al. 2006)	*Hc avr-14 (gbr-2)*	Hc GluCl α3A (Hc GBR-2A) Hc GluCl α3B (Hc GBR-2B)	Both varients expressed in nerve ring, motor neurones and amphid neurones (Jagannathan et al. 1999; Portillo et al. 2003)
avr-15	GluCl α2A GluCl α2B	Pharyngeal mucles pm4 and pm5. Some head neurones. Dorsal and ventralsublateral nerve cords. Neurones DA9 ans VA12 (Dent et al. 1997)	-	-	
-	-		*Hc GluCl α*	Hc GluCl α	Inhibitory motor neurones(Portillo et al. 2003)

Table 1. Summary of known *C. elegans* genes, GluCl subunits and expression patterns and the equivalent orthologues in *H. contortus.*

[1] Unpublished information taken from www.wormbase.org.

GluCl Subunit	GluCl gene	EC_{50} Glutamate	Hill coeff. Glutamate	KD IVM (or $IVMPO_4$)	Hill coeff. IVM	Reference
C. elegans mRNA	-	300 µM	1.7	90 nM	1.1	(Arena et al. 1991; Arena et al. 1992)
C. elegans pharynx	-	166 µM	No data	2.7 nM	-	(Pemberton et al. 2001)
Ce GluClα1	*glc-1*	No Response	-	140 nM	1.5	(Cully et al. 1994)
Ce GluClβ	*glc-2*	380 µM	1.9	-	-	(Cully et al. 1994)
Ce GluClα1 β	-	1.36 mM	1.7	190 nM	2.5	(Cully et al. 1994)
Ce GluClα 2A	*avr-15*	2.0 mM	1.5	-	-	(Dent et al. 1997)
Ce GluClα 2B	*avr-15*	208.3 µM	2.1	108 nM	1.6	(Laughton et al. 1997; Vassilatis et al. 1997)
Ce GluClα 2Bβ	-	62 µM	2.4	103 nM	1.85	(Vassilatis et al. 1997)
Ce GluClα 3A	*avr-14 / gbr-2*	No Response	-	-	-	(Dent et al. 2000)
Ce GluClα 3B	*avr-14 / gbr-2*	Response at 10 mM	-	-	-	(Dent et al. 2000)
Ce GluClα 4 (GLC-3)	*glc-3*	1.9 mM	1.5	400 nM	4.9	(Horoszok et al. 2001)

Table 2. Summary of the pharmacological properties of known *C. elegans* channels.
EC50 and Hill slope values are expressed as mean ± SEM

GluCl Subunit	GluCl gene	EC_{50} Glutamate	Hill coeff. Glutamate	KD IVM (or $IVMPO_4$)	Hill coeff. IVM	Reference
Hc CluCl α (HG5)	HcGluClα	8.4 µM	2.13	131 nM	1.15	(Forrester et al. 2003)
Hc GluClβ (HG4)	Hcglc-2 /HG4	-	-	No IVM binding	-	(Cheeseman et al. 2001)
HcGluClα3A (Hc-GBR-2A) (HG2)	Hc avr-14 /gbr-2-	-	-	No IVM binding	-	(Cheeseman et al. 2001)
HcGluClα3B (Hc-GBR-2B) (HG3)	Hc avr-14/ gbr-2	unknown	unknown	70pM	-	(Cheeseman et al. 2001)

Table 3. Summary of the pharmacological properties of known parasitic nematode channels expressed in either *Xenopus* oocytes or COS-7 cells
EC50 and Hill slope values are expressed as mean ± SEM

Our current understanding of GluCl pharmacology has been elucidated from several experimental approaches, the most important has been two-electrode voltage clamp recordings taken from *Xenopus* oocytes expressing GluCls or tissue preparations and radioligand binding studies on either nematode membrane or membrane taken from cultured cell lines expressing GluCls. Obtaining pharmacological data using ivermectin has over the years proven difficult due to its viscous consistency and highly hydrophobic nature. As a result many data was derived from experiments using Ivermectin-phosphate ($IVMPO_4$) a far more soluble compound.

In *C. elegans* there are six GluCl genes, at least two of which are alternatively spliced giving at least eight functional subunits (Yates et al. 2003). The *avr-15* and *avr-14* genes are alternatively spliced to create two subunits each (Cully et al. 1994; Dent et al. 1997; Laughton et al. 1997; Vassilatis et al. 1997; Horoszok et al. 2001). Homologues for one of these alternatively spliced genes (avr-14) were also found in *Haemonchus contortus* (see table i) along with GluClβ (Cheeseman et al. 2001).

GluClα1a and GluClβ were the first subunits to be isolated and characterised by expression in oocytes (Cully et al. 1994). Oocytes expressing both subunits gave electrophysiological responses to both glutamate and $IVMPO_4$, which was comparable to earlier studies in which *C. elegans* mRNA was injected directly into oocytes (Arena et al. 1991; Arena et al. 1992). The responses showed a classic fully reversible inward chloride current on addition of glutamate; this was blocked on the addition of 100 μM picrotoxin (PTX) the chloride channel blocker by 68%. (Cully et al. 1994) 100μM PTX also blocked the inward currents of the channels activated by 1μM $IVMP0_4$ by 61% (Cully et al. 1994). This blocking action was also repeated with the addition of flufenamic acid in similar concentrations used to the same effect in the oocytes injected with *C. elegans* mRNA (Arena et al. 1992). The GluClα1β heteromers were also activated by the structural analogue of glutamate: ibotenate, but were insensitive to NMDA, AMPA, acetylcholine, kainate and muscimol at 1mM and GABA, L-aspartate, glycine, histamine, β-alanine and taurine at 10mM (Cully et al. 1994; Dent et al. 1997; Vassilatis et al. 1997; Horoszok et al. 2001).

The GluClα1β heteromers were also activated by the structural analogue of glutamate: ibotenate, but were insensitive to NMDA, AMPA, acetylcholine, kainate and muscimol at 1 mM and GABA, L-aspartate, glycine, histamine, β-alanine and taurine at 10mM (Cully et al. 1994; Dent et al. 1997; Vassilatis et al. 1997; Horoszok et al. 2001).

Both of these subunits show the ability to form homomeric channels, with the GluClα1 pentamers insensitive to glutamate but responsive to IVMPO_4, although, it was later demonstrated that the GluClα1 subunits can bind glutamate but cannot trigger the gating mechanism (Etter et al. 1996). Conversely the GluClβ pentamers are readily activated by the addition of glutamate but insensitive to IVM. Homologues to the *glc-2* gene (GluClβ) have been found in *Cooperia oncophora* and *Haemonchus contortus.* (Delany et al. 1998; Cheeseman et al. 2001; Njue et al. 2004)

The alternatively spliced *C. elegans* GluCl α2A and GluCl α2B subunits are also able to form homomeric pentamers sensitive to both glutamate and IVM. Prior to splice variants being characterized the GluCl α2B subunit (or GluCl α2 as it was known) was also shown to co-assemble and form heteromeric channels with GluClβ (Vassilatis et al. 1997). This increased its sensitivity to glutamate compared to either homomeric pentamers but stopped the weak blocking by PTX shown in the homomer (Vassilatis et al. 1997). The *glc-3* gene product GluClα4 has been shown to form homomeric channels sensitive to glutamate and IVM (Horoszok et al. 2001) and are blocked by insect-GABA blockers BIDN and Fipronil but are, interestingly, insensitive to the action of PTX (Hosie et al. 1995; Hosie et al. 1995; Rauh et al. 1997; Hamon et al. 1998; Horoszok et al. 2001).

Of the two splice variants created by the *C. elegans avr-14* gene the GluClα3A when expressed alone was found to be neither glutamate nor IVM sensitive, in contrast, GluClα3B subunit forms homomeric channels that are both activated by glutamate and irreversibly opened by IVM (Dent et al. 2000). Homologues of *C. elegans avr-14* gene have been identified in *H. contortus, Haemonchus placei* and *Difilaria immitis,* and *C. oncophora* have shown to form similar splice variants. *Avr-14* homologues which produce only one subunit (GluClα3) have been discovered in *Ascaris suum* and *Onchocerca volvulus* (Cully et al. 1996; Jagannathan et al. 1999; Cheeseman et al. 2001; Yates et al. 2003; Njue et al. 2004; Njue et al. 2004).

Another subunit has been found in *H. contortus*, which doesn't appear to have an obvious homologue in *C. elegans, Hc GluClα* which encodes the Hc GluClα subunit forms homomeric channels which are both glutamate gated and to which

IVM binds with high affinity. (Forrester et al. 1999; Cheeseman et al. 2001; Forrester et al. 2002; Forrester et al. 2003)

The macrocyclic lactones work potently against all manner of invertebrates and are powerful insecticides and acaricides and it may be possible to gain insights into the anthelmintic action of these compounds, and of resistance to them, by looking at their modes of action and resistance in insects. As the IVM sensitive GluCl subunits are thought to be the major target of the anthelmintics it is reasonable to believe that mutations in or loss of the invertebrate GluCls may confer resistance to the AMs. Several insect LGCC are sensitive to avermectins, including the glutamate- and histamine-gated chloride channels (HisCl) (Gisselmann et al. 2002; Zheng et al. 2002). Mutations in the *ort* gene, encoding one of the HisCl subunits of *D. melanogaster,* alters the susceptibility of the flies to the avermectins (Iovchev et al. 2002), but specific resistance-associated polymorphisms have yet to be identified in this channel. An amino-acid substitution (P299S) in the *Drosophila* GluClα subunit confers a tenfold level of resistance to ivermectin and nodulisporic acid (Kane 2000). The affected proline residue is located just after the second transmembrane region and is ubiquitous in all known glutamate-, glycine- and GABA-gated chloride channels. Homomeric channels were expressed in *Xenopus* oocytes and two voltage clamp electrophysiology carried out to determine the pharmacological effects of the mutation. The P299S mutation conferred a tenfold loss of glutamate sensitivity, from 19.5 μM in the wild type subunits to 201 μM in the P299S DmGluClα subunits. The loss of sensitivity to ivermectin was even more marked with a 14 fold loss of sensitivity from 25 nM in the *wt* to 340 nM in the P299S DmGluClα (Kane 2000). However, these are laboratory strains and there is no information on the mechanism of insect resistance to the ML from the field.

The GABA-gated chloride channel is the site of action of the cyclodiene insecticides. Resistance to these is conferred by a SNP at position 302 of Rdl, a GABA-gated chloride channel subunit, with an alanine being replaced with either a serine or a glycine (ffrench-Constant RH et al. 1993). The A302S/A302G substitutions are in the important second transmembrane region (M2) of the GABA subunit. Interestingly some later expression studies were carried out in *Xenopus* oocytes have shown that the *Rdl* mutation also results a 3.3 fold decrease in sensitivity to ivermectin (Kane 2000), and it has been reported that the GluCl and Rdl subunits can be co-

immunoprecipitated, suggesting that either the GABA and glutamate-gated channels are part of the same complex or that Rdl and GluClα co-assemble into a functional receptor (Ludmerer et al. 2002): other workers have found that the insect glutamate- and GABA-gated channels co-exist and function separately (Zhao et al. 2004). Very recently, Eguchi *et al.* (2006) have found that the *Musca domestica* GluClα assists in the expression of Rdl when the two are co-expressed in the same *Xenopus* oocyte.
It is worth noting that the *Drosophila* mutations that confer resistance to ivermectin in both GABA receptors and GluCls are in, or very close to, M2, the membrane-spanning region that lines the pore and undergoes a conformational change to open the channel. This could highlight this part of the receptor as a potential 'hotspot' for resistance-associated polymorphisms. In nematodes, we have most information about the free-living species, *C. elegans*. Ivermectin kills *C. elegans* at therapeutic concentrations making it a suitable model system to investigate the mechanism of resistance and consequently ML resistance has been extensively studied in this species. There are a large number of *C. elegans* genes predicted to encode proteins with homology to LGCC subunits and there has been very little work done to date to examine the role many of these receptors may play in avermectin sensitivity and resistance. Nonetheless, several genes have been found that contribute to IVM resistance, however Dent et al. (2000) concluded that the GluCls are the physiologically relevant mediators of ivermectin toxicity.

Ivermectin activates GluCl channels that contain α-type subunits; such as the *avr-14*, *avr-15, glc-1* and *glc-3* gene products that all individually form ivermectin-sensitive channels as described above (Cully 1994; Dent et al. 1997; Vassilatis et al. 1997; Dent et al. 2000; Horoszok 2001), and so these are obvious candidate resistance-associated genes. Functionally null mutations in any one of the *avr-14*, *avr-15* and *glc-1* genes do not lead to significantly resistant worms, however a triple GluCl mutant displays high level resistance of > 4, 000 fold (Dent et al. 2000); double mutants in any two of the genes lead to an intermediate level of resistance. Even in the model nematode, this may reflect the necessity for changes in multiple genes to cause high-level target-site mediated ML resistance. Other *C. elegans* gene products may interact with the GluCls to mediate ML sensitivity: in particular gap junctions, which are composed of the innexins, may allow the drug-induced hyperpolarisation to spread to other cells. In the absence of the innexins (UNC-7 and UNC-9 in *C.*

elegans) ML toxicity might be restricted to only those cells expressing GluCl, preventing systemic effects (Dent et al. 2000). Both *unc-7* and *unc-9* genes contribute to ivermectin sensitivity, but neither bind ivermectin directly. An additional pathway for resistance in *C. elegans* is controlled by genes that mediate cuticle permeability. The dye-filling (*dyf*) mutants are unable to take up fluorescent dyes from the environment through the amphids. When the Dyf gene *osm-1* is mutated, all genetic backgrounds show reduced effects of ivermectin, presumably due to lower uptake of the drug (Dent et al. 2000). The GluCl and the *Dyf* genes can also act together, as the *avr-15*; *osm-1* double mutant is significantly more resistant than the *osm-1* single mutant though the *avr-14*; *osm-1* mutant is not.

In reality, the big deletions or insertions causing the above artificial mutations are relatively unlikely to occur *in vivo* in comparison to coding single nucleotide polymorphisms (SNPs) are the most likely to occur. Coding SNPs that result in changes to the tertiary structure which, in turn cause changes to the ligand or drug binding site, may cause defect in trafficking and channel assembly. This may also reduce the number of effective target sites. Alternatively changes to the tertiary structure of the pore lining transmembrane regions could lead to the inability of the channel to fully open or close, even with successful ligand binding. Although traditionally dismissed, non-coding SNPs can have recently been proven to cause the alteration of splice sites and reduction in mRNA stability. Non- coding SNPs may be detectable in cDNA, but not obvious. They can cause changes in expression level or pattern (perhaps less likely) due to promoter/enhancer polymorphisms. Due to their non-coding nature these SNPs would not be detectable in cDNA (Kimchi-Sarfaty et al. 2007). Larger deletions, insertions, transposable elements etc are likely to cause major changes in gene expression as seen in the previously discussed *C. elegans* studies

In nematodes single nucleotide polymorphisms in targets show dramatic effects on the efficacy of drugs, for example the β-tubulin codon 200 TTC/TAC (F200Y) SNP in many nematode species that confers high level resistance to benzimidazole, it is logical to predict that a similar mechanism may be at work in macrocyclic lactone resistance. There have been several reported cases of SNPs in various nematodes that confer limited levels of resistance.

It is suggested that polymorphisms in the GluCl subunits can confer resistance in parasitic nematodes. A Canadian group cloned two full-length glutamate-gated chloride channel (GluCl) cDNAs, encoding GluClα3 from *Cooperia oncophora*, the subunit which is homologous to the *C. elegans* and *H. contortus* GluCl α3B channel subunit, from ivermectin-susceptible (IVS) and -resistant (IVR) *C. oncophora* adult worms. The IVS and IVR GluClα3B subunits differed at three amino acid positions, E114G V235A and L256F all of these SNPs were located in the N terminal domain of the *C. oncophora* GluClα3 subunit, the ligand binding site area, although it is important to note the actual ivermectin/ moxidectin binding sites are still unknown (Njue et al. 2004), but are thought to be in the transmembrane regions due to the hydrophobic nature of the macrocyclic lactone drugs.

The subunits carrying the candidate SNPs were cloned and expressed in *Xenopus laevis* oocytes. Electrophysiological whole-cell voltage-clamp recordings showed that the L256F mutation in the GluClα3 was the only one that caused a small but significant threefold loss of sensitivity to glutamate from an EC_{50} of 29.7± 4 μM to 100.6 ± 0.21 μM. The efficacy of the macrocyclic lactones ivermectin and moxidectin were also significantly reduced with this mutation with the EC_{50} increasing from 0.5 ± 0.12 in IVS worms to 1.2 ± 0.11μM in channels carrying the L256F mutation. It is also important to note that the GluClα3 channels from the Ivermectin resistant population had EC_{50} comparable to those carrying the L256F mutation, 96.1 ± 4.4 μM for glutamate and 1.3 ± 0.11 μM for ivermectin/moxidectin (IVR) (Njue et al. 2004). Whether this mutation alone is enough to confer resistance of the nematodes to the macrocyclic lactones is unclear.

1.4 Aim of Project

Few studies have actually examined the molecular nature of macrocyclic lactone action in organisms such as parasitic nematodes (Cheeseman et al. 2001; Forrester et al. 2002) which is suprising considering the worldwide expenditure on anthelmintics and the emergence of resistance.

The aim of my project was to characterise the *H. contortus* GluClα3B subunit, and, investigate candidate polymorphisms found in field isolates of IVR nematodes and insects to determine whether they confer resistance, and thus to gain understanding of the interactions between the GluCls and their agonists.

The first stage of the project was to characterise the *wt H. contortus* GluClα3B subunit. This particular subunit was chosen because it had been implicated in IVM resistance in *C. oncophora* (Njue et al. 2004), and had already been proven to form homomeric channels when expressed in *Xenopus* oocytes that elicit a robust inward current that is reproducible in response to glutamate and is also sensitive to IVM.

The second stage of the project was to investigate GluClα3B-agonist interactions further by introducing mutations into the channel. IVR associated SNPs were introduced into the IVS GluClα3B. The mutations that were introduced had largely been implicated in IVM resistance, including SNPs found exclusively in the GluClα3 subunit of isolates of IVR *C. oncophora* (Njue et al. 2004), the $GABA_A$ and Dm GluClα of IVR *Drosophila melanogaster* (ffrench-Constant et al. 1993; Kane et al. 2000) and SNPs found in populations of IVR *H. contortus* (Jagannathan 1998). The position of the mutations were visualised using molecular modelling to create a homology model of the N-terminal domain of the GluClα3B subunit which would aid in the understanding of pharmacological data obtained.

Chapter 2: Methods and materials

2.1 Materials

2.1.1 Molecular biology reagents

Molecular biology grade chemicals and kits were purchased from Sigma chemical company Ltd, (Dorset, UK), PAA laboratories (Somerset, UK), Promega or Fisher scientific (Leicestershire, UK), Ambion (Texas, USA) or promega (Hampshire, UK)

2.1.1.2 Composition of general buffers and solutions

Buffer	Components
50x TAE	2 M tris-acetate, 50 mM EDTA; pH 8.0
10x TBE	1 M Tris, 0.9 M Boric Acid, and 0.01 M EDTA; pH 8.0
PBS	140 mM NaCl, 2.7 mM KCl, 10mM Na_2HPO_4, 1.76 mM KH_2PO_4; pH 7.4
TE	10 mM Tris-Cl, 1mM EDTA; pH 7.6
10x MOPS (500ml)	20.9 g MOPS in 350 ml DEPC H_20, 10 ml 1 M sodium acetate, 10 ml EDTA adjusted to 500 ml with DEPC H_20. filter sterilised
6x loading buffer	12 ml H_2O, 10ml 0.05M EDTA, 0.05 g Bromophenol Blue, 0.05 g Xylene cyanol
Agarose gel	1% agarose in 1x TBE or TAE, heated until mixed and molten, 5 µg/ml ethidium bromide added

2.1.1.3 Composition of culture media and buffer

Buffer/ solutions	Components/ L
Luria Broth (LB)	25 g Luria broth powder (or 10g tryptone, 10g NaCl, and 5g yeast extract). Autoclaved
LB Agar	25 g Luria broth powder and 15 g BactoAgar. Autoclaved
DYT Broth	16g tryptone, 10g NaCl, and 5g yeast extract. Autoclaved
NZY+ Broth	10g casein hydrolysate, 5g NaCl, and 5g yeast extract. Autoclaved Supplemented before use with 12.5ml 1 M $MgCl_2$, 12.5 ml 1 M $MgSO_4$, 10 ml 2 M glucose
SOC medium	20 g bacto-tryptone, 5g yeast extract, 10 mM NaCl, 2.5 mM KCl, 10 mM $MgCl_2$, 10 mM $MgSO_4$, 20mM glucose

2.1.1.4 Composition of *Xenopus* oocyte electrophysiology reagents

All buffer constituents and drugs were supplied by Sigma.

Buffer/ solutions	Components
Collagenase	Collagenase IA 75mg in 50ml OR-2, filter sterilised.
Frog Ringer	100.0 mM NaCl, 1.0mM MgCl2, 1.8 mM $CaCl_2$, 2.0mM KCl, 5.0 mM HEPES pH adjusted to 7.5 with NaOH
ND-96 complete	96 mM NaCl, 2 mM KCl, 1 mM MgCl2, 1.8 mM CaCl2, 5 mM HEPES, pH adjusted to 7.5 with NaOH. To 500ml, add 0.5ml 2.5M sodium pyruvate and 5ml heat inactivated, dialysed (vs ND96 inc. 1x) FBS. Filter sterilise
OR-2	82.5 mM NaCl, 2 mM KCl, 1 mM MgCl2, 5 mM HEPES, pH adjusted to 7.5 with NaOH

2.1.1.5 Bacterial strains

***E coli* strain**	**Genotype**	**Supplier**
XL-Blue	*sup*E44 *hsd*R17 *rec*A1 *end*A1 *gyr*A46 *thi rel*A1 *lac*$^-$ F$^-$ [*pro*AB]$^+$ *lac*I^q *lac*Z ΔM15 Tn*10* (*tet*^{r}0]	Stratagene Ltd Cambridge, UK
OP50	*sup*E44 *hsd*R17 *rec*A1 *end*A1 *gyr*A46 *thi rel*A1 *lac*$^-$ F$^-$ [*pro*AB]$^+$ *lac*I^q *lac*Z ΔM15 Tn*10*]	Stratagene
JM110	*rpsL* (Str^r) *thr leu thi-1 lacY galK gal Tara tonA tsx dam dcm supE44* Δ*(lac-proAB*) [F' *traD36 proAB lacI*^{q} ZΔM15]	Stratagene

2.1.1.6 Enzymes

Enzyme	**Buffer components (1X)**
T4 DNA ligase	30 mM Tris-HCl, pH 7.8; 10 mM $MgCl_2$, 10 mM DTT, 1mM ATP
BamH I	Buffer E: 6 mM Tris-HCl, pH 7.5; 6 mM $MgCl_2$, 100 mM NaCl, 1 mM DTT
EcoR I	Buffer H: 90 mM Tris-HCl, pH 7.5, 10 mM $MgCl_2$ 50 mM NaCl
Not I	Buffer D: 6 mM Tris-HCl, pH 7.9; 6 mM $MgCl_2$, 150 mM NaCl, 1 mM DTT
Pst I	Buffer H: see above
Sal I	Buffer D: see above
Xba I	Buffer H: see above
Xho I	Buffer D: see above

2.1.1.7 Antibiotic solutions

Antibiotic	Stock concentration	Working concentration
Ampicillin	50 mg/ml in ddH_2O	50 µg/ml
Kanamycin	50 mg/ml in ddH_2O	50 µg/ml

2.1.1.8 Mammalian cell-culture reagents

COS-7 (African green monkey kidney cells) were supplied by the European Collection of Cell Cultures (Sailsbury, UK). Cells were maintained in Dulbecco's Modified Eagles Medium (DMEM) (Sigma) supplemented with 10% (w/v) Foetal Bovine Serum, 2mM L-glutamine, 100,000 units/ 500 ml penicillin and 100mg/ 500ml streptomycin (all from PAA). Trypsin EDTA was supplied by Sigma.

2.1.1.9 Radioligand binding

Coomassie Plus protein assay Reagent kit supplied by Pierce (Rockford, USA). [^{3}H] ivermectin (specific activity 1.44 TBq/mmol) was custom synthesised by Amersham International (Bucks., UK) and was a gift from Pfizer Animal Health (Sandwich, UK). Unlabelled IVM, HEPES, PEI, Triton-X and PMSF were all supplied by Sigma.

2.2 Basic Methods

2.2.1 Agarose gel electrophoresis

Agarose gels were made by the addition of 1% (w/v) agarose to 1x TAE or 1x TBE. The agarose was dissolved by heating for short (10-20 second) bursts in a microwave oven. Visualisation of DNA was enabled by the addition of 5 µg/ml ethidium bromide to the slightly cooled molten agarose. The gels were formed by pouring the molten agarose into gel rigs and allowed to set. Gels were run in a solution of 1x TAE or 1x TBE.
DNA samples were run after the addition of ~0.25 vol of 6x loading dye. DNA molecular weight ladders were also run for estimation of DNA fragment sizes.

2.2.2 Restriction endonuclease digestion of DNA

1-5 µg of DNA sample were digested with either 1 or 2 restriction enzymes using a two to tenfold excess of enzyme over DNA in the presence of acetylated BSA made up in the buffer recommended by the manufacturer for the particular enzyme(s) in use. Reactions were then incubated at the optimal temperature for the enzyme used (usually 37°C) for 1-4 hours.

Typical reaction.

Sterile deionized water	14.5 µl
RE Buffer 10x	2 µl
Acetylated BSA 1µg/µl	2 µl
DNA 1µg/µl	1 µl
Restriction enzyme 10u/µl	0.5 µl
Total	20 µl

2.2.3 Preparation of *E. coli* competent cells

A single colony of *E. coli* was taken and grown up in 100 ml of LB with shaking for ~ 3 hours or until it reached OD600. The broth was transferred to an ice-cold 5 ml polypropelene tube and cooled on ice for 10 minutes. The broth was centrifuged for 10 minutes at 2700 x g and 4°C after which the supernatant was discarded and the pellet resuspended in 30 ml ice cold 80 mM $MgCl_2$. 20mM $CaCl_2$. The resuspension was again centrifuged under the same conditions. The supernatant was discarded and the pellet resuspended in 4 ml of ice cold 3 M $CaCl_2$.

2.2.4 Transformation of *E. coli* cells

Competent cells (300 µL) were mixed with 5µg of plasmid cDNA in pre-chilled microfuge tubes and left to incubate on ice for 30-45 minutes. Cells were heat shocked at 42°C for 90 seconds followed by a further 2 minutes on ice. 800µL of LB was added and the cells allowed to recover at 37°C for 45 minutes. 200 µL of transformed competent cells was then added to LB- ampicillin plates or 5 ml of LB-ampicillin medium and incubated at 37°C overnight with shaking.

2.2.5 Small scale preparation of plasmid DNA

GenElute™ plasmid miniprep kit (Sigma- Aldrich) was used to isolate plasmid DNA from overnight bacterial cultures. 1.5 ml of bacterial broth are harvested via centrifugation at 12000 x g for 1 minute, the supernatant discarded and the pellet resuspended in 200 µl resuspension solution. This is then subjected to a modified alkaline-SDS lysis by addition of 200 µl of lysis buffer for 5 minutes. The lysis is halted by the addition of 350 µl neutralization buffer. The protein and bacterial debris are removed by centrifugation at 12000 x g for 10 minutes. The supernatant is added to a spin column and centrifuged at 12000 x g for 1 minute for the DNA to be

adsorbed onto silica in the presence of high salts. Contaminants are then removed by a simple wash step of 750 µl wash buffer and 12000 x g for 1 minute. Bound DNA is eluted in 100 µl water or Tris-EDTA buffer with a final centrifugation at 12000 x g for 1 minute.

2.2.6 Large scale preparation of plasmid DNA

GenElute™ HP Plasmid Maxiprep Kit (Sigma-Aldrich) was used to isolate a 100 ml overnight recombinant *E. coli* culture were harvested by centrifugation at 5000x g for 10 minutes, the supernatant discarded and the cells resuspended in 12 ml of resuspension solution using. The cells were then subjected to a modified alkaline-SDS lysis procedure by the addition of 12 ml lysis buffer for 5 minutes. The lysis was halted after addition of 12 ml of neutralization solution and 9 ml of binding solution. The lysate is cleared with a filter syringe. The columns were prepared for DNA biding by the addition of 12 ml column preparation solution and centrifuged at 3000 x g for 2 minutes. The eluate was discarded. The filtered solution was passed down the prepared centrifuge column and the DNA was bound to the silica-based membrane at 3000 x g for 2 minutes, the eluate was discarded and the centrifugation repeated. The remaining contaminants were removed by two wash steps; the wash solution was added to the column and centrifuged for 3000 x g for 2 minutes, the eluate is discarded, this is repeated with two different wash buffers. Finally, the bound DNA is eluted in 3 ml of buffer or water with a final centrifugation of 3000 x g for 5 minutes.

2.3 Site-directed mutagenesis of GluClα3B cDNA

2.3.1 DNA linearization and site directed mutagenesis

SNP's were introduced into the linear cDNA of *H. contortus* IV susceptible clones using oligonucleotide primers containing mutations for single amino acid substitutions.

Site directed Mutagenesis was carried out using Stratagene QuickChange mutagenesis kit (Stratagene, La Jolla, USA).

2.3.2 Primer design

The oligonucleotide primers were designed individually across the area of sequence to be altered with at least 12-15 bp of unchanged sequence either side of the target base(s). Both the forward and reverse primers contained the desired mutation, annealed to the same sequence on opposite strands of the plasmid and were between 25 and 45 bases in length, with a melting temperature (Tm) of ≥78°C.

2.3.3 Mutagenesis reaction

The mutation was introduced via a PCR reaction where the mutation was incorporated into the template with each amplification.

A typical reaction mixture contained

5 µl	10× reaction buffer*
10 ng	dsDNA template
125 ng	oligonucleotide primer #1
125 ng	oligonucleotide primer #2
1 µl	dNTP mix
H_2O	to a final volume of 50 µl

Then
1 µl of *PfuTurbo* DNA polymerase (2.5 U/µl)

The Reaction was put into the thermocycler with the following program

95°C	30 seconds	
95°C	30 seconds	16 cycles
55°C	1 minute	
68°C	1 minute/kb of plasmid length	

Following the temperature cycling the reactions were cooled to 37°C

2.3.4 Removal of parental dsDNA

Dpn I restriction enzyme (10 U/µl) was added directly to each amplification reaction and then immediately incubated at 37°C for 1 hour to digest the parental (i.e., the nonmutated) supercoiled dsDNA.

2.3.5 Transformation of mutated plasmid into supercompetent cells

XL1-Blue supercompetent cells were thawed on ice. For each control and sample reaction to be transformed, 50 µl of the supercompetent cells were aliquoted a prechilled 15-ml polypropylene round-bottom tube.
1 µl of the *Dpn* I-treated DNA from each control and sample reaction to was added to separate aliquots of the supercompetent cells. The transformation reactions were mixed gently and incubated on ice for 30 minutes. This was followed with a heat shock of 45 seconds in a 42°C water bath and then cooled on ice for 2 minutes. 0.5 ml of NZY+ broth prewarmed to 42°C was added and the transformation reactions were incubated at 37°C for 1 hour with shaking at 225–250 rpm. 250 µl of each transformation reaction was plated on large LB–ampicillin agar plates containing 80 µg/ml X-gal and 20 mM IPTG, and incubated overnight at 37°C.

A number of successfully transformed colonies were picked and grown overnight in LB- broth containing ampicillin. The plasmid was then extracted and tested for successful mutation by sequencing.

2.4 In vitro transcription of cRNA

2.4.1 DNA linearization

Stocks of pcDNA3.1 vectors containing the HcGluClα3b subunit were linearized using *Xba* I and incubated at 37°C for four hours. The linear DNA was checked on an agarose gel.

DNA was isolated using a phenol: chloroform extraction. The DNA was 5 μl reaction mixture was added to 205 μl nuclease-free H_2O and 300 μl Phenol: Chloroform: Isoamyl alcohol (for DNA, 25:24:1). The mixture was vortexed well and centrifuged at 5000 x g for 2 min at RT. The upper aqueous layer was retained and 1 vol (~ 300 μl) chloroform added, Vortexed and centrifuged at 5000 x g for 2 minutes. Again the upper layer was kept and 30 μl 3M sodium acetate pH 5.2 and 720 μl 100% ethanol added, mixed well, precipitated at –20°C overnight. The precipitated DNA was centrifuged at 4°C for 15min+ at 5000 x g. The supernatant removed ~200 μl 70% ethanol (4°C) added as a wash. The mixture was centrifuged at 4°C for 10min+. The pellet was resuspended in 10 μl DEPC or nuclease-free H_2O. Quality of DNA was checked by running on an agarose gel and measuring absorbance at 260/280 on a spectrophotometer.

2.4.2 RNA in vitro transcription

RNA in vitro transcription was carried out using the mMESSAGE mMACHINE kit, (Ambion).

The following reaction was assembled using RNase free pipette tips and tubes

3 μl nuclease-free H_2O

10 μl 2x NTP/CAP

2 μl 10x Reaction Buffer*

2 μg linear template DNA

2 μl enzyme mix†

* 10X Reaction Buffer contains 100mM KCl, 100mM $(NH_4)_2SO_4$, 200mM Tris-HCl (pH 8.8), 20mM $MgSO_4$, 1% Triton X-100 and 1mg/ml nuclease-free bovine serum albumin (BSA).

The reaction was incubated at 37°C for 2hrs for the transcription to occur 1 μl DNase (2 U/μl) was added and mixed well to destroy the linear template DNA. This was incubated at 37°C for a further 15 min. 115 μl Nuclease-free H_2O and 15 μl Ammonium Acetate Stop Solution (kit) was added to halt the DNase activity.

RNA was extracted with 1vol (150 μl) phenol: chloroform (5:1 nuclease-free). The upper aqueous layer was retained and further extracted with 1vol (150 μl) chloroform (nuclease-free). Again the top layer was retained. 1 vol isopropanol (nuclease-free) was added, mixed well and chilled at –20°C overnight. The RNA precipitate was centrifuged for 5000 x g at 4°C for 15min. The supernatant was removed and the remaining supernatant allowed to evaporate at RT.
The RNA was re-suspended in 10 μL nuclease-free H_2O and preferably used fresh to inject into oocytes. Alternatively the RNA was aliquoted into 5x 2 μL and stored at –80°C.

* 10X reaction buffer comes exclusively with Ambion mMESSAGE mMACHINE kit and is labelled as containing salts, buffer, dithiothreitol, and other ingredients.
† Enzyme mix comes exclusively with Ambion mMESSAGE mMACHINE kit and is labelled as containing 50% buffered glycerol containing RNA polymerase, RNase inhibitor and other components

2.4.3 RNA Reducing gel

RNA reducing gels were prepared by making up a 2% (w/v) agarose gel in a solution of 1x MOPS containing 20% formaldehyde (37% w/v).

To 2 μl of the RNA samples from the transcription reaction was added:

2 μl RNA (or 5 μl RNA ladder NEBL),
2 μl 10x MOPS
4 μl Formaldehyde

10 μl Formamide

1 μl Ethidium bromide (200 μg/ml)

The samples were prepared for running on RNA reducing gel by heating the sample mixture containing at 75°C for 10 min then adding loading buffer e.g. 3 μl 6x.
The gel tanks were washed with 3% H_2O_2 or RNase Away before use. The gels were run in 1x MOPS. Photo gel at ½ sec f5.6

2.5 Expression of cDNA in *Xenopus* oocytes for electrophysiology

2.5.1 Isolation of *Xenopus* oocytes

Ovarian tissue was isolated from mature female *Xenopus laevis* by a simple surgical procedure. The frogs were by euthanized by immersion in benzocaine solution 0.2 % w/v. The isolated ovarian lobes were placed in a 50 ml centrifuge tube containing OR-2 calcium-free buffer and washed three times in fresh buffer using a sterile glass Pasteur pipette on an aspirator. The lobes were then placed in a dish and dissected into smaller clumps of oocytes. These were rinsed several times in OR-2, and gently shaken in OR2 containing 4 mg/ml collagenase type 1A (Sigma) for 75 minutes at cool room temperature (20°C). The oocytes were rinsed thoroughly in OR2 before being placed incomplete ND96 buffer. The largest oocytes were manually selected and allowed to recover overnight in fresh ND-96 with gentle shaking at 18°C.

2.5.2 Injection of oocytes

50nL of cRNA (~1 ng) in RNAse-free water was injected cytoplasmically into each oocyte using a micro-injector on a micromanipulator. Injected oocytes were maintained at cool room temperature (20°C) in ND96 and electrophysiological recordings were performed at room temperature (22–25°C) 2–3 days after injection. The ND96 medium was changed daily

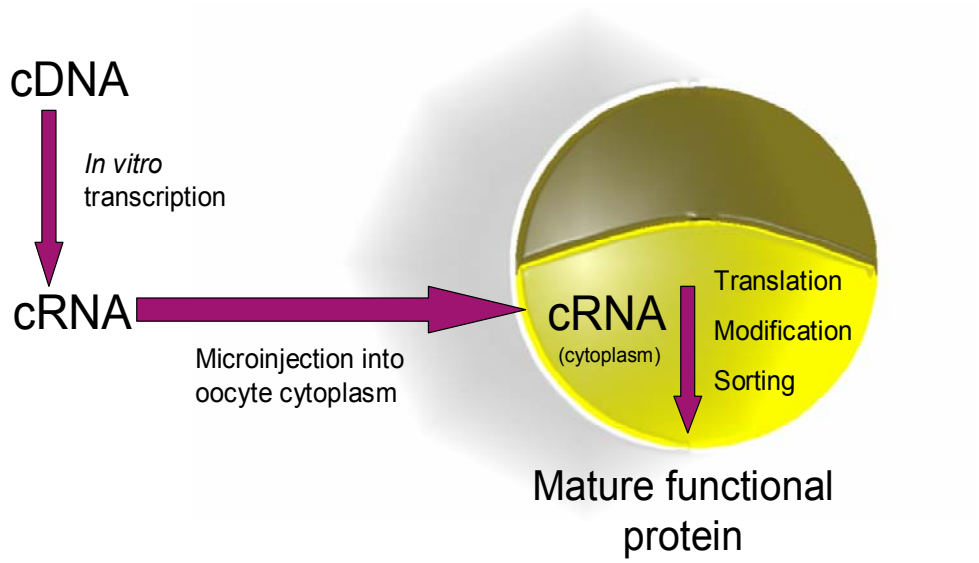

Figure 12: overview of the basic processes involved in the production of GluCl channels in *Xenopus* oocytes.

2.5.3 Electrophysiology

Whole-cell currents were recorded from oocytes using the two-electrode voltage-clamp technique. Oocytes were voltage-clamped at a holding potential of –80 mV and continually superfused with frog ringer. Recording microelectrodes were filled with 3 M potassium chloride, and had tip resistances of 0.5-5 MΩ. Oocytes were held in a 0.13 ml bath, and continually superfused with frog ringer at a rate of 0.8 ml/min. Drugs were applied by superfusion in the same way as the ringer at the same rate, the duration of the drug application was 10-20s. For the dose–response experiments, recordings were made sequentially from the lowest to the highest drug concentration, with an interval of 5 min between applications. Glutamate and ibotenate was dissolved in frog ringer. Ivermectin was prepared as 10 mM stock solutions in dimethyl sulfoxide (DMSO) and again diluted in frog ringer.

2.5.4 Electrophysiology data analysis

Data were analysed using Graphpad prism 4 (San Diego, USA). Non linear regression analysis was used to fit a sigmoidal dose-response curve of variable slope to normalised data using the following equation

.

$$I = I_{min} + (I_{max} - I_{min}) / 1+10^{[\log EC50-[ag]\ H]}$$

I_{max} and I_{min} represent the (percentage) maximal and inward current induced by the agonist. The EC_{50} is the concentration of agonist required to elicit half the maximum response, H is the Hill slope coefficient and [ag] is the agonist concentration.
The student's t-test was used to calculate the whether differences in the EC_{50} and Hill numbers was significantly different.

2.6 Expression of GluCl cDNA in mammalian cell lines for ligand binding

2.6.1 Maintenance of COS-7 primate kidney fibroblast cells.

Cells were grown in either 25cm^3 or 75 cm^3 flasks containing in an appropriate volume of supplemented DMEM. The flasks were incubated at 37°C with 5% CO_2 . The cells were split once they have reached ~ 90% confluence. The cells were washed with sterile PBS warmed to 37°C, 1-2 ml of trypsin/EDTA was added and cells incubated at 37°C until floating then trypsin activity was inactivated by adding 8-10 ml fresh pre warmed supplemented DMEM. Cells were split at a ratio 1:8 – 1:10 into new flasks containing supplemented DMEM. Using this method the cells reached confluence in 3-4 days.

2.6.2 Preparation of cells for storage in liquid nitrogen.

Cells were grown in a 75 cm^3 flask and, at approximately 80-85% confluence were washed with pre warmed PBS, and harvested using 1 ml trypsin/EDTA until floating

and then made up to 10 ml with supplemented DMEM. In a 15 ml sterile centrifuge tube the cells were centrifuged at 1500x g for 5 minutes and the supernatant discarded. The cells were resuspended in 1ml of freezing medium and transferred into cryotubes. The cells were cooled in the gaseous phase of liquid nitrogen for 24h before transfer to liquid nitrogen. Alternatively the cells were placed in a StrataCooler® Cryo preservation module (Stratagene) which was kept in a -80°C freezer overnight to cool the cells at a controlled rate. The cells were transferred to liquid nitrogen the following day.

2.6.3 Re-establishment of frozen COS-7 cells

Frozen aliquots of cells were removed from liquid nitrogen and quickly thawed in a 37°C water bath and added to a 75 cm^3 flask containing pre warmed supplemented DMEM. Once the cells had established and adhered to the flask surface, the Supplemented DMEM was replaced to get rid of any residual DMSO from the freezing medium.

2.6.4 Transfection of COS-7 cells

Lipofectamine™ 2000 was used to transiently transfect COS7 cells. Most transfections were carried out in 10 cm^3 tissue culture dishes or on coverslips in 6 well plates.

Complexes were prepared using a DNA (µg) to Lipofectamine™ 2000 (µl) ratio of 1:2 to 1:3 for most cell lines.
One day before transfection, dishes were seeded in 12 ml of DMEM supplemented with L-glutamine but in the absence of antibiotics so that cells will be 90-95% confluent at the time of transfection.
Plasmid DNA was diluted in 50 µl of Opti-MEM® I Reduced Serum Medium without antibiotics. In another non-polypropelene tube Lipofectamine™ 2000 was mixed gently with 50 µl of Opti-MEM® I Medium. This was incubated for 5 minutes at room temperature. After which the DNA and Lipofectamine™ were combined, mixed gently and incubated for 20 minutes at room temperature to allow forming

complexes. 100 µl of the complexes were then added to each well containing cells and medium and mixed gently by rocking the plate back and forth. Medium was changed after 4-6 hours.
Cells were incubated at 37°C in an incubator with 5 % CO_2 for 18-48 hours prior to testing for transgene expression or harvesting membrane protein.

2.6.5 Preparation of membranes from cultured cells

Transiently transfected COS-7 cells were harvested after 48hours in a 100cm^3 cell culture plate, at this point the cell were usually between 85-90% confluent.
Control cells were also harvested at ~85% confluence .The culture medium was removed by aspiration from the plate and the cells washed three times with room temperature 50 mM HEPES with 0.01% (w/v) sodium azide (pH 7.4). Cells were harvested with a cell scraper in 5 ml of the 50 mM HEPES with 0.01% (w/v) sodium azide and placed in a 15 ml universal centrifuge tube. The cells were further disrupted by sonication in 3x 10 second bursts on medium power.
The medium was made up to 10 ml with more 50mM HEPES with 0.01% sodium azide and added to a 10 ml ultracentrifuge tube. The cells were centrifuged at 28,000 rpm (75,000g) for 30 minutes at 4°C. The supernatant was discarded and the cells resuspended in 1 ml 50 mM HEPES with 0.01% (w/v) sodium azide and 0.2 mM PMSF.

2.6.6 Measuring protein concentration

The protein was concentration was measured using the Coomassie plus protein assay reagent kit (Pierce, Rockford, USA)
Prior to the first use a standard curve was established using known concentrations of protein (bovine serum albumin) supplied with the kit.
5 µl of each standard or unknown sample was added into the appropriate microplate wells. 250 µl of the Coomassie Reagent was added to each well and mixed with

plate shaker for 30 seconds. Plates were incubated for 10 minutes at room temperature (RT). The absorbance was measured at or near 595 nm with a plate reader. The average 595 nm measurements for the Blank replicates were subtracted from the 595 nm measurements of all other individual standard and unknown sample replicates. A standard curve was prepared by plotting the average Blank-corrected 595 nm measurement for each BSA standard vs. its concentration in µg/ml. The standard curve was used to determine the protein concentration of each unknown sample.

10 µl of membrane preparation or 10 µl of blank solution was added to 300 µl of Coomassie reagent and mixed on a shaker, incubated for 10 minutes at room temperature and then the absorbance was measured at 595 nm with a plate reader. The average 595 nm measurement for the Blank replicates was subtracted from the 595 nm measurements of all sample replicates and the protein concentration calculated by reading the absorbance vs. protein concentration of the standard curve.

2.6.7 Binding of [^{3}H]-ivermectin to membrane preparations

[3H]-ivermectin binding studies were carried out in 5ml polypropylene tubes. Membrane preparations were incubated with [^{3}H]-ivermectin in 50 mM HEPES (pH 7.4) with 5-40 µg protein (10 µg standard). Non specific binding was determined by binding in the presence of 10 µM of unlabeled (cold) ivermectin, the final assay volume was made up to 1 ml with 50 mM HEPES. The reactions were incubated at room temperature for 2 hours. The binding reaction was terminated by dilution with 3ml cold wash buffer of HEPES with 0.01% (w/v) sodium azide and 0.25% (v/v) Triton X-100. The halted reactions were filtered through type A/B glass fibre filters (Whatman, Kent, UK) which had been pre-soaked in 3% (v/v) Polyethyleneimine (PEI) in wash buffer. The filters were rinsed 3 times in wash buffer and placed in individual mini vials to which 5 ml of Optiphase Safe was added (Wallac, Bucks, UK). Bound radioactivity was determined by liquid scintillant spectrometry.

2.6.8 Radioligand binding data analysis

Data were analysed using Graphpad prism 4 (San Diego, USA). Non linear regression analysis was used to determine the disassociation constant for the equilibrium binding of the radiolabel ligand (K_d) fitted to a single-site binding model. Data were fitted to the equation

$$Y= (Bmax)[[3H] ligand])/ Kd + ([3H] ligand)$$

The student's t-test was used to calculate the whether differences in the K_d was significantly different.

2.7 Homology modeling

2.7.1 Template search and selection

A BLAST search (Altschul et al. 1997) through NCBI was used to identify homologous structures by searching the structural database of protein sequences in the protein data bank (PDB) (Berman et al. 2000). The program modeller 9v2 was also used in a parallel study to find the best template. This program searches for potentially related sequences of known structure and is performed by the profile.build() command of MODELLER. This command initializes the ‘environment’ for the modeling run, by creating a new ‘environ’ object then creates a new ‘sequence_db’ object, calling it ‘sdb’? 'sequence_db' objects are used to contain large databases of protein sequences. The program then reads a text format file containing non-redundant PDB sequences at 95% sequence identity into the sdb database. Sequences which have fewer than 30 or more than 4000 residues are discarded, and non-standard residues are removed. A binary machine-specific file is written and creates a new 'alignment' object, calling it 'aln'. Profiles contain similar information to alignments, but are more compact and better for sequence database searching. Searches the sequence database 'sdb' for our query profile 'prf'. Matches from the sequence database are added to the profile. Modeller then writes a profile of the query sequence and its homologs. The equivalent information is also written out in standard alignment format.

Two searches were compared and the best match decided. The crystal structure of the acetyl binding protein from *Lymnea stagnalis* (PDB code: 1I9BA) was selected as a template for the homology modeling for the GluClα3B subunit.

2.7.2 Sequence – template alignment

The amino acid sequences of GluClα3B and 1I9B were aligned using align2d() command in MODELLER, which aligns multiple sequences using a pairwise progressive alignment algorithm. The alignments were checked for any deletions or insertions in the structurally conserved and structurally variable regions between the template and target sequences.

2.7.3 Model generation

Homology models of *wt* and Mutant Gluclα3B were constructed using Modeller 9v2 (default parameters), based upon the individual sequence/template alignments. Modeller is a comparative modelling methodology which automatically generates a 3D homology model of a protein sequence based on a given sequence alignment to a known 3D protein structure (Sali et al. 1993). Modeller was downloaded from http://salilab.org/modeller/download_installation.html. Modeller was installed and used to model 3D structure of protein by satisfaction of spatial restraints on the structure of the amino acid sequence. The restraints operate on the distances, angles, dihedral angles and pairs of dihedral angles and other spatial features defined by atoms. Modeller automatically derives the restraints only from known related structures and their alignment with the target sequence. The output is a 3D structure that satisfies these restraints as well as possible (Sali et al. 1993)
All structures and models were visualised using the protein explorer 2.80 (file:///C:/Program%20Files/Protein_Explorer_2.80/protexpl/frntdoor.htm).

2.7.4 Model Assessment

The stereochemical, volume and surface properties of the models were evaluated using modeller and procheck (Laskowski et al. 1993) which can be accessed from www.bichem.ucl.ac.uk/~roman/procheck/procheck.html.

Chapter 3: Characterising the Molecular Pharmacology of the *H. contortus* GluClα3B Subunit.

3.1 Introduction

Previous work carried out in the laboratory isolated five partial cDNAs from *H. contortus* by reverse transcription-polymerase chain reaction (RT-PCR) amplified from primers matching highly conserved areas of ligand gated chloride channels (Laughton 1993). Two of the cDNAs were first identified as HG2 and HG3 which are actually splice variants of the same gene *Hcavr-14* later renamed GluClα3A and GluClα3B. It was demonstrated by rapid amplification of cDNA ends (RACE) PCR that the *avr-14* gene was present in *H. contortus* eggs (Jagannathan 1998) and that the pattern of alternative splicing first identified in the *C. elegans avr-14* gene (Laughton et al. 1997) was conserved in *H. contortus.* Similar splice variants of the same gene have been found in other species such as *Haemonchus placei* and *D. immitis* (Jagannathan et al. 1999; Cheeseman et al. 2001; Yates et al. 2004) although not in other species such as *C. oncophora, A. suum, or Onchocerca volvulus* (Cully et al. 1996; Njue et al. 2004; Njue et al. 2004). Of the splice variants GluClα3A appears was found not to form functional channels when expressed in *Xenopus* oocytes and did not bind to ivermectin when expressed in mammialian cells (Cheeseman et al. 2001). The GluClα3B subunit does bind ivermectin with high affinity (Cheeseman et al. 2001) and produce functional homomeric channels when expressed in *Xenopus* oocytes (Rogers unpublished) which were activated by glutamate and irreversibly opened with IVM. GluClα3B has also been implicated in IVM resistance in *C. oncophora* (Njue et al. 2004), indicating that this subunit was an important target for IVM and possibly a site of interest in the development of anthelmintic resistance, and as a result the decision was made to characterise the pharmacology of the subunit more fully. Some preliminary work had already been carried out using electrophysiology by Adrian Rogers, a former worker in the lab, he had first expressed the GluClα3B subunit in *Xenopus* oocytes and ascertained that the channel was sensitive to Glutamate and irreversibly opened with IVM, that the irreversibly opened channel could be blocked with picrotoxin, however further work was required to quantify these data.

Full length clones of the GluClα3B subunit were translated into mRNA and injected into *Xenopus* oocytes where the subunits were transcribed and assembled into functional subunits on which electrophysiological experiments could be carried out. The GluClα3B cDNA was also transfected into COS-7 cells and the resultant expressed protein collected and used for ligand binding studies using [^{3}H]-IVM.

3.2 Results

3.2.1 Action of glutamate on oocytes injected with GluClα3B cDNA

Full length cDNA encoding the GluClα3B subunit was transcribed by *in vitro* transcription to produce cRNAs that were expressed in *Xenopus* oocytes. It was found that injection of 1 ng cRNA injected was sufficient to produce a robust and reliable electrophysiological response up to ~5000nA (The cRNA was produced and stored in 2 µl aliquots in thin walled 200 µl PCR tubes at -80°C for no more than two months). Recordings were made between 48 hours and 5 days post injection. At a holding potential of -80 mV, L-glutamate elicited robust inward currents in all oocytes successfully expressing the GluClα3B subunits. The responses were dose dependent with increasing inward currents corresponding to increasing concentrations of glutamate and were extremely rapid in onset and reversible (see Figure 13) creating a dose response curve generating an EC_{50} value of 27.6 ± 2.7 µM. The maximal response for glutamate in IVS GluClα3B channels is at 300 µM with 100 µM giving a 95% maximal response. The Hill coefficient of the homomer to glutamate is 1.89 ± 0.35 clearly suggesting that more than one molecule of glutamate is required to gate the channel. Control oocytes that were either un-injected or injected with 50 nl ddH_20 failed to elicit any response to glutamate at concentrations of 0.1, 1, 10 and 100 mM.

A

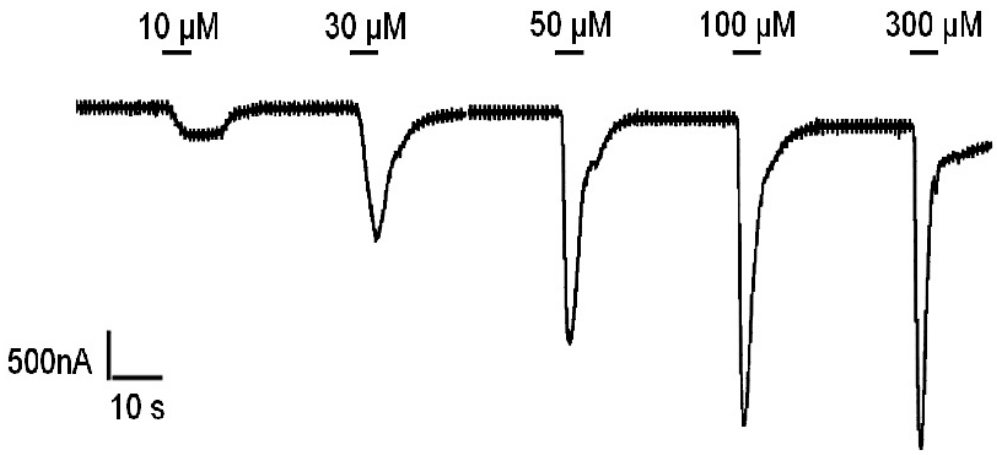

B

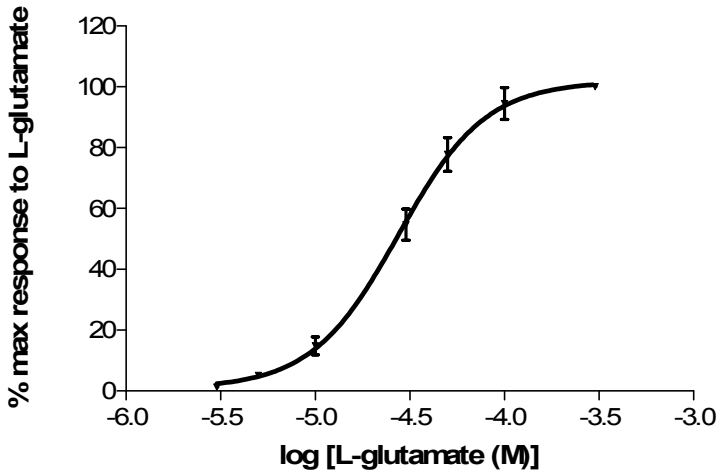

Figure 13: Activation of GluClα3B homomeric channels by glutamate.

A) Representative current traces from oocytes when activated with glutamate at the concentration shown above each trace. Horizontal bars relate to the duration of the glutamate application.

B) Glutamate dose-response curve for oocytes injected with *H. contortus* GluClα3B cRNA. Data were normalised to the maximum glutamate responses seen with each oocyte, and are shown as the standard error of the mean of seven oocytes (taken from four individual frogs)

3.2.2 Action of ibotenate on oocytes injected with GluClα3B cDNA

Ibotenate elicited a visually similar electrophysiological response to glutamate (Figure 14). Ibotenate is a structural analogue of glutamate known to open GluCls (Lea et al. 1973; Arena et al. 1992; Cully et al. 1994) On addition to the GluClα3B channel it elicited a response, with kinetics similar to those shown by glutamate. The EC_{50} for glutamate is 27.6 ± 2.7 μM and for ibotenate 87.7 ± 3.5 μM. At 300 μM glutamate shows a maximal response (100%) with ibotenate eliciting a response 69 ± 5.2 % of the maximum See (Figure 14). The Hill coefficient of the homomer to glutamate is 1.89 ± 0.35 indicating cooperativity, this is a trend that is followed with ibotenate that has a Hill number of 1.70 ± 0.36, which, although lower than glutamate is still indicative of a level of cooperativity. These data suggest that it is a partial agonist at GluCl α3B receptors.

A)

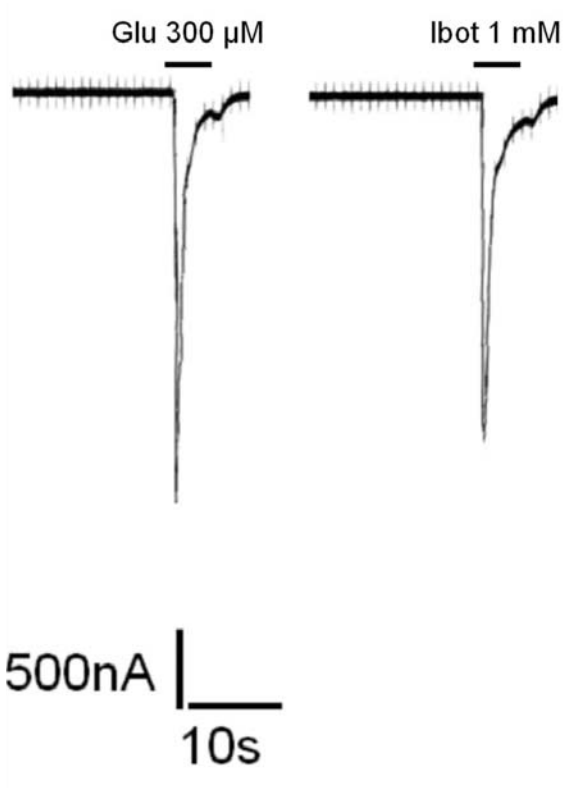

B)

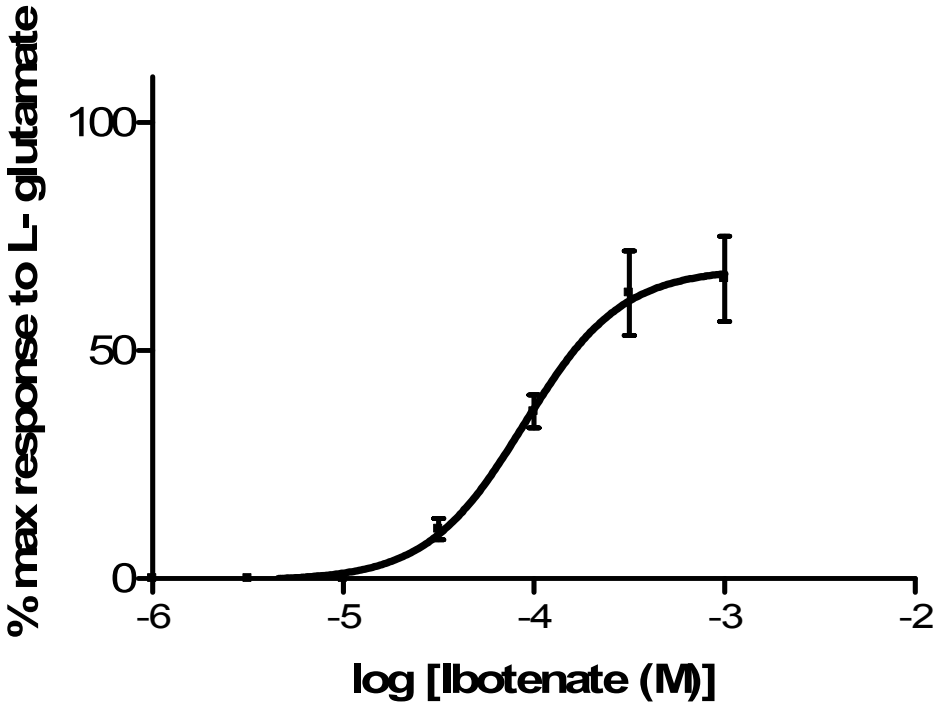

Figure 14: Typical electrophysiological response of GluClα3B homomeric channel to ibotenate.

A) Representative current traces from oocytes when activated with glutamate and ibotenate at the concentration shown above each trace. Horizontal bars relate to the duration of agonist application.

B) Ibotenate dose-response curve for oocytes injected with *H. contortus* GluClα3B cRNA. Data were normalised to the maximum glutamate responses seen with each oocyte, and are shown as the standard error of the mean of six oocytes (taken from three individual frogs)

3.2.3 Action of IVM on oocytes injected with GluClα3B cDNA

The effects of IVM were also tested on the homomeric channel. Unlike the glutamate and ibotenate response the effect of IVM was a slow and irreversible activation. The current did not return to the baseline even after periods of prolonged washing (>15 minutes) with drug-free ND96 buffer. Application of 300 μM glutamate after addition of maximal response to IVM did not elicit any additional response. No response to IVM was observed in either group of control oocytes, one group being un-injected the other being injected with 50 nl sterile water. It was observed that IVM would elicit a maximal response, even with the addition of low concentrations, and addition of higher concentrations of IVM affected the speed of activation rather than the magnitude, with even picomolar concentrations activating a current higher than the maximal response to glutamate. This made the production of the IVM standard curve laborious and difficult and results in large standard errors. Despite the practical difficulties data suggest an EC_{50} of 0.14 ± 1.01 nM for IVM in oocytes expressing the GluClα3B channels.

2A)

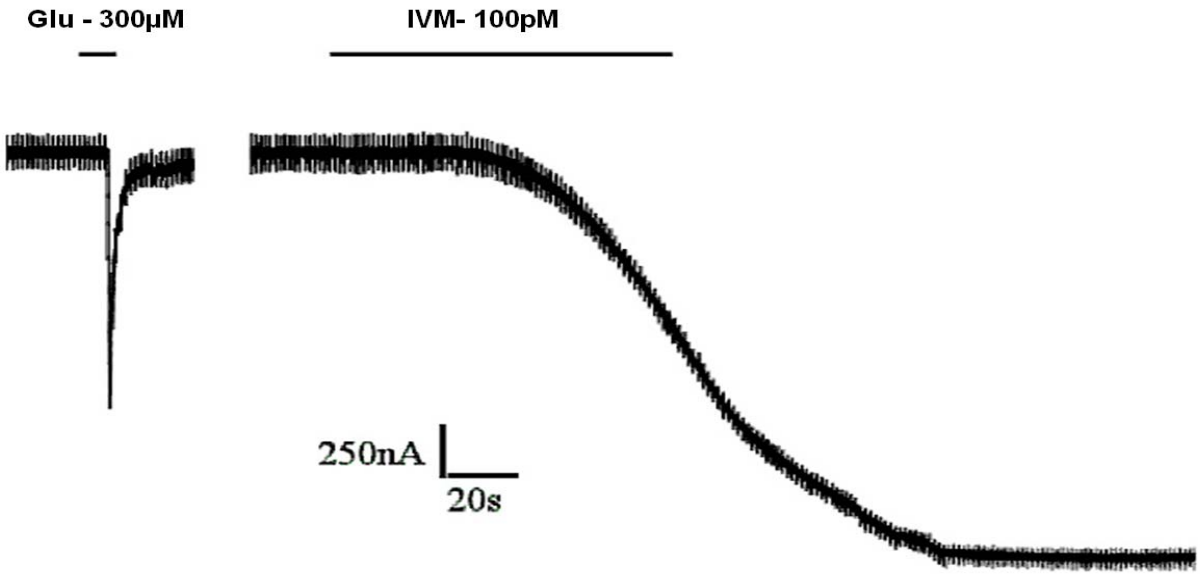

B)

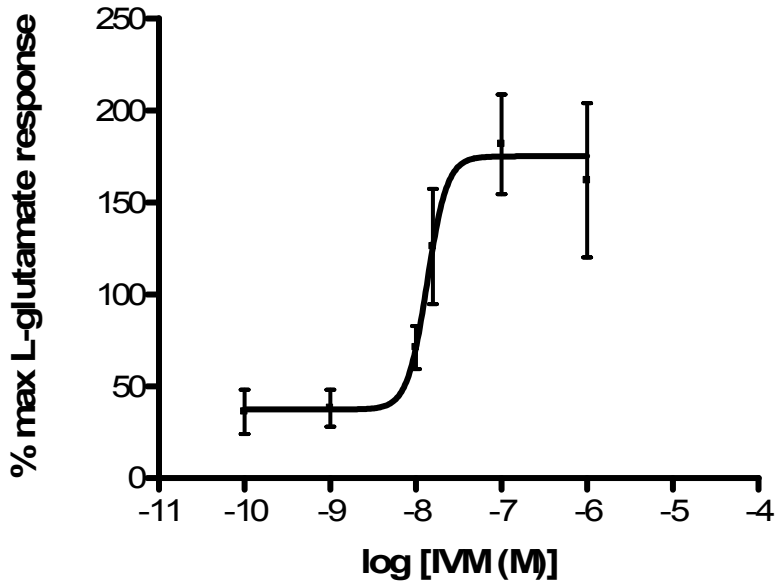

Figure 15: Activation of GluClα3B homomers by ivermectin (IVM),

A) Representative current traces from oocytes when activated with glutamate and IVM at the concentration shown above each trace. Horizontal bars relate to the duration of the glutamate application.

B) IVM dose-response curve for oocytes injected with *H. contortus* GluClα3B cRNA. Data were normalised to the maximum glutamate responses seen with each oocyte, and are shown as the standard error of the mean of nine oocytes (taken from six individual frogs).

3.2.4 Action of PTX and fipronil on oocytes injected with GluClα3B cDNA

Work carried out by Adrian Rogers in the Wolstenholme lab investigated the effect of common agonists picrotoxin (PTX) and fipronil. Fipronil was shown to partially but irreversibly block glutamate. The channels remained blocked after prolonged periods of washing (see Figure 16). PTX was shown to completely block GluClα3B channels with an approximate IC_{50} of 40 μM (Rogers 2004-unpublished), but the effect is fully reversible after washing. In addition PTX acts to partially reverse the effects of IVM (see Figure 17).

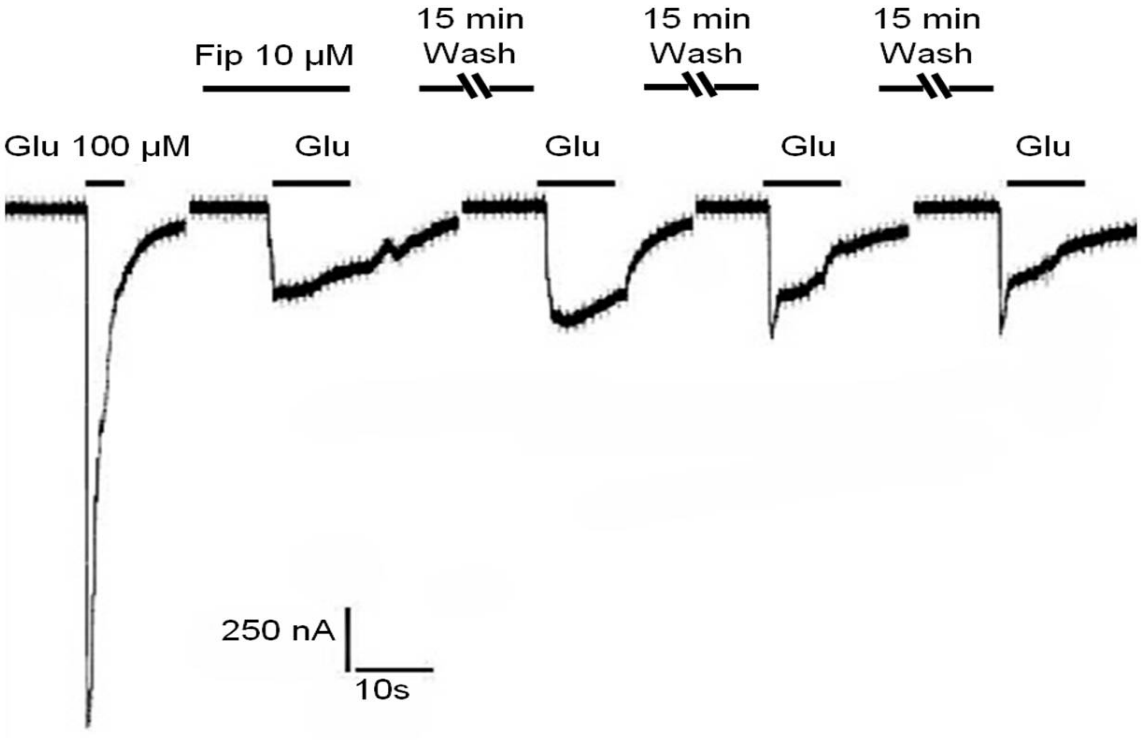

Figure 16: Fipronil partially blocks GluClα3B channels irreversibly
Figure shows a typical Glutamate reaction which is blocked on application with fipronil. Normal glutamate action is not recovered even with prolonged washing. (Rogers 2004-unpublished)

A

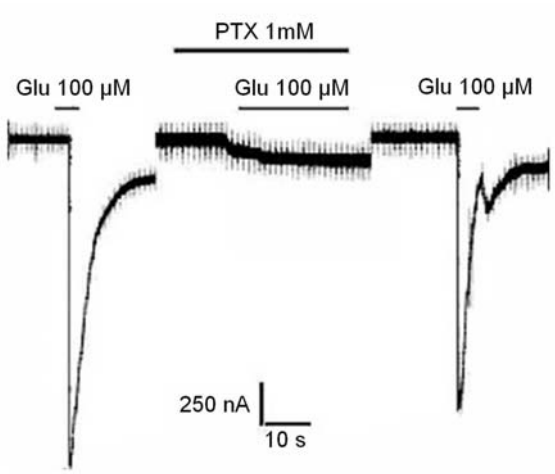

B

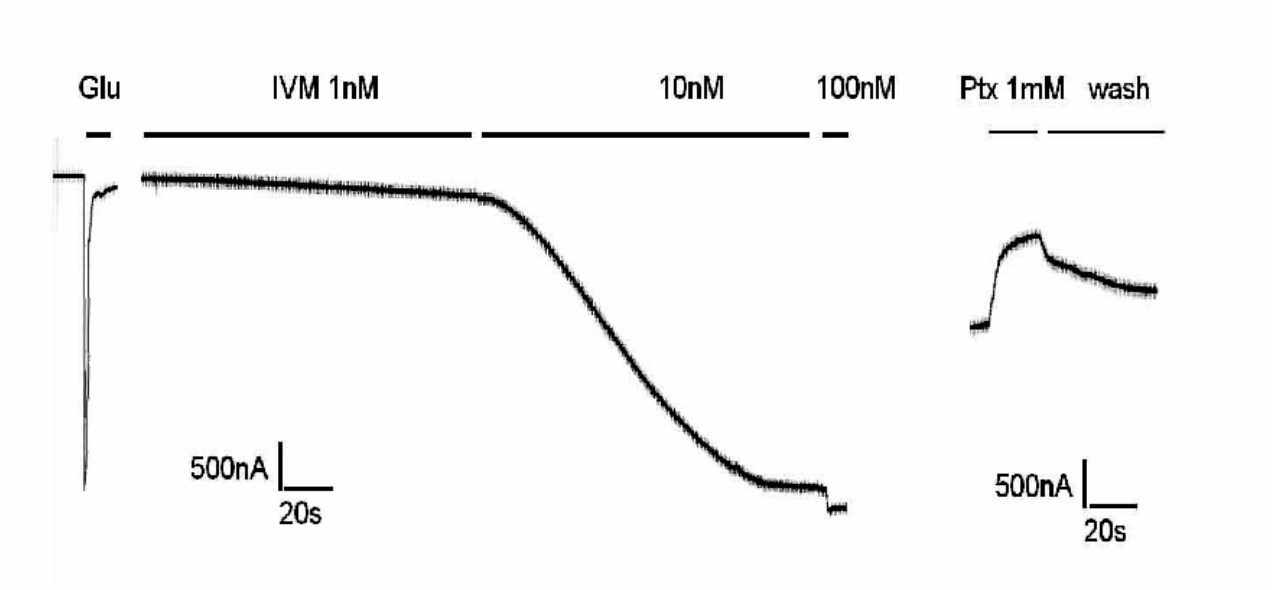

Figure 17: Picrotoxin blocks homomeric GluClα3B channels reversibly
A. Responses to Glutamate, before during and after application with PTX
B. Typical relative responses of GluCl α3B to ivermectin. There is incomplete reversal of ivermectin with PTX. (Rogers 2004- unpublished)

3.2.5 Action of [3H]-IVM binding on membrane preparations expressing GluClα3B subunits.

Due to the difficult nature of quantifying IVM standard curves using electrophysiology, investigation into the effects of IVM binding on GluClα3B subunits with candidate SNPs was carried out using [^{3}H]-Ivermectin. Previous experiments have shown that GluClα3B binds [^{3}H]-IVM with high affinity at a K_d of 70 ± 19 pM in COS-7 membrane preparations transiently transfected with the GluClα3B (Cheeseman et al. 2001). COS-7 cells were transiently transfected with GluClα3B cDNA and membrane preparations taken. Initially binding was determined by incubating increasing concentrations of membrane protein 1 µg-50 µg with 0.5 nM [^{3}H]-IVM for two hours at 18-22°C. Specific binding appeared to increase in a linear fashion with increasing concentration. A concentration of 10 µg protein was decided upon for all further experiments because it is a high enough concentration to show high levels of specific binding. Non specific binding was determined by incubation the presence of unlabelled IVM. No specific binding was seen when the [^{3}H]-IVM was incubated with either non-transfected COS-7 membrane preparations, or membrane preps transfected with empty pcDNA3.1 vector.

3.2.6 Saturation analysis of [^{3}H]-IVM binding to GluClα3B

Specific high affinity [^{3}H]-IVM binding was observed to membranes from GluClα3B transfected cells. Initial experiments were carried out measure the level of total, specific and non specific binding of [^{3}H]-IVM to 10µg of total protein taken from GluClα3B transfected COS-7 cells (Figure 18). Non- specific binding accounted for approximately 35-40% of the total binding.

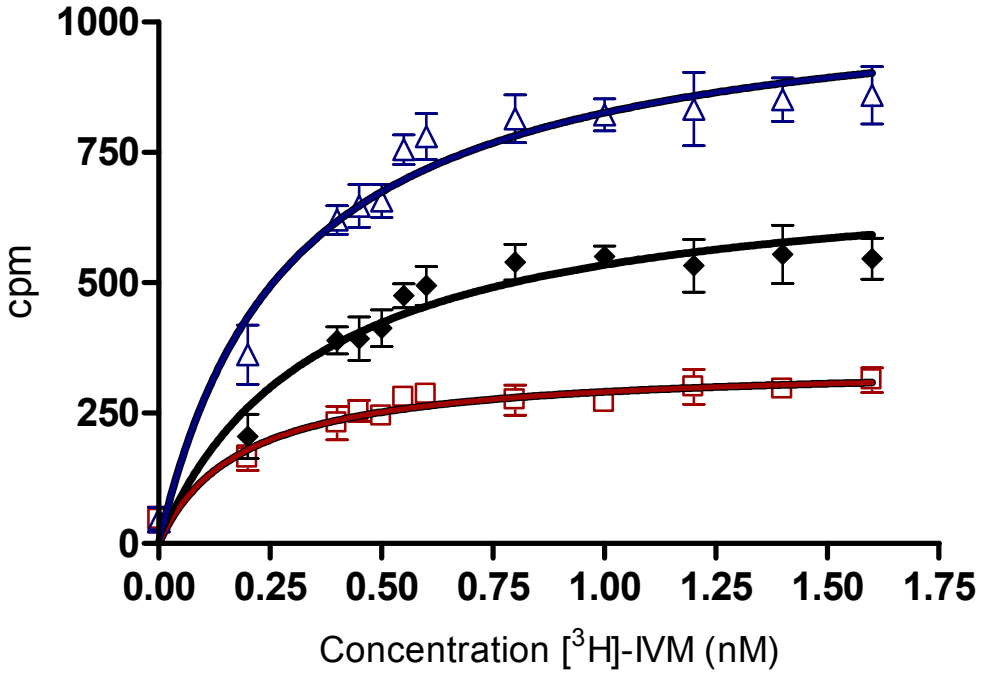

Figure 18. Raw saturation data of 10 µg COS-7 membrane preparations transiently expressing IVS *wt* GluClα3B with [^{3}H]-IVM.
10 µg of membrane protein was incubated with various concentrations of [^{3}H]-IVM for 2 hours at room temperature. Non specific binding was determined in the presence of 10µM unlabelled IVM
The blue curve respresents total [^{3}H]-IVM binding, the red line shows non-specfic [^{3}H]-IVM binding and the specific binding is illustrated with the black line.

The raw specific binding data was analysed and the specific [^{3}H]-IVM binding in fmol/mg was calculated. The [^{3}H]-IVM binding reached saturation with a B_{max} value of 0.83 ± 0.06 pmol/ mg and k_d of 0.35 ± 0.10 nM. Variation in B_{max} between transfection reactions was not significant. Each reaction was repeated eight times using membrane preparations from five different transfection reactions.

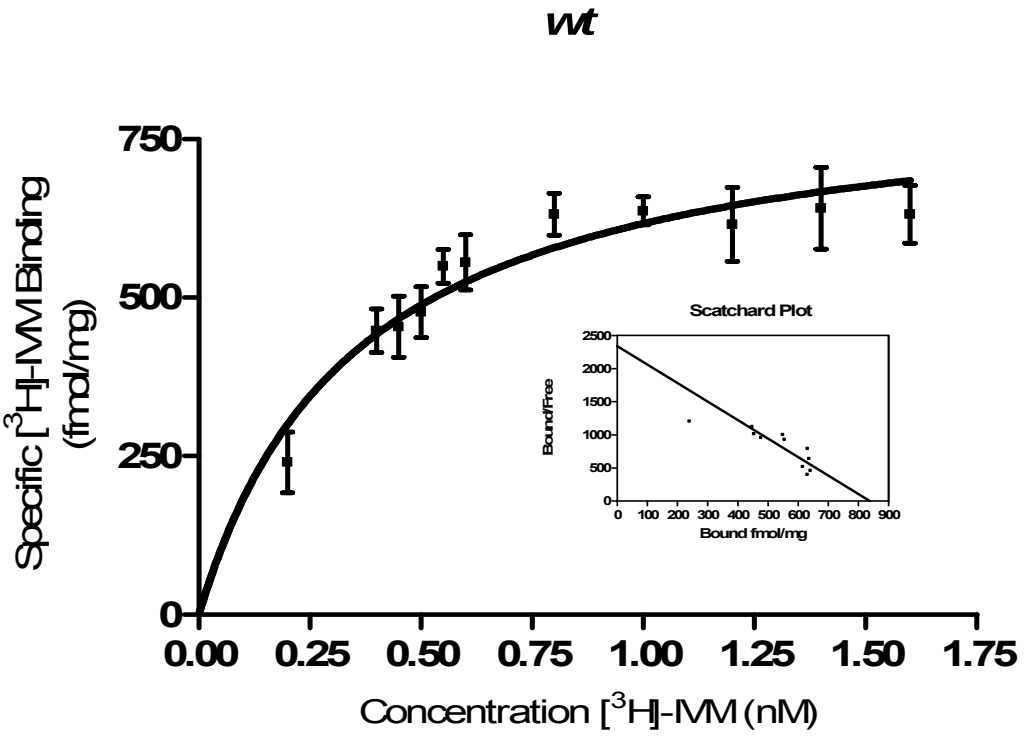

Figure 19: Saturation of COS-7 membrane preparations transiently expressing IVS *wt* GluClα3B with [^{3}H]-IVM. Inset is the Scatchard plot.
10 µg of membrane protein was incubated with various concentrations of [^{3}H]-IVM for 2 hours at room temperature. Non specific binding was determined in the presence of 10 µM unlabelled IVM

3.3 Discussion

It has been known for several years that GluClα3B subunits form homomeric channels when expressed in *Xenopus* oocytes, the channels are gated by both glutamate and ibotenate in a reversible manner and by ivermectin (IVM) which opens the channel irreversibly (Cheeseman et al. 2001). Picrotoxin is a nonselective blocker of GABA that is known to block *C. elegans* GluClβ and CluClα (Etter et al. 1999) so it is unsurprising that it has a similar effect in *H. contortus.* Fipronil is an insecticide that also acts on GABA receptors and other closely related channels such as the GluCls (Horoszok et al. 2001).

The *H. contortus* data is comparable *C. elegans* data published by Yates et al in 2003 shows *C. elegans* GluClα3B has a EC_{50} 2.23 ± 1.2 mM and a Hill coefficient of 0.72 ± 0.08 in direct comparison to the *H. contortus* values of 27.6 ± 2.7 μM and Hill value of 1.89 ± 0.35. Evidently the *H. contortus* subunit is far more sensitive to glutamate and also displays a level of cooperativity not seen in *C. elegans*. Data from the *C. oncophora* GluClα3 subunit was also published in 2004 and showed an EC_{50} to glutamate of 13.4 ± 2.5 μM and a Hill coefficient of 1.9 ± 0.28 (Njue et al. 2004), these are similar in magnitude to the *H. contortus* values. It could be argued that the channel sensitivity to glutamate may be parasite specific, although with data available from such a limited number of parasite species it is still unclear.

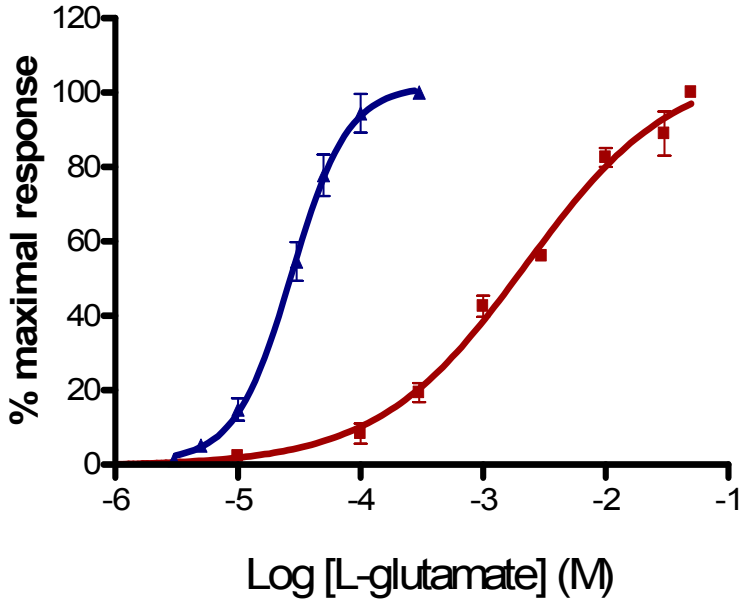

Figure 20: Comparison Glutamate dose-response curve for oocytes injected with of *H. contortus* (blue) and *C. elegans* (red) GluClα3B cRNA.
C. elegans data taken from (Yates et al. 2003)

Species	EC_{50} Glutamate	Reference
H. contortus	28 µM	-
C. elegans	2.2 mM	(Yates et al. 2003)
D. immitis	~ 1 mM	(Yates et al. 2004)
C. oncophora	30 µM	(Njue et al. 2004)

Table 4: Summary of GluClα3B subunit sensitivities to glutamate

The saturation curve for ivermectin shows a K_D of 0.35 ± 0.10 nM, which is a factor of 10 higher than the previous experimentally derived value of 70 ± 6 pM (Cheeseman et al. 2001). This may be due relative transformation efficiency of the COS-7 cells; both experiments were carried out on 10 µg of transfected membrane preparation that contains GluClα3B protein as well as endogenous COS-7 membrane protein. Higher transformation efficiency would result in proportionally

more GluClα3B protein, resulting in more ligand binding per µg protein. In both sets of experiments COS-7 cells were used. The batch of cells used in the experiments described here were new with fewer than 20 passages, the age of the cells in previous experiments is unknown. It is known that the sequence of the GluClα3B cDNA was identical in both sets of experiments (excluding introduced mutations) and the same pcDNA 3.1 vector was used, ruling out loss of IVM affinity due to unnoticed mutations in the sequence. It is also possible that small changes in the activity of the radioactive ligand could play a part. that different preparations of [^{3}H]-IVM were used. Differences in the relative activity of different batches of the same radioactive ligand have been repeatedly observed over the years and considered a pitfall in an otherwise excellent technique (Keen 1995). The batches of [^{3}H]-IVM used in both my experiment and in the previous experiments were made by different companies, thus opening up the possibility of numerous differences in manufacture that could explain the differences in K_D. In addition to the manufacturing process, minor changes in experimental procedure and simply calculation error could play their part, including differences in the efficiency of different scintillation counters. The fact that in both cases the SEM is well within an acceptable range indicates that both data sets are essentially correct and comparable to other data sets carried out with the same reagents under the same conditions, this is further supported by the subsequent experiments discussed in the next chapter using mutated versions of the GluClα3B subunit.

Comparison of the inward current elicited by the agonists of the GluCl show marked differences. The maximal inward current is produced by concentrations of glutamate of over 300 µM, but the inward current elicited by the irreversible agonist IVM is on average ~ 170% of the maximal glutamate current. Therefore it could be argued that glutamate is only a partial agonist of the homomeric GluClα3B channel and the channel only requires a partial opening to be effective. Alternatively glutamate is capable of fully opening all channels desensitising is occurring so fast that the electrophysiology equipment in incapable of recording the full extent chloride influx. Another question raised is whether glutamate is therefore required to be present before IVM irreversibly opens the channel. Experimentally, when IVM was applied to the oocytes it was only done on the oocytes that had shown positive responses to glutamate, therefore had previous exposure to it. This was done because it was the

only way of telling whether successful production of channels had occurred. The oocytes were then washed for 5-10 minutes with frog ringer before application with IVM. However we cannot be certain that this was sufficient to wash all the glutamate away. One possible mode of action for IVM is the agonist activates the channel and then holds it open allowing the influx of chloride ions, another theory might suggest that the presence of an agonist at the traditional binding site is required and that IVM in its hydrophobic nature is able to gain access to a position between the helices of the transmembrane region and “wedge” open the channel. From the data presented here it is impossible to say from these experiments whether either is the case.

In order to further characterise the interaction between agonists and the GluClα3B subunit, mutations were introduced into the subunit and electrophysiology and ligand binding studies undertaken to see whether they elicit a change in subunit activity.

Chapter 4: Analysis of the effect of Single Amino Acid substitutions have on *H. contortus* GluClα3B pharmacology

4.1 Introduction

It is suggested that polymorphisms in the GluCl subunits can confer resistance to parasitic nematodes. A Canadian group cloned two full-length glutamate-gated chloride channel (GluCl) cDNAs, encoding GluClα3 from *Cooperia oncophora*, the subunit which is homologous to the *C. elegans* and *H. contortus* GluClα3B channel subunit, from ivermectin-susceptible (IVS) and -resistant (IVR) *C. oncophora* adult worms. The IVS and IVR GluClα3B subunits differed at three amino acid positions, E114G V235A and L256F. All of these SNPs were located in the N terminal domain of the *C. oncophora* GluClα3 subunit, the ligand binding site area, although it is important to note the actual ivermectin/ moxidectin binding sites are still unknown (Njue et al. 2004), but are thought to be in the transmembrane regions due to the hydrophobic nature of the macrocyclic lactone drugs.

The subunits carrying the candidate SNPs were cloned and expressed in *Xenopus laevis* oocytes. Electrophysiological whole-cell voltage-clamp recordings showed that the L256F mutation in the GluClα3 was the only one that caused a small but significant threefold loss of sensitivity to glutamate from an EC_{50} of 29.7± 4 μM to 100.6 ± 0.21 μM. The efficacy of the macrocyclic lactones ivermectin and moxidectin were also significantly reduced with this mutation with the EC_{50} increasing from 0.5 ± 0.12 in IVS worms to 1.2 ± 0.11 μM in channels carrying the L256F mutation. It is also important to note that the GluClα3 channels from the Ivermectin resistant population had EC_{50} comparable to those carrying the L256F mutation, 96.1 ± 4.4 μM for glutamate and 1.3 ± 0.11 μM for ivermectin/moxidectin (IVR) (Njue et al. 2004). Whether this mutation alone is enough to confer resistance of the nematodes to the macrocyclic lactones is unclear.

Surprisingly few studies have actually examined the molecular nature of macrocyclic lactone action in organisms such as parasitic nematodes (Cheeseman et al. 2001; Forrester et al. 2002) for which these drugs have important economic implications. Therefore, our current research has focused on examining the relationship between IVM and potential parasite targets such as the GluCl.

The initial objective of this project was to elucidate pharmacological data on the *H. contortus* GluClα3B subunit using site directed mutagenesis to create single point mutations in the cDNA that had been found in populations of IVM-resistant parasitic nematodes of two species *C. oncophora* and *H. contortus*, and to see if the mutations conferred a change in affinity of the subunit to with the natural agonist glutamate and the anthelmintic drug ivermectin using both two-voltage clamp electrophysiology and ligand binding experiments using [^{3}H]-ivermectin.

4.2 Results

4.2.1 Results of site directed mutagenesis

The PCR product of the mutagenesis for all reactions was sequenced in an area localised to the mutation. Three of the mutations (E114G, V235A and L256F) were originally discovered as polymorphisms in *Cooperia oncophora* (Njue et al. 2004). L256F was discovered to confer loss of sensitivity in *C. oncophora* and in *H. contortus* so alternative aromatic amino acid substitutions at the same position were incorporated. The T300S mutation was discovered by our lab as a polymorphism between IVS and IVR *H. contortus* (Jagannathan 1998), The V69E, S295T and T362A mutations were discovered as differences between in IVR and IVS *H. contortus* (Walsh et al, unpublished). Several mutations found in *Drosophila melanogaster* have been found to cause resistance to IVM. A mutation in the Dm $GABA_A$ (A302S) has been implicated in IVM resistance (ffrench-Constant et al. 1993; ffrench-Constant et al. 1993) and a mutation in the Dm GluClα (P299S) also causes a loss of sensitivity to IVM, glutamate and nodulisporic acid (Kane et al. 2000). The equivalent mutations (A308S and P316S) were incorporated into *H. contortus* GluClα3B (A summary of the mutations studied is shown in Table 5).

GluCl α3 mutant	Nucleotide change	Amino Acid Change	Experiments carried out
T300S	ACA to TCA	T to S	Electrophysiology, Ligand binding
E114G	GAG to GGG	E to G	Electrophysiology, Ligand binding
V235A	GTT to GCT	V to A	Electrophysiology, Ligand binding
L256F	CTC to TTC	L to F	Electrophysiology, Ligand binding
L256W	CTC to TGG	L to W	Ligand binding
L256V	CTC to GTC	L to V	Ligand binding
L256Y	CTC to TAC	L to Y	Ligand binding
V69E	GTG to GAG	V to E	Ligand binding
A308S	GCA to TCA	A to S	Ligand binding
P316S	CCA to TCA	P to S	Ligand binding
S295T	TCT to ACT	S to T	Ligand binding
T362A	ACG to GCG	T to A	Ligand binding

Table 5. C. *oncophora* and *H. contortus* mutants tested

Full length cDNAs encoding *H. contortus* ivermectin susceptible clones are kept as lab stocks. The mutations were successfully incorporated into the IVS cDNA and confirmed sequencing cDNA (see Figure 21). The mutations E114G and V235A are a result of transitional substitutions at the second codon position while mutations L256F and T300S are caused by substitution of the first codon position. All three mutations found in *C. oncophora* are thought to be in the N-terminal extracellular domain of the GluCl receptor (Njue et al. 2004). As the longest extracellular domain of the subunit this part of the channel is implicated in ligand binding. The mutation from *H. contortus* is found in the second transmembrane region.

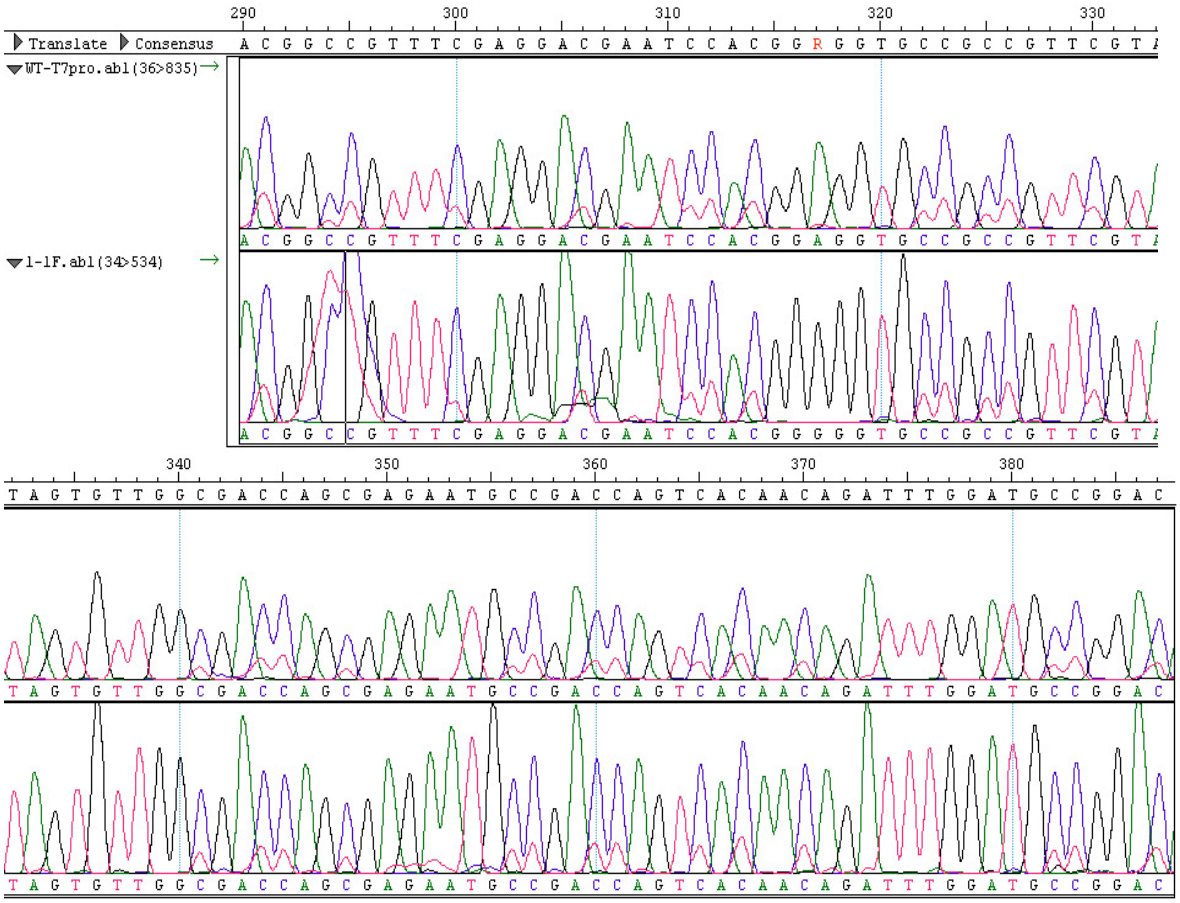

Figure 21: Chromatogram showing sequencing results after successful incorporation of a single base change for the mutation E114G.
The point mutation is highlighted by the red R in the consensus box

4.2.2 Actions of glutamate on oocytes injected with mutated GluClα3B cRNA

In an attempt to determine whether the SNP's contributed to an altered response to glutamate, the SNPs found in populations of IVR *C. oncophora,* (Njue et al. 2004) and a SNP found in IVR *H. contortus* were incorporated into the *H. contortus* GluClα3B subunit cDNA and transcribed into cRNA. The mutants, each representing one mutation were expressed individually in *Xenopus* oocytes. The T300S mutant,

when expressed alone failed to respond to glutamate and when expressed with *wt* at a ratio of 1:1 the resultant channels elicit responses identical to those of the *wt* channels alone, indicating that the T300S mutants are either not expressing protein, or that a functional channel is failing to assemble. Of the mutants that did express E114G and V235A showed dose-response curves similar to the IVS *wt* receptor with EC_{50} values of 31.5 ± 3.2 and 26.2 ± 2.5 μM respectively. Conversely the L256F mutation caused a significant ($p>0.0001$) 3.3 fold increase in the EC50 to 92.2 ± 3.5 μM (See, Table 6). Unlike in the wild type channels the concentration at which the L256F reach a maximal inward current is increased from 300 μM to 1mM. For the L256F mutation there is also a significant ($p=0.0016$) decrease in the Hill coefficient from 1.89± 0.35 in the wild type to 1.09 ± 0.16 indicating a loss of cooperativity for glutamate binding. The E114G mutation also shows a slightly shallower standard curve with a corresponding reduction in Hill number to 1.48 ± 0.31, although this is not significantly different. The V235A mutation has a Hill number very similar to that of the *wt* at 1.97 ± 0.35.

GluCl α3B mutant	EC50 (μM)	Hill Number	Oocytes (n)
IVS *wt*	27.6 ± 2.7	1.89 ± 0.35	7
E114G	31.5 ± 3.2	1.48 ± 0.31	6
V235A	26.2 ± 2.5	1.97 ± 0.35	6
L256F	92.2 ± 3.5	1.09 ± 0.16	8
T300S	No Channel	No Channel	-

Table 6. Summary of effects of glutamate on mutant GluClα3B homomeric channels.
EC50 and Hill slope values are expressed as mean ± SEM

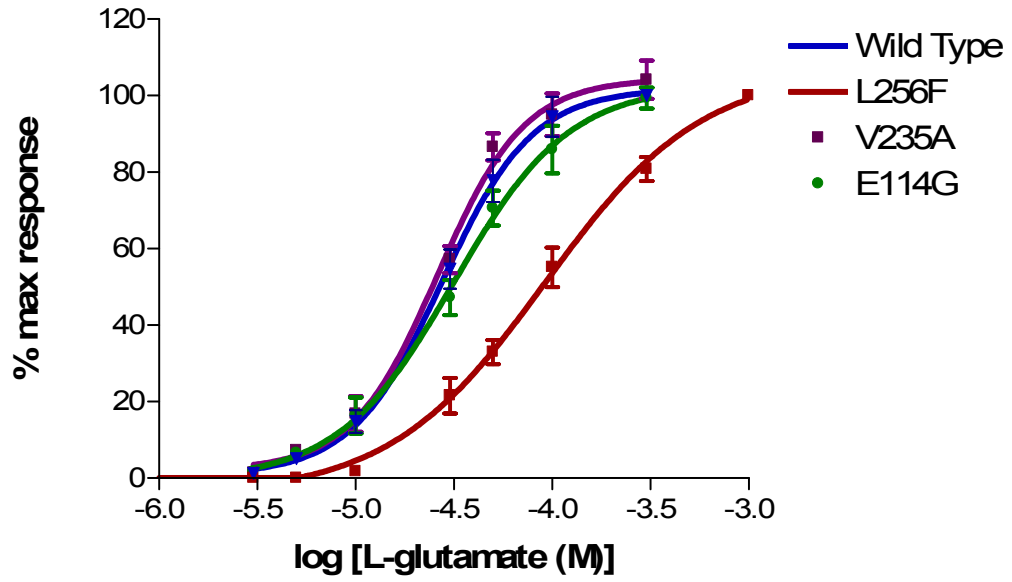

Figure 22: Dose-response curves of wild type and mutant dose- response curves for glutamate.

Glutamate dose-response curves for oocytes injected with *wild type* or Mutant *H. contortus* GluClα3B cRNA. Data were normalised to the maximum glutamate responses seen with each oocyte, and are shown as the standard error of the mean of seven oocytes for the *wt,* six oocytes each for E114G and V235A mutants and eight oocytes for the L256F mutant.

4.2.3 Saturation analysis of [^{3}H]-IVM binding to GluClα3B mutants at position 256

Studies on [^{3}H]-IVM binding to GluClα3B with the L256F SNP caused a significant change in B_{max} and K_d to the IVS *wt* GluClα3B. The L256F mutant shows a 6.5 fold increase in K_d from 0.35 ± 0.10 nM for *wt* to 2.26 ± 0.78 nM (see Figure 23A and Table 7). The *wt* shows a B_{max} of 0.83 ± 0.06 pmol/mg, which is increased to 1.41 ± 0.33 pmol/mg, with the L256F substitution a 1.7 fold increase. Due to these interesting results further substitutions to the leucine at position 256 were carried out and analysed. The L256Y substitution has B_{max} of 1.16 ± 0.20 pmol/mg and a K_d of 1.84 ± 0.49 nM both significantly higher ($p>0.0001$) than the *wt* (Figure 23B and Table 7). This trend continues with the L256W mutation which shows a B_{max} of 1.22 ± 0.21 pmol/mg and a K_d of 2.02 ± 0.52 nM (Figure 23C and Table 7). The L256V mutation does not show such a large difference to the *wt* with a B_{max} of 0.93 ± 0.14 pmol/mg and a K_d of 0.79 ± 0.24 nM but is still significant ($p=0.0217$) (Figure 23D and Table 7).

A

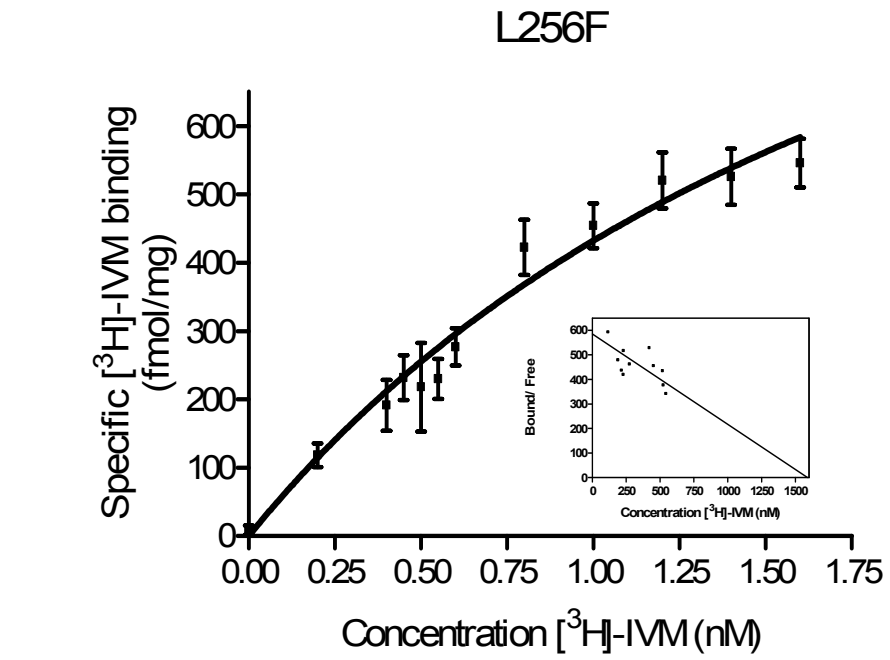
L256F
Specific [3H]-IVM binding (fmol/mg)
600
500
400
300
200
100
0
0.00
0.25
0.50
0.75
1.00
1.25
1.50
1.75
Concentration [3H]-IVM (nM)
Bound/ Free
0
250
500
750
1000
1250
1500
Concentration [3H]-IVM (nM)

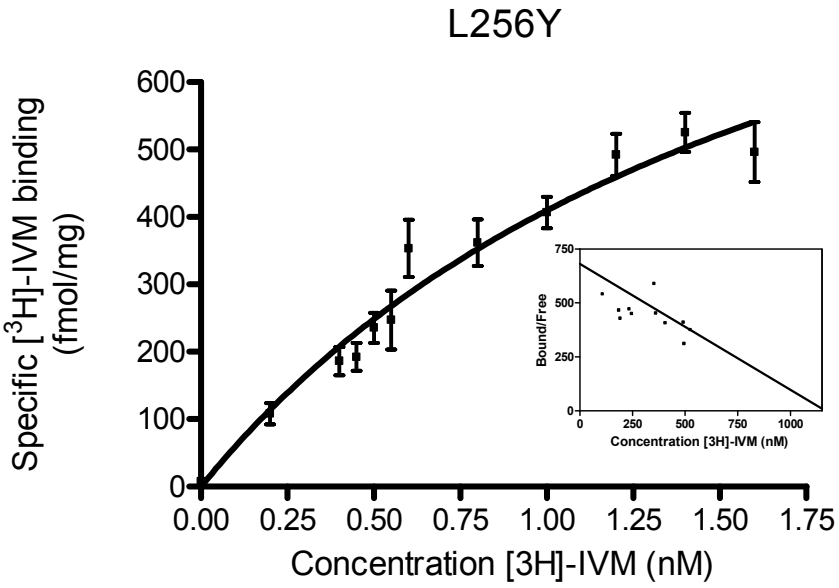
L256Y
Specific [3H]-IVM binding (fmol/mg)
600
500
400
300
200
100
0
0.00
0.25
0.50
0.75
1.00
1.25
1.50
1.75
Concentration [3H]-IVM (nM)
Bound/Free
750
500
250
0
250
500
750
1000
Concentration [3H]-IVM (nM)

C

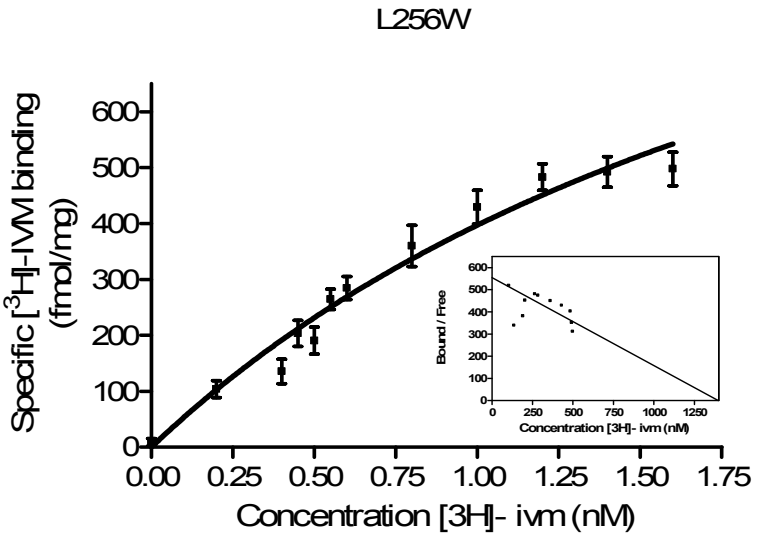

D

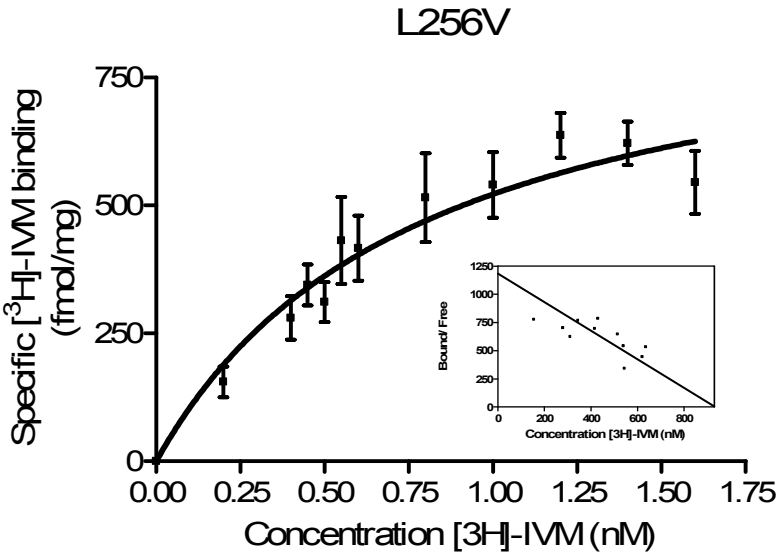

Figure 23: Saturation of COS-7 membrane preparations transiently expressing mutant GluClα3B with [^{3}H]-IVM. Inset is the Scatchard plot for each mutation.

A) Saturation data for L256F mutant GluClα3B protein.
B) Saturation data for L256Y mutant GluClα3B protein.
C) Saturation data for L256W mutant GluClα3B protein.
D) Saturation data for L256V mutant GluClα3B protein.

For each reaction 10µg of membrane protein was incubated with various concentrations of [^{3}H]-IVM for 2 hours at room temperature. Non specific binding was determined in the presence of 10µM unlabelled ivermectin.

4.2.4 Saturation analysis of [^{3}H]-IVM binding to GluClα3B mutants.

Specific high affinity [^{3}H]-IVM binding was observed to membranes from GluClα3B transfected cells carrying single-amino acid substitutions were assessed. The two SNPs found in IVR *C. oncophora* E114G and V235A (Figure 27A and B) showed no significant change in either B_{max} when compared to the *wt* indicating that these mutations have no effect on ivermectin binding with B_{max} values of 0.87 ± 0.06 and 0.79 ± 0.07 pmol/mg respectively. The K_d values are also similar to that of the *wt* channel with the E114G SNP having a K_d of 0.39 ± 0.07 nM and V235A 0.32 ± 0.09nM (Table 7). The T300S mutation failed to produce a functional channel when expressed in *Xenopus* oocytes but is expressed and binds ivermectin when expressed in COS-7 cells with a B_{max} of 1.01 ± 0.16 pmol/mg which is just ~ 18% higher than *wt* and K_d 0.76 ± 0.25 nM which is more than double that of *wt.* Another mutation V69E resulted in a very similar pharmacology to that of the T300S mutation with very similar B_{max} and K_d values 1.06 ± 0.15 pmol/mg and 0.80 ± 0.24 nM respectively.

A

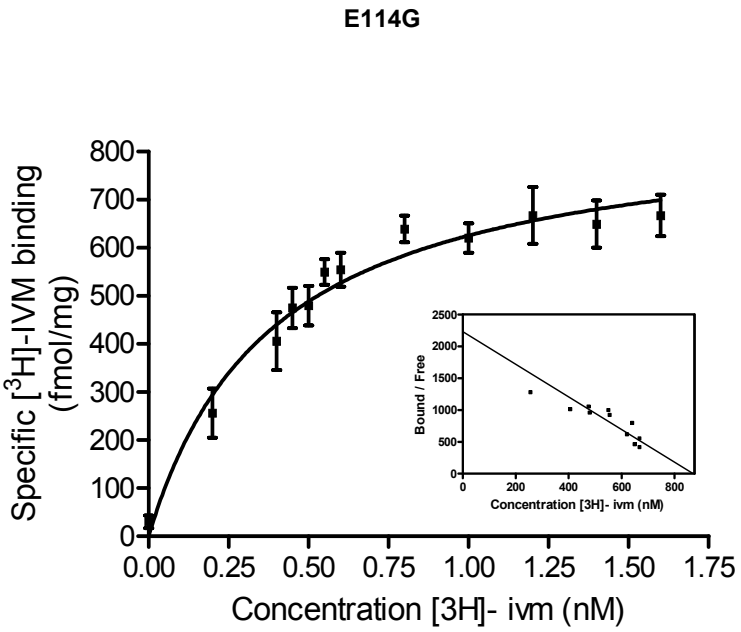

B

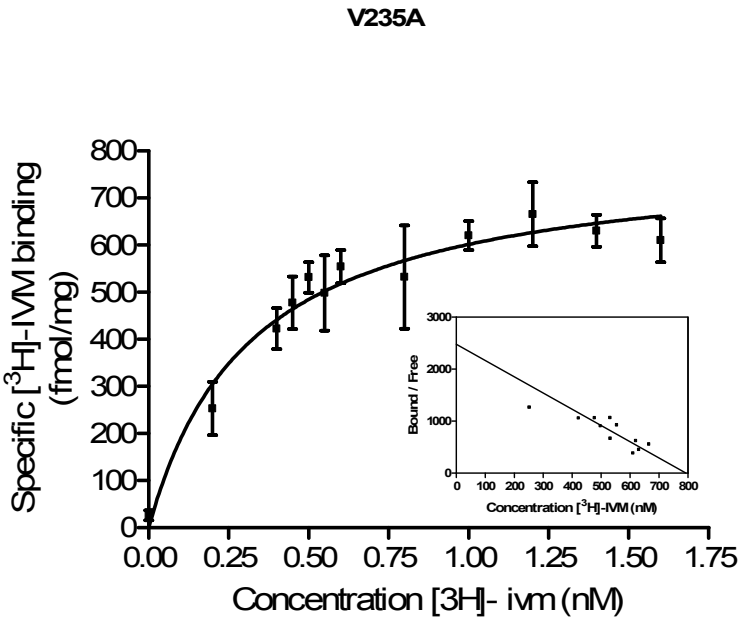

Figure 24: Saturation of COS-7 membrane preparations transiently expressing mutant GluClα3B with [^{3}H]-IVM. Inset is the Scatchard plot for each mutation.

A) Saturation data for E114G mutant GluClα3B protein.

B) Saturation data for V235A mutant GluClα3B protein

For each reaction 10µg of membrane protein was incubated with various concentrations of [^{3}H]-IVM for 2hours at room temperature. Non specific binding was determined in the presence of 10µM unlabelled ivermectin.

C

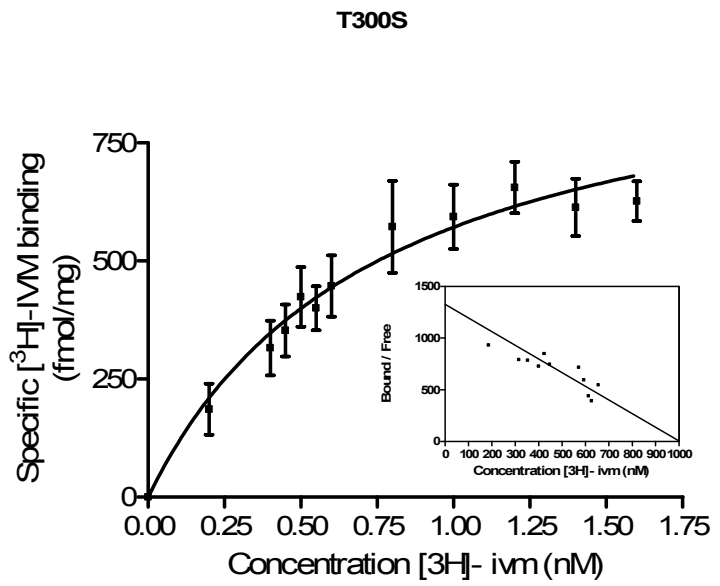

D

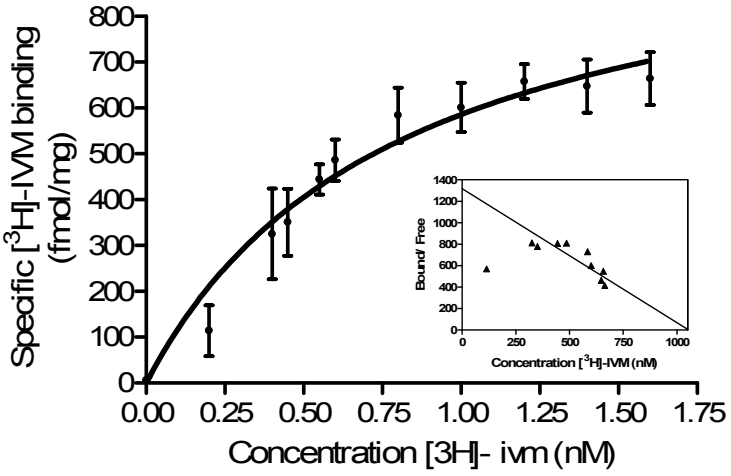

Figure 25: Saturation of COS-7 membrane preparations transiently expressing mutant GluClα3B with [^{3}H]-IVM. Inset is the Scatchard plot for each mutation.

C) Saturation data for T300S mutant GluClα3B protein.

D) Saturation data for V69E mutant GluClα3B protein

For each reaction 10µg of membrane protein was incubated with various concentrations of [^{3}H]-IVM for 2hours at room temperature. Non specific binding was determined in the presence of 10µM unlabelled ivermectin.

E

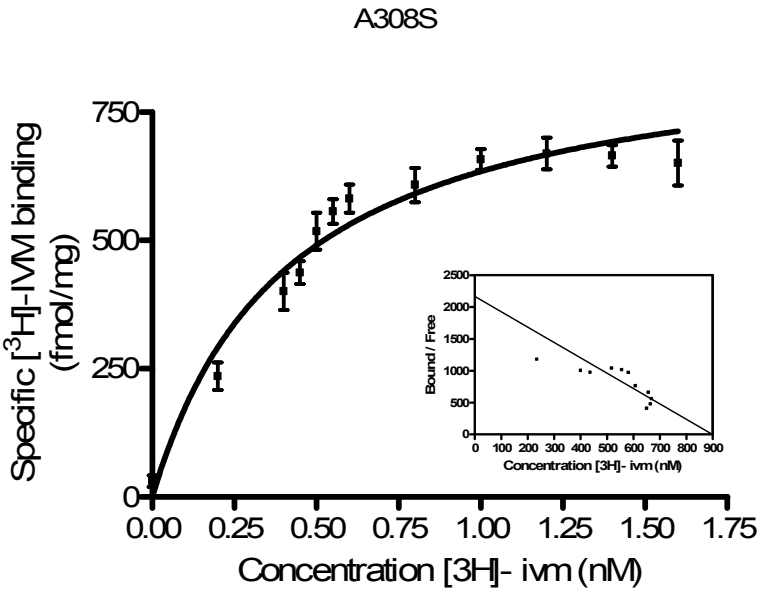

F

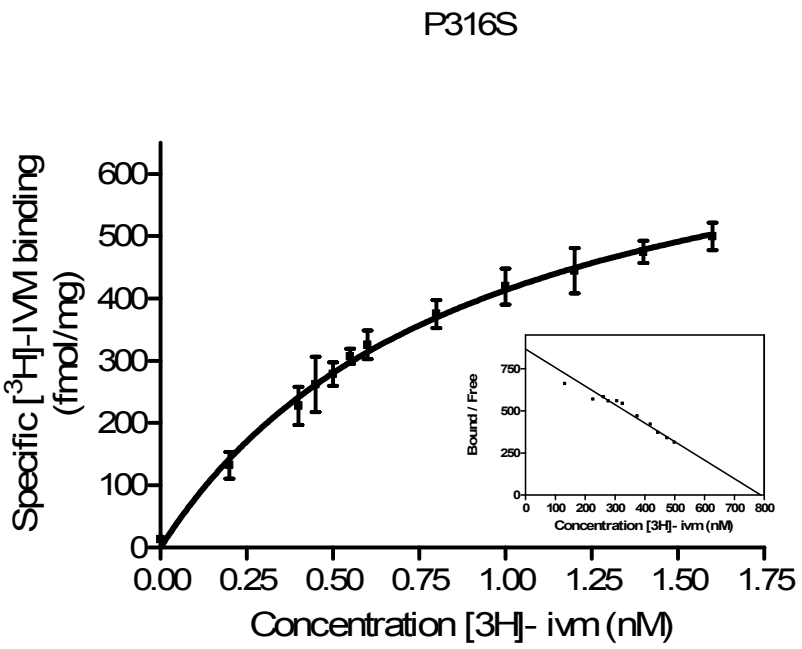

Figure 26: Saturation of COS-7 membrane preparations transiently expressing mutant GluClα3B with [^{3}H]-IVM. Inset is the Scatchard plot for each mutation.

E) Saturation data for A308S mutant GluClα3B protein.
F) Saturation data for P316S mutant GluClα3B protein

For each reaction 10µg of membrane protein was incubated with various concentrations of [^{3}H]-IVM for 2hours at room temperature. Non specific binding was determined in the presence of 10µM unlabelled ivermectin.

G

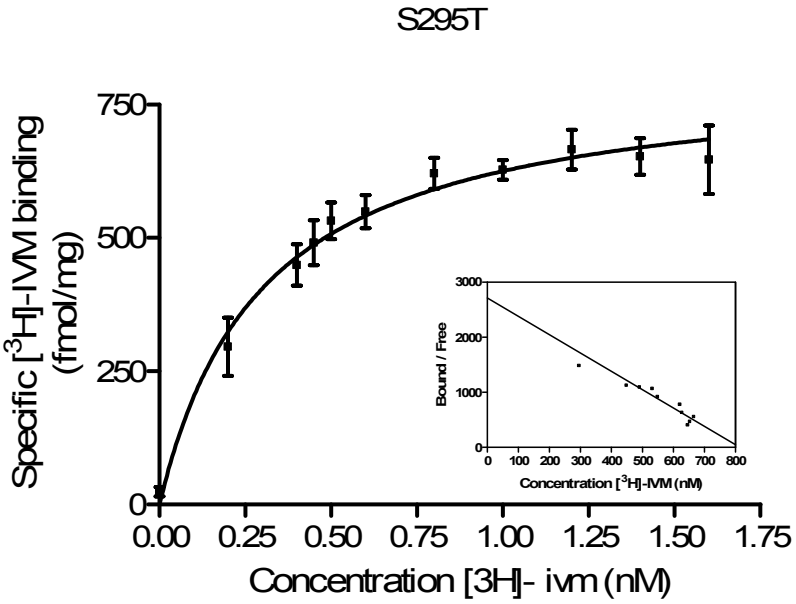

H

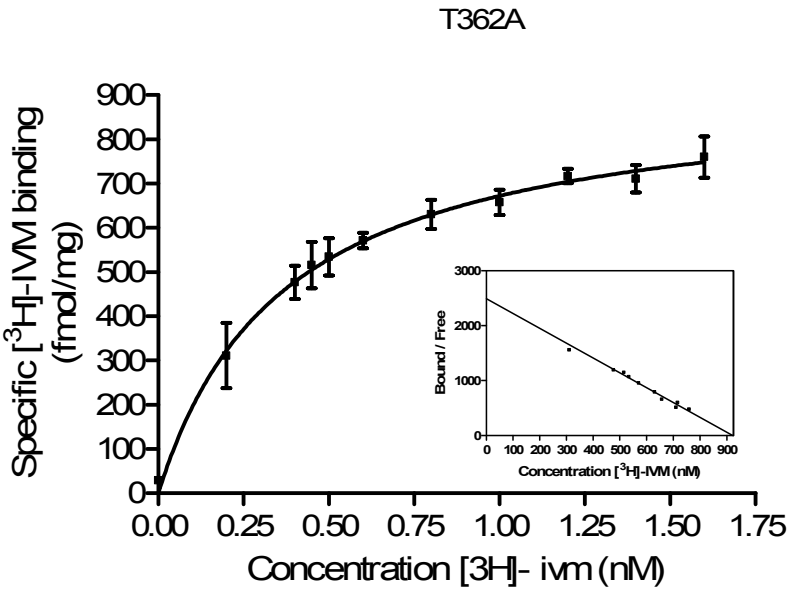

Figure 27: Saturation of COS-7 membrane preparations transiently expressing mutant GluClα3B with [^{3}H]-IVM. Inset is the Scatchard plot for each mutation.

G) Saturation data for S295T mutant GluClα3B protein

H) Saturation data for T362A mutant GluClα3B protein

For each reaction 10µg of membrane protein was incubated with various concentrations of [^{3}H]-IVM for 2hours at room temperature. Non specific binding was determined in the presence of 10µM unlabelled ivermectin.

mutation	B_{max} pmol/mg	K_d nM	n (n of transfection reactions)
wt	0.83 ± 0.06	0.35 ± 0.10	8 (4)
L256F	1.41 ± 0.33	2.26 ± 0.78	8 (5)
L256Y	1.16 ± 0.20	1.84 ± 0.49	6 (4)
L256V	0.93 ± 0.14	0.79 ± 0.24	6 (6)
L256W	1.39 ± 0.28	2.51 ± 0.70	6 (3)
E114G	0.87 ± 0.06	0.39 ± 0.07	6 (3)
V235A	0.79 ± 0.07	0.32 ± 0.09	6 (3)
T300S	1.01 ± 0.16	0.76 ± 0.25	8 (5)
V69E	1.06 ± 0.15	0.80 ± 0.24	6 (4)
A308S	0.90 ± 0.05	0.41 ± 0.06	6 (4)
P316S	0.79 ± 0.07	0.92 ± 0.16	6 (3)
S295T	0.81 ± 0.05	0.30 ± 0.06	5 (2)
T362A	0.92 ± 0.05	0.37 ± 0.07	5 (2)

Table 7. Summary of B_{max} and K_d from radioligand binding studies with [^{3}H]-IVM
Wt values are highlighted in green and mutations that elicit more than two-fold increase in EC_{50} are highlighted in blue

4.3 Discussion

Assessment of the mutations found in populations of ivermectin resistant *Cooperia oncophora* was essential to determine whether they conferred resistance. Studies carried out on the *C. oncophora* GluClα3 concluded that a 3 fold loss of sensitivity to glutamate and a 2.5 fold loss of sensitivity to IVM (Njue et al. 2004) and led us to investigate whether these mutations played a similar role in other parasite species such as *H. contortus.* The potential importance of these particular mutations was due to the fact that they had occurred *in vivo,* and therefore could potentially occur

naturally in closely related species. To determine whether all three mutations in the IVR GluCl α3B contribute to loss of glutamate and ivermectin sensitivity, each mutation was introduced alone into the IVS GluCl α3B using site-directed mutagenesis. From preliminary studies the responses of Mutation E114G and mutation V235A receptors were similar to those of the IVS GluCl α3B receptor with, suggesting that the mutations at these positions had no influence on ligand binding. There is little difference caused by the E114G and V235A mutations concerning the sensitivity of the channels to IVM with the mutations having very little effect of [^{3}H]-IVM binding. It is clear that these mutations have no obvious individual effect of the pharmacology of the channel. Although both mutations are found in the N-terminal domain of the GluCLα3B channel neither mutation is located in the glutamate binding pocket. In contrast, L256F mutant channels were less sensitive to glutamate with an ~ 3 fold increase in EC_{50} to 92.2 ± 3.5 μM , which proved a similar loss of sensitivity in *C. oncophora* to the IVR GluCl α3 receptor responses (Njue et al. 2004), suggesting that the L256F mutation accounted for the difference between IVS and IVR GluCl α3 channels in response to these two ligands. The Hill number for the L256F mutant is 1.09 ± 0.16 whereas the IVS channels it is 1.89 ± 0.35. This indicates a loss of cooperativity between ligand molecules binding to the channel. The effect of the mutations on the sensitivity of the GluCl α3B showed a decrease in sensitivity to glutamate with the L256F mutation there was a shift to the right. The maximal response for glutamate in IVS GluCl α3B channels is ~ 300 μM with 100 μM giving a 95% maximal response. With the L256F mutation the maximal response is increased, with 1 mM eliciting an average 20% higher response than 300 μM. This was not found in the parallel *Cooperia* study where the maximal response remained constant between mutations and IVS channels. This may be due to differences between experimental procedures or between the two nematode species.

The ligand binding studies show a reduction in sensitivity to [^{3}H]- IVM binding with a 6.5 fold increase in K_d for L256F. This mutation, causing an amino acid change from a leucine to a larger amino acid like phenylalanine with an aromatic group could cause a conformational change that influences ligand binding. Alternatively, leucine may contribute directly to ligand binding, and the substitution to a different amino acid may have changed the tertiary structure of the ligand binding site. This prompted the creation of further substitutions with different amino acids at the 256 position for ligand binding studies. The alternative substitutions at the 256 position

all show significant differences in their K_d to that of the *wt,* with L256V producing 0.79 ± 0.24 nM, significantly less than the L256F K_d but higher than *wt*. This could be due to the nature of the amino acid substitution. All amino acids chosen to substitute with leucine were neutral. Valine is the smallest amino acid substituted and most similar in structure to leucine, valine does not carry aromatic an aromatic ring and is highly hydrophobic like leucine with a hydropathy number of 4.2 (Kyte et al. 1982). It is possible that the similarities between these amino acids explain the smaller difference in the resulting K_d and very similar B_{max}. The tyrosine substitution (L256Y) caused a K_d of 1.84 ± 0.49 nM and tryptophan (L256W) 2.51 ± 0.70 nM. Both these substitutions and the original phenylalanine (L256F) cause the greatest change in K_d. and all contain aromatic rings the most reactive of which is tryptophan as it contains a non-carbon atom (nitrogen) in the aromatic ring system and is considered more reactive than phenylalanine but less than tyrosine (Betts et al. 2003). This is represented in the results with tryptophan substitution causing the largest (7- fold) increase in K_d followed by phenylalanine and then tyrosine. To further study the amino acid substitutions carried out in the N-terminal domain of the subunit, *in silico* modelling of this region were undertaken and will be described in chapter 4.

From the data shown it is clear that the L256F mutation confers loss of sensitivity to glutamate and ivermectin in *H. contortus* as seen with *Cooperia*. Ivermectin studies were carried out using [^{3}H]-IVM because experiments carried out on *Xenopus* oocytes have limited success; because ivermectin is irreversible it is difficult to obtain dose response curves using the same oocytes. The only way of doing this is to add ivermectin in increasing doses over one electrophysiological reading. This does not allow for the normal recovery time between doses, it has also been observed that all concentrations of ivermectin can cause an “all or nothing reaction” with the even low concentrations (~1nM) resulting in a fully open channel with the time taken to open the channel decreasing with increasing concentration. The *C. oncphora* study states that there is a three fold decrease in sensitivity to ivermectin with the L256F mutation. But with an n of 2 oocytes for the ivermectin studies for L256F mutation and an n of 3 for the IVS (Njue et al. 2004), the low n raises concerns over the statistical significance of this result especially due to the variable nature of electrophysiology with ivermectin (as previously discussed in chapter 3). However, the work *H. contortus* L256F mutation complements the results in *Cooperia* which uses an n of 3. Electrophysiology with ivermectin is also made more difficult with the

fact that only one oocyte can be treated with ivermectin each day due to the nature of the drug. Ivermectin is hydrophobic and 'sticky' even in low concentrations (10nM) and remains stuck to the plasticware long after an application of the drug. A separate perfusion system was used solely for ivermectin but it must be soaked in ethanol overnight to remove all traces of ivermectin between applications. As a result, it is easier and more reliable to conduct IVM studies using radiolabelled ligands at low concentrations avoiding the difficulties described above.

The GluClα3B subunits carrying the T300S mutation did not respond to either glutamate or IVM. It was not known if the channel successfully assembled on the surface or if the mutation triggered a problem in the protein synthesis or assembly pathways. Successful expression in the COS-7 cells indicated that the problem was not in the synthesis of the protein subunit as the subunit bound IVM with high affinity. The ligand binding studies do not require the formation of functional channels on the surface of the cell like the electrophysiology experiments, rather, all that is necessary is any protein found in the membrane that has a functional IVM binding site. This may be suggestive of an assembly or trafficking problem as protein, stuck undergoing post translational modification in the endoplasmic reticulum or vesicles will also be collected in the membrane preparation. Alternatively, the problem may lie in the channel expression in *Xenopus* oocytes, the mutation may cause a problem in the endogenous *Xenopus* protein synthesis apparatus of the cell and it may be able to express a functional channel in another expression system. With the current information we have it is impossible to say what caused the lack of electrophysiological data. The T300S mutation caused an increase in the K_d from 0.35 ± 0.10 nM to over double this value at 0.76 ± 0.25 nM, However neither the K_d or the B_{max} for T300S are significantly different from *wt* (p=0.0585). I would not have expected a big change from *wt* in either electrophysiology or radioligand binding studies due to the very subtle substitution of threonine to serine which is effectively just the loss of a methyl group. Both amino acids are polar, neutral and have hydropathy index of -0.8 to -0.7 (Kyte et al. 1982) respectively showing them to be slightly hydrophobic which is common for amino acids found in transmembrane regions. The 2-fold increase in K_d may be due to the T300S mutation being involved in the IVM- binding domain, so even a subtle amino acid change may cause a noticeable effect on ligand binding. The actual binding site of IVM is still unknown,

but from earlier competition studies it is known that IVM does not share a binding site with glutamate (Cheeseman et al. 2001), from the hydrophobic nature of the IVM molecule it can be hypothesised that the IVM would stay in the cell membrane and bind the channel on the transmembrane regions the TM2 region where the T300S mutation is found is inaccessible when the channel is closed but due to the twisting mechanism of channel opening would become available to proteins in the cell membrane when open (Hucho 1986; Celie et al. 2004). This makes the TM2 region a feasible participant in IVM binding, although this would suggest that glutamate or another agonist would need to be present for IVM action. Due to the unknown nature of IVM binding, further study of the structure of GluCl channels needs to be undertaken and only when a clearer picture of the structure has been determined can experiments targeting the IVM binding sites be designed. The values elucidated for T300S mutation are very similar to those found for the V69E mutation despite this mutation being located in the N-terminal region of the subunit and not the membrane region like the T300S. V69E causes a 2-fold increase in K_d from *wt* at 0.35 ± 0.10 nM to 0.80 ± 0.24 nM in IVM despite being nowhere near the proposed IVM binding site. The substitution of valine to glutamic acid is a big change. With glutamic acid being polar, acidic and extremely hydrophilic where valine is nonpolar and neutral and also very hydrophobic (Betts et al. 2003). Further study was carried out to determine if the changes in these properties at the V69 position caused any conformational changes in the tertiary structure of the subunit that may explain this result (See chapter 4).

The GluClα3B belongs to the same LGIC superfamily with with nicotinic acetylcholine receptors (nAChR), which are found in all organisms and are drug targets for insecticides known as the neonicotinoids, such as imidacloprid. The L256F mutation does not map onto any of the equivalent six domains of the nAChR subunits that form the acetylcholine binding site (Corringer et al. 1995; Corringer et al. 2000; Brejc et al. 2001) although alignment of these domains with the GluCl α3B is not totally clear. The fact that this mutation is not found in critical regions nAChR may explain the modest loss of agonist sensitivity observed (Njue et al. 2004). In *Drosophilia melanogaster* a single mutation in the M2-M3 linker region of Dm GluClα gene confers over 20-fold resistance to the novel insecticide, nodulisporic acid. Although the basis of the drug's insecticidal activity was not known, recent studies indicate that nodulisporic acid acts by a mechanism similar to that of ivermectin

(Kane et al. 2000; McHardy M. Smith et al. 2000) Electrophysiological studies of wild-type and mutant channels expressed in *Xenopus* oocytes revealed that nodulisporic acid directly activates Dm GluClα and that the mutation P299S renders the channel less sensitive to activation by nodulisporic acid, ivermectin, and the endogenous glutamate (Kane et al. 2000). It has also been found mutation in the TM2 region of the *rdl* gene that codes for a GABA-gated channel confers high-level resistance to the insecticide dieldrin. This mutation not only identifies a single amino acid conferring high levels of resistance to the important GABA receptor antagonist picrotoxin (PTX) but also, by conferring resistance to cyclodienes (ffrench-Constant et al. 1993). These *drosophila* SNPs were also incorporated into the GluClα3B subunit to undergo radioligand binding analysis and the equivalent mutation in *H. contortus* was at the position P316S and resulted significant ($p=0.0006$) loss of sensitivity to IVM with a 2.6- fold increase in K_D.

In conclusion it has been shown that several single amino acid substitutions introduced into GluClα3B subunit have a significant effect on agonist affinity. In order to further characterise these pharmalogical effects, it is necessary to understand the position and importance of each amino acid that has been substituted. With current understanding of the secondary and tertiary structure of the GluCls, the amino acid positions can only be allocated into general areas. The next chapter focuses on trying to pinpoint the position of amino acids within the N-terminal domain and therefore to elicit a greater understanding of the importance of mutations such as L256F in relation to the subunit as a whole.

Chapter 5: Analysis of the position of Single Amino Acid substitutions in the N-terminal region of the *H. contortus* GluClα3B subunit using homology modelling

.

5.1 Introduction

Our understanding of the structure of the ligand gated chloride channels is still far from complete, but great headway has been made in understanding the structure of the primary family member: the nicotinic acetylcholine receptor. Understanding this structure is essential for creating a template for understanding the conserved regions in all the ligand gated ion channels including ionotropic, glutamate and 5HT channels.

Ligand gated ion channels are vastly important in several fields of research. They make up crucial parts of the excitory and inhibitory pathways in the central and peripheral nervous systems and implicated in mammalian diseases such as Alzheimer's, Parkinson's and epilepsy amongst many others. They are excellent drug targets for a whole range of drugs. Understanding how these incredible and highly important channels are built and organised will be helpful in targeting research more usefully and carefully.

Although high-resolution crystal structures of other receptors or their domains have become commonplace, the ligand gated ion channel field has had to make do with low-resolution electron microscopy images of nAChR (Unwin 2005) (4 Å) or with the structure of a remote water-soluble homolog from *Lymnea stagnalis* (Brejc et al. 2001). Last year a new high-resolution crystal structure of the extracellular portion of the nAChR α1 subunit bound to α bungarotoxin at 1.94 Å resolution (Dellisanti et al. 2007). This paper provides a significant breakthrough, putting existing data into perspective and supplies high-resolution insights (Sixma 2007). With channels that have membrane spanning domains it is extremely difficult to crystallize a single ligand binding domain of the nAChR in isolation. The nAChR ion channels have five homologous or identical subunits, with an extracellular domain that binds ligands at an aromatic site that lies at the interface of an α subunit and its neighbour (Sixma 2007). Ligand binding triggers a gating signal in the transmembrane domain, which opens its gate for ions to pass through the channel pore. In all members of the

superfamily, the extracellular domain has a conserved loop of 13 amino acids that is flanked by a disulfide bridge. Therefore, the superfamily of pentameric ligand-gated ion channels, which also includes GluCls $GABA_A$, 5HT3 serotonin and glycine receptors, is also known as the family of cys-loop receptors. Although the extracellular domains are separate units that can even be exchanged between receptors, it has been remarkably difficult to engineer soluble ligand-binding domains. (Sixma 2007)

In recent years advances in homology modelling have allowed scientists to create potential models of proteins based on similarities to existing data of known crystal structures. Previously this technique was the reserve of the few scientists with strong backgrounds in several programming languages such as Perl and modelica but the release and development of the Modeller program has allowed scientists to use a more user friendly method of molecular modelling (Sali et al. 1993), each new version that became available became easier to use. The Modeller 9 version 2 that came out in 2007 was the first that required little or no knowledge of programming and allowed non- computer experts to use it. This new user-friendly tool and the advances in nicotinic crystal structure analysis allowed us to attempt to create the first homology models of GluClα3B subunits, although, at the present only the extracellular portion can be modelled as only crystal structures of the extracellular domains of nAChRs are available to use as templates.

The main objective of creating molecular models of the N-terminal domain of GluClα3B subunit is to understand the position and importance of the mutations of interest discussed in previous chapters.

5.2 Results

All computations and simulations were carried out using a Sony vaio VGN-A397XP laptop computer running Microsoft windows XP professional. Modelling was only carried out on the N-terminal domain of the GluClα3B subunit. This is because known crystal structures have only been created using soluble proteins. The hydrophobic nature of the transmembrane regions make the creation of crystals and the subsequent X-ray experiments very difficult, therefore the decision was made to concentrate on the extracellular domain as this is the site of ligand binding.

5.2.1 Selecting the template

GluClα3B N-terminal amino acid sequence was compared, using BLAST, to those in the protein structure database (PDB). BLAST is a pair-wise sequence alignment program based on approximation of dynamic programming algorithms. The program looks for local alignments, short stretches of identical residues, in both the query and database sequences. A parallel comparison was also carried out using the modeller 9v2 program.

For the modeller GluClα3B query sequence the top alignments came out as 1i9BA-E. These same resultant sequences of acetylcholine binding protein came out with the BLAST search; although not the top match, it was the best match over 50 amino acids long. As a result the acetylcholine binding protein subunit from *Lymnea stagnalis* was chosen as the template. Interestingly the majority of the remaining 50 matches were alternative crystal structures of the acetylcholine binding protein as indicated from the similar E- values and other data shown in Figure 28. The Expect value (E) is a parameter that describes the number of hits one can "expect" to see by chance when searching a database of a particular size. It decreases exponentially as the Score (S) of the match increases. Essentially, the E value describes the random background noise. For example, an E value of 1 assigned to a hit can be interpreted as meaning that in a database of the current size one might expect to see 1 match with a similar score simply by chance. Consequently the E-value can be used to assess the level of confidence in the alignment, and the smaller it is, is due to homology rather than chance. The E-value

of $0.17x10^{-5}$, a very low number that proves that the sequence homology between the GluClα3B subunit and the 1i9B is very unlikely to be down to chance, and that the two structures are, in fact, similar

```
# Number of sequences:     51
# Length of profile  :    263
# N_PROF_ITERATIONS  :      1
# GAP_PENALTIES_1D   :   -500.0   -50.0
# MATRIX_OFFSET      : -450.0
# RR_FILE            : ${LIB}/blosum62.sim.mat
```

1	GluCla3B	s	0	263	1	263	0	0	0	0.	0.0
2	1i9bA	X	1	205	66	250	26	187	155	30.	0.17E-05
3	1i9bB	X	1	205	66	250	26	187	155	30.	0.17E-05
4	1i9bC	X	1	205	66	250	26	187	155	30.	0.17E-05
5	1i9bD	X	1	205	66	250	26	187	155	30.	0.17E-05
6	1i9bE	X	1	205	66	250	26	187	155	30.	0.17E-05
7	1uv6A	X	1	205	66	250	26	187	155	30.	0.17E-05
8	1uv6B	X	1	205	66	250	26	187	155	30.	0.17E-05
9	1uv6C	X	1	205	66	250	26	187	155	30.	0.17E-05
10	1uv6D	X	1	205	66	250	26	187	155	30.	0.17E-05
11	1uv6E	X	1	205	66	250	26	187	155	30.	0.17E-05
12	1uv6F	X	1	205	66	250	26	187	155	30.	0.17E-05
13	1uv6G	X	1	205	66	250	26	187	155	30.	0.17E-05
14	1uv6H	X	1	205	66	250	26	187	155	30.	0.17E-05
15	1uv6I	X	1	205	66	250	26	187	155	30.	0.17E-05
16	1uv6J	X	1	205	66	250	26	187	155	30.	0.17E-05
17	1uw6A	X	1	208	66	250	27	188	155	30.	0.17E-05
18	1uw6B	X	1	206	66	250	27	188	155	30.	0.17E-05
19	1uw6C	X	1	206	66	250	27	188	155	30.	0.17E-05
20	1uw6D	X	1	208	66	250	27	188	155	30.	0.17E-05
21	1uw6E	X	1	206	66	250	27	188	155	30.	0.17E-05
22	1uw6F	X	1	208	66	250	27	188	155	30.	0.17E-05
23	1uw6G	X	1	206	66	250	27	188	155	30.	0.17E-05
24	1uw6H	X	1	206	66	250	27	188	155	30.	0.17E-05
25	1uw6I	X	1	206	66	250	27	188	155	30.	0.17E-05
26	1uw6J	X	1	206	66	250	27	188	155	30.	0.17E-05
27	1uw6K	X	1	206	66	250	27	188	155	30.	0.17E-05
28	1uw6L	X	1	206	66	250	27	188	155	30.	0.17E-05
29	1uw6M	X	1	208	66	250	27	188	155	30.	0.17E-05
30	1uw6N	X	1	208	66	250	27	188	155	30.	0.17E-05
31	1uw6O	X	1	206	66	250	27	188	155	30.	0.17E-05
32	1uw6P	X	1	206	66	250	27	188	155	30.	0.17E-05
33	1uw6Q	X	1	206	66	250	27	188	155	30.	0.17E-05
34	1uw6R	X	1	208	66	250	27	188	155	30.	0.17E-05
35	1uw6S	X	1	206	66	250	27	188	155	30.	0.17E-05
36	1uw6T	X	1	208	66	250	27	188	155	30.	0.17E-05
37	1ux2A	X	1	207	66	250	28	189	155	30.	0.17E-05
38	1ux2B	X	1	206	66	250	27	188	155	30.	0.17E-05
39	1ux2C	X	1	207	66	250	28	189	155	30.	0.17E-05
40	1ux2D	X	1	207	66	250	28	189	155	30.	0.17E-05
41	1ux2E	X	1	206	66	250	27	188	155	30.	0.17E-05
42	1ux2F	X	1	207	66	250	28	189	155	30.	0.17E-05
43	1ux2G	X	1	206	66	250	27	188	155	30.	0.17E-05
44	1ux2H	X	1	207	66	250	28	189	155	30.	0.17E-05
45	1ux2I	X	1	206	66	250	27	188	155	30.	0.17E-05

Figure 28: Result of template search for GluClα3B- N-terminal region.
The most important columns in the profile.build() output are the second, tenth, eleventh and twelfth columns. The second column reports the code of the PDB sequence that was compared with the target sequence. The PDB code in each line is the representative of a group of PDB sequences that share 95% or more sequence identity to each other and have less than 30 residues or 30% sequence length difference. The eleventh column reports the percentage sequence identities between GluClα3B- N-terminal region and a PDB sequence normalized by the lengths of the alignment (indicated in the tenth column). In general, a sequence identity value above approximately 25% indicates a potential template unless the alignment is short (i.e, less than 100 residues). A better measure of the significance of the alignment is given in the twelfth column by the e-value of the alignment.

5.2.2 Aligning the sequences

Since the accuracy of the homology model is related to the degree of sequence identity and similarity between the template and target, particular attention was paid to the structural template selection and sequence alignment steps which are crucial in any homology modelling. The GluClα3B query was aligned using the modeller 9v2. According to the values generated by the modeller program the sequence identity between the template and the query is 30% (See Figure 28). The minimum requirement for a potential template is 25% identity over more than 100 amino acids (Sali et al. 1993).

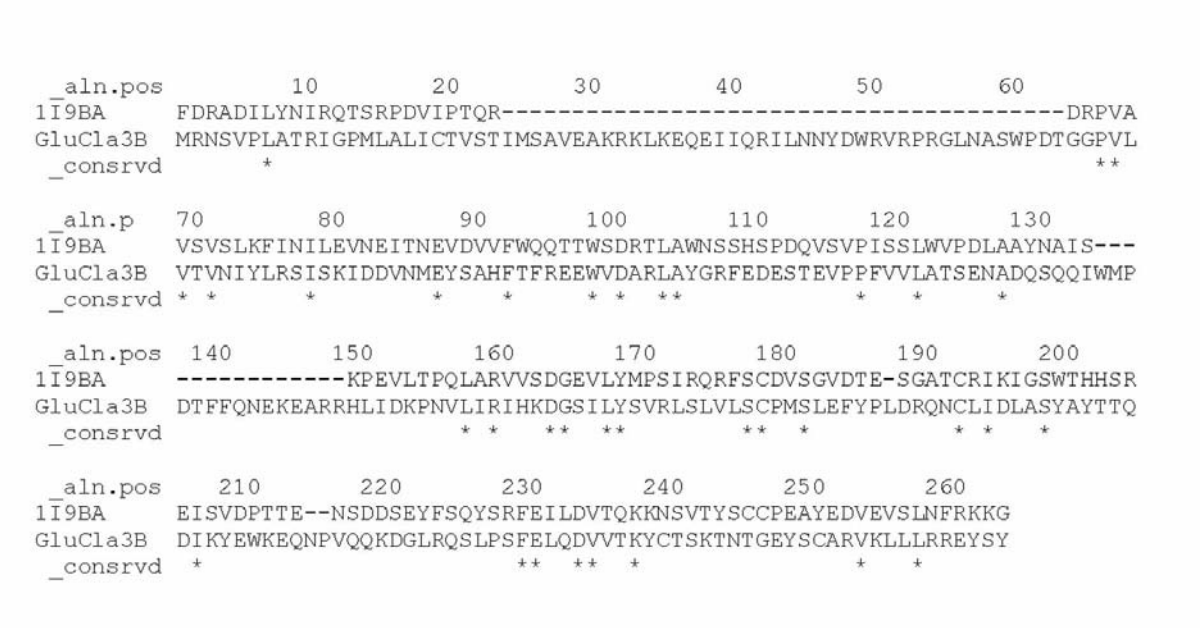

Figure 29: Modeller alignment of GluClα3B N-terminal domain
The asterisks indicate exact matches between the two sequences.

In order to better understand the nature of the similarities between the proposed template and GluClα3B further study was carried out to determine structurally conserved and variable regions, the query sequences were annotated using the secondary structure of the template using ESPript 2.2. The Risler Matrix was used, which is derived from amino acid substitutions in aligned 3D structures rather than the commonly used PAM model which is designed to track the evolutionary origins of

proteins or the BLOSUM matrix, used to identify only conserved domains. The Risler Matrix also provides an added layer of refinement by in identifying amino acids of interest (Mount 2004).

A multiple alignment of the IVS *wt* GluClα3B N-terminal region vs. the *Lymnea stagnalis* amino acid sequence was carried out using ClustalW and then the resultant file was uploaded to the ESPript 2.2 web-interface. The resultant alignment expands on the information showing not just identical residues but ones with similar properties. It is also useful to note that the areas that are more highly conserved are usually areas important to the secondary structure (Figure 29). The N-terminal regions of the GluClα3B subunits carrying mutations in this region were also studied to elucidate whether the mutations were carried in conserved regions where it would be easy to see if they have a conformational effect on the channel. Of the mutations in the N-terminal region the V69E mutation is the only one in a conserved area on the first β-sheet.

It is also worth noting that the extracellular portion of the GluClα3B subunit is significantly longer than that of the template at 263 amino acid residues in length compared to 205 in the template. The areas of extra sequence are found in one major area, the first N-terminal region prior to any conserved secondary structures, this is due to the presence of a signal peptide. There are also several stretches of extra residues between two and seven amino acids in length throughout the subunit (see Figure 31). These areas that don't have a template will still be modeled using mathematical parameters but due to the lack of template will not be as reliable.

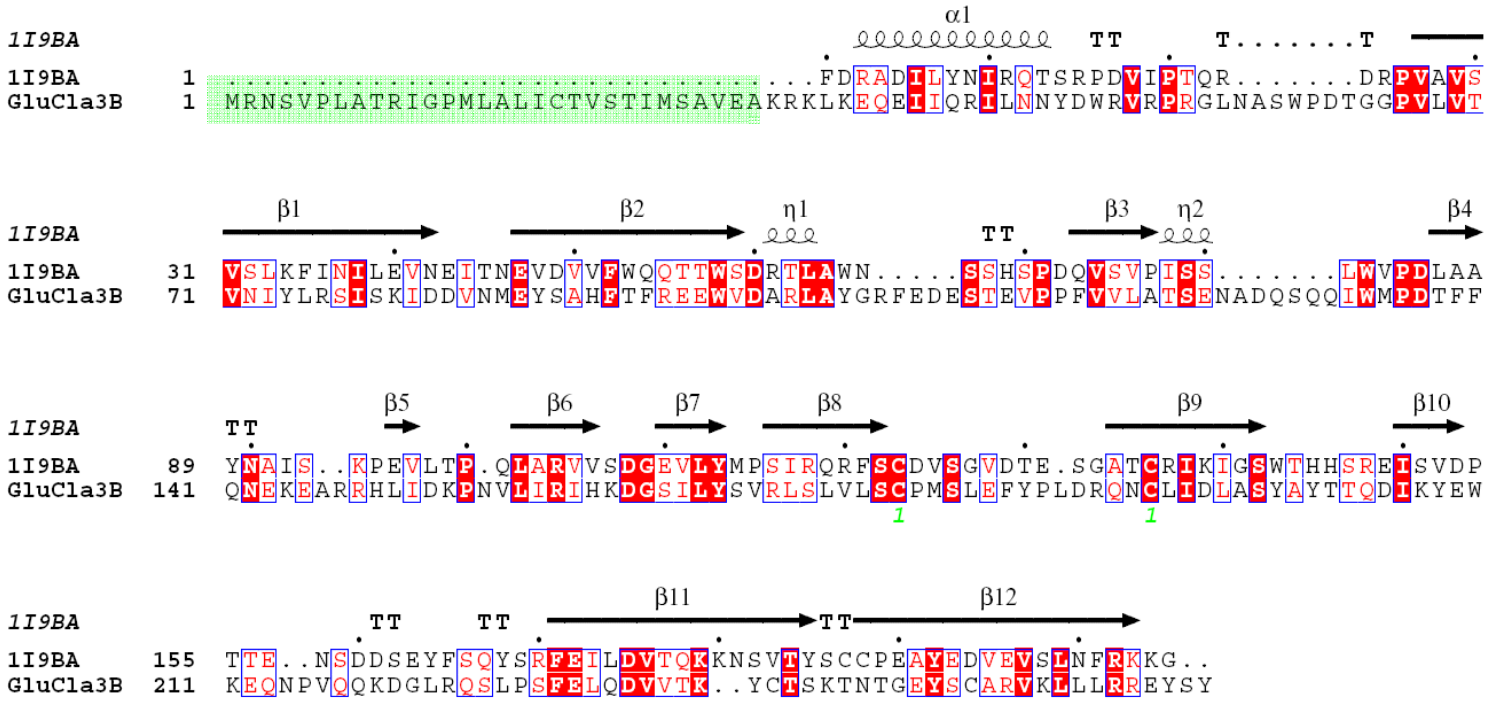

Figure 30: sequence alignment of acetylcholine binding protein (pdb 1I9B) and GluClα3B N-terminal domain.
The secondary structure of the acetylcholine binding protein is shown above the alignment. Identical residues are shown as white letters on a red background and similar residues are shown as red on a white background. The βn represents β sheets, αn represent alpha helicies, TT shown above the residues indicates a sharp β-turn. The disulphide bridge caused by paired cysteine residues are illustrated with green numbers. The black dots above the sequence are space markers every 10 residues. The signal peptide is shown in the green box.

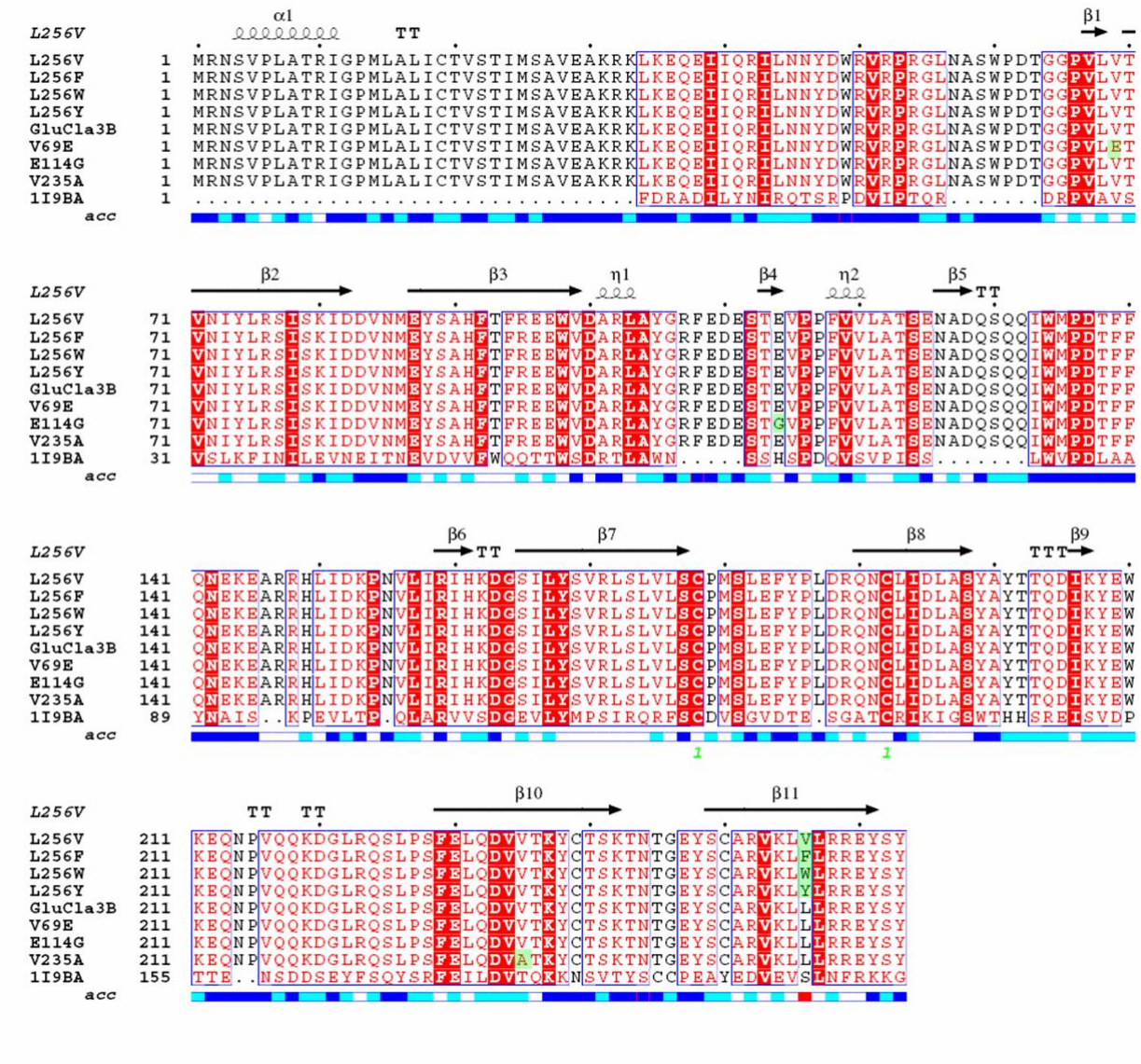

Figure 31: sequence alignment of acetylcholine binding protein (pdb 1I9B) and Mutant GluClα3B N-terminal domain.

The secondary structure of the acetylcholine binding protein is shown above the alignment. Identical residues are shown as white letters on a red background and similar residues are shown as red on a white background. The βn represents β sheets, αn represent alpha helices', TT shown above the residues indicates a sharp β-turn. The disulphide bridge caused by paired cysteine residues are illustrated with green numbers. The black dots above the sequence are space markers every 10 residues. Introduced SNPs are highlighted in green

5.2.3 Building and choosing the models

Due to the relatively low homology to the template 50 models were built using Modeller 9v2 for each of the *wt* and mutant GluClα3B N-terminal subunits and the corresponding homomeric subunits. Each putative model was attributed a Modeller-generated energy score known as the objective function (molpdf) which is essentially the sum of all the restraint functions and has no units. This score can be used to assess the energy of the protein model and the model returning the lowest energy score, for each target sequence, was selected as the best probable structure.

5.2.4 Assessing the models

Each of the potential models were assessed with Modeller 9v2 using the standard evaluate-model script. In addition to the propriety Modeller energy score, this is being minimised by the algorithm when building the model to satisfy spatial restraints, the script also generates a DOPE score, which has no units, that assesses the energy of the overall protein model . Although using different criteria, both scores are similar and should correlate, i.e. a good model will have a low energy score and a low DOPE value. An ideal model would have DOPE and energy scores similar to that of the template.

All objective function and DOPE scores- as calculated by Modeller are listed in Table 8. Due to the relatively low homology between the GluClα3B subunit and the acetylcholine binding protein some discrepancy was expected and in the case of the objective function this is the case with the template having a lower energy value compared to that of the GluClα3B subunit 5456.7 compared to >8000. This can be explained by the fact that the template sequence in significantly shorter than the query subunit and will have fewer restraint functions. The DOPE scores are considered to be a far better way of assessing the suitability of the model and in this case the scores are far more similar. The GluClα3B subunit, *wt* and mutant, show DOPE values lower then the template indicating that they are structurally more stable than the template, this is indicative of a good model.

Table 8. Evaluation of pentameric template and pentameric models by Modeller evaluation scripts.

Name	Objective Function (no units)	DOPE Score (no units)
1I9BA (template)	**5456.7**	**-118049.9**
GluClα3B	8321.2	-120249.6
L256F	8242.1	-122581.3
L256Y	8759.3	-122218.0
L256W	8519.1	-120885.8
L256V	8299.4	-120672.7
V235A	8483.8	-120598.3
E114G	8315.6	-121138.8
V69E	8557.2	-119848.9

The final selected structure (Figure 32) shows a GluClα3B single asymmetric subunit consisting of an N-terminal α-helix, two shorter 310 helices, which are arranged in a typical right-handed helical structure with each amino acid, corresponds to a 120° turn in the helices, and a core of 10 major β- strands, forming a β sandwich. The order of the β assembly conforms to the modified immunoglobin (Ig) topology noted in the nAChRs (Copley et al. 1994). There is also a short length of a β strand found prior to the β-sandwich structure known as β1 on Figure 31.

In the structure, the N and C termini are located at 'top' and 'bottom' of the pentamer, respectively. In the ion channels the transmembrane domains are at the C-terminal end of the LBD, at the 'bottom' of the GluClα3B structure, starting directly at the end of β-strands 10 and 11.

The pentameric structure fits together in a energetically favourable manner and shows the characteristic “petal like” conformation when viewed along the five–folds axis Figure 32b.

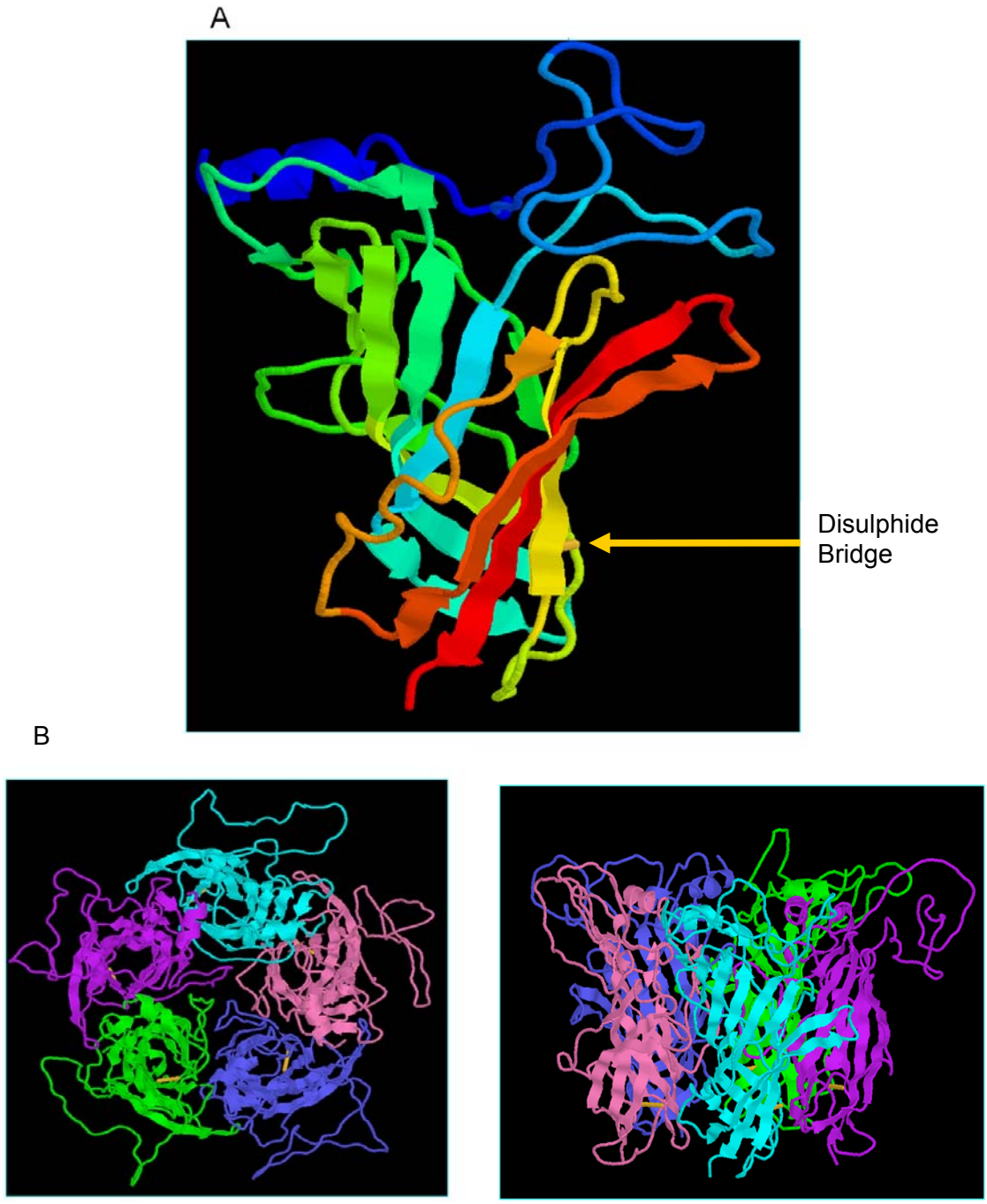

Figure 32: Model of the final *wt* GluClα3B models
A) Side view of a cartoon model of a single GluClα3B subunit. Rainbow colours illustrate the progression from the N-terminus (blue) to the C-terminus (red).
B) Top and side views of cartoon model of the pentameric structure of the *wt* channel. Each subunit is illustrated with a different colour.

5.2.5 Model of GluClα3B V69E mutant.

Amino acid 69 is a region of the GluClα3B channel that is conserved with the AChBP template (see Figure 31). Molecular modeling of the subunit shows that this residue interacts with amino acids at positions 67, 70, 96, 97, 98, 208 and 209 (see Table 9 and Figure 31). Position 69 is found in the core of the β-sandwich and as a result is not involved in any subunit-subunit interactions (Figure 33A and Figure 32).

The valine at position 69 in the *wt* channel is the first amino acid of the first β-strand, the substitution of valine to glutamic acid results in a loss of participation in the β-strand. Valine is hydrophobic, and prefers to be buried in protein hydrophobic cores. However, like isoleucine, and threonine it is C-β branched. Whereas most amino acids contain only one non-hydrogen substituent attached to their C-β carbon, these three amino acids contain two resulting in a higher density of molecular structures close to the protein backbone, meaning these amino acids are more restricted in the conformations the main-chain can adopt. Perhaps the most pronounced effect of this is that it is more difficult for these amino acids to adopt an alpha-helical conformation, though it is easy and even preferred for them to lie within beta-sheets (Betts et al. 2003). Glutamic acid is larger and negatively charged and polar, therefore more likely to be found on the outside edge of the extracellular domain, it is also more flexible in the backbone area resulting in the shortening of the first β-stand.

From the ball and stick part of Figure 34 we can see that in the V69 model the valine primarily interacts with E96, but following the V69E substitution the two negatively charged glutamic acids repel each other and the E69 leans closer to the Y208 residue.

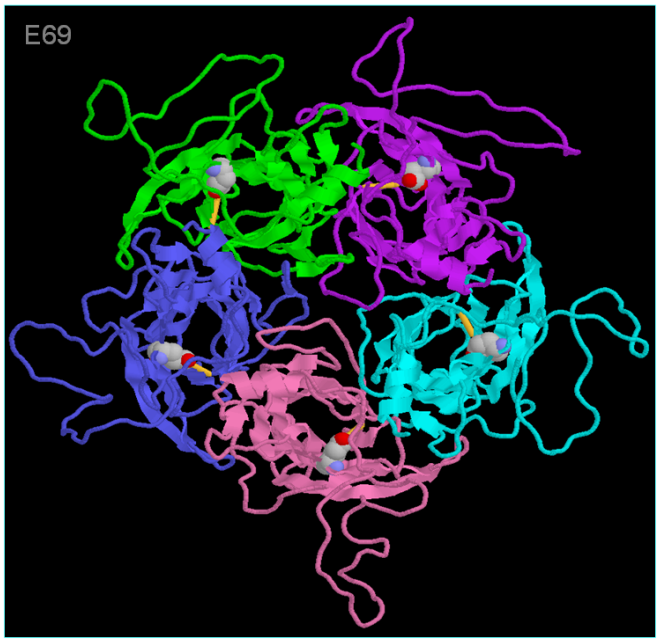

Figure 33: Model representation of the pentameric homomer of the V69E GluClα3B subunit.
The structure is shown as a cartoon representation with each subunit a different colour. The Glutamic acid at position 69 is shown as a spacefill molecule.

Position	Residue	Representative colour
69	**Valine/Glutamic acid**	**Natural grey**
68	Leucine	Blue
70	Threonine	Light Blue
208	Tyrosine	Light orange
209	Glutamic acid	Orange
96	Glutamic acid	Pink
97	Glutamic acid	Purple
98	Tryptophan	Red

Table 9. Table summarising the amino acids in contact with V69E in the GluClα3B subunit.
The table also describes the colour of the residues illustrated in Figure 34

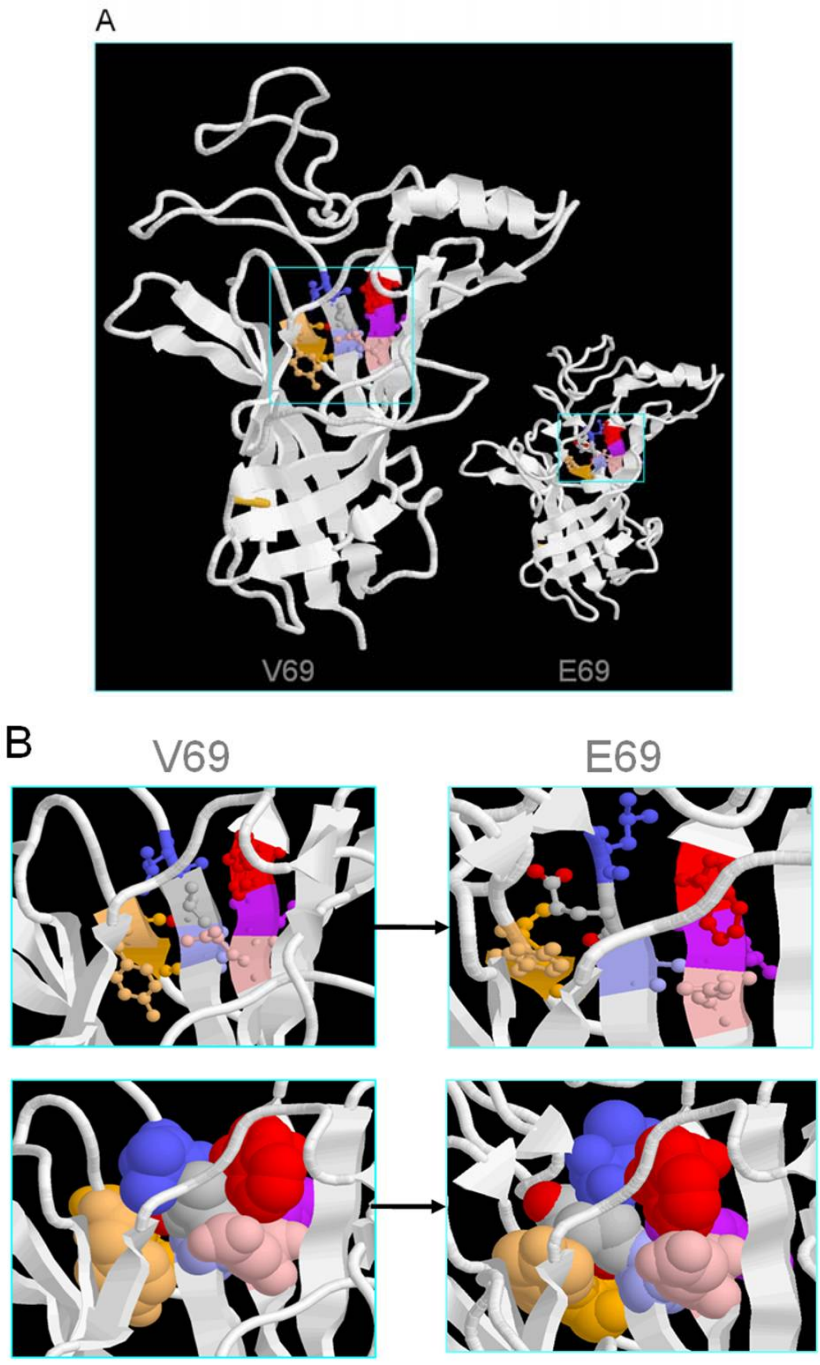

Figure 34: Model of the GluClα3B N-terminus carrying the V69E mutation
A) Cartoon model of the side view of a single GluClα3B subunit. Inset cartoon of model carrying the V69E mutation. The blue box represents the areas enlarged in 7B)
B) Cartoon model of the pentameric structure of the *wt* channel with ball and stick (top) and spacefill (bottom) illustrations of the residues including and contacting position 69. The pictures on the left are of a Valine at residue 69 and the pictures of the right are of a glutamic acid at position 69.

5.2.6 Model of GluClα3B E114G mutant

Residue 114 is found in an area of the subunit that has no direct conservation with the template, but is in the middle of an otherwise conserved area. It has a limited range of interactions, but according to the model interacts primarily with the proline at position 6.It is also relatively close to the edge of the subunit but is too high to be involved in subunit-subunit interactions.

Glutamic acid is a negatively charged, polar amino acid. Being charged and polar, glutamatic acid generally prefers to be on the surface of proteins, exposed to an aqueous environment. (Betts et al. 2003). Any interaction between E114 and P6 is lost when the E114G substitution takes place. Glycine is a unique amino acid in that in contains hydrogen as its side chain (rather than a carbon as is the case in all other amino acids). This means that there is much more conformational flexibility in glycine. What this means is that glycine can reside in parts of protein structures that are forbidden to all other amino acids (e.g. tight turns in structures). In the case of this mutation it is the fact that glycine is much smaller than glutamic acid that causes change. From Figure 36 we can see that the original amino acid meets the P6, but the glycine is so small it is barely visible after the substitution.

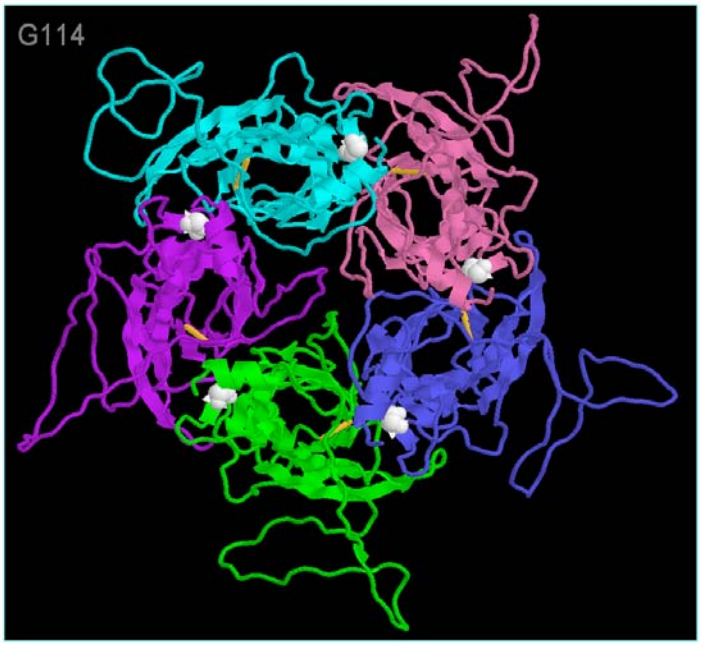

Figure 35: Model representation of the pentameric homomer of the E114G GluClα3B subunit.
The structure is shown as a cartoon representation with each subunit a different colour. The glycine at position 114 is shown as a spacefill molecule.

Position	Residue	Representative colour
114	**Glutamic acid/ Glycine**	**Natural grey**
113	Threonine	purple
115	Valine	Light purple
6	Proline	Green
7	Leucine	Light green

Table 10. Table summarising the amino acids in contact with E114G in the GluClα3B subunit.
The table also describes the colour of the residues illustrated in Figure 34

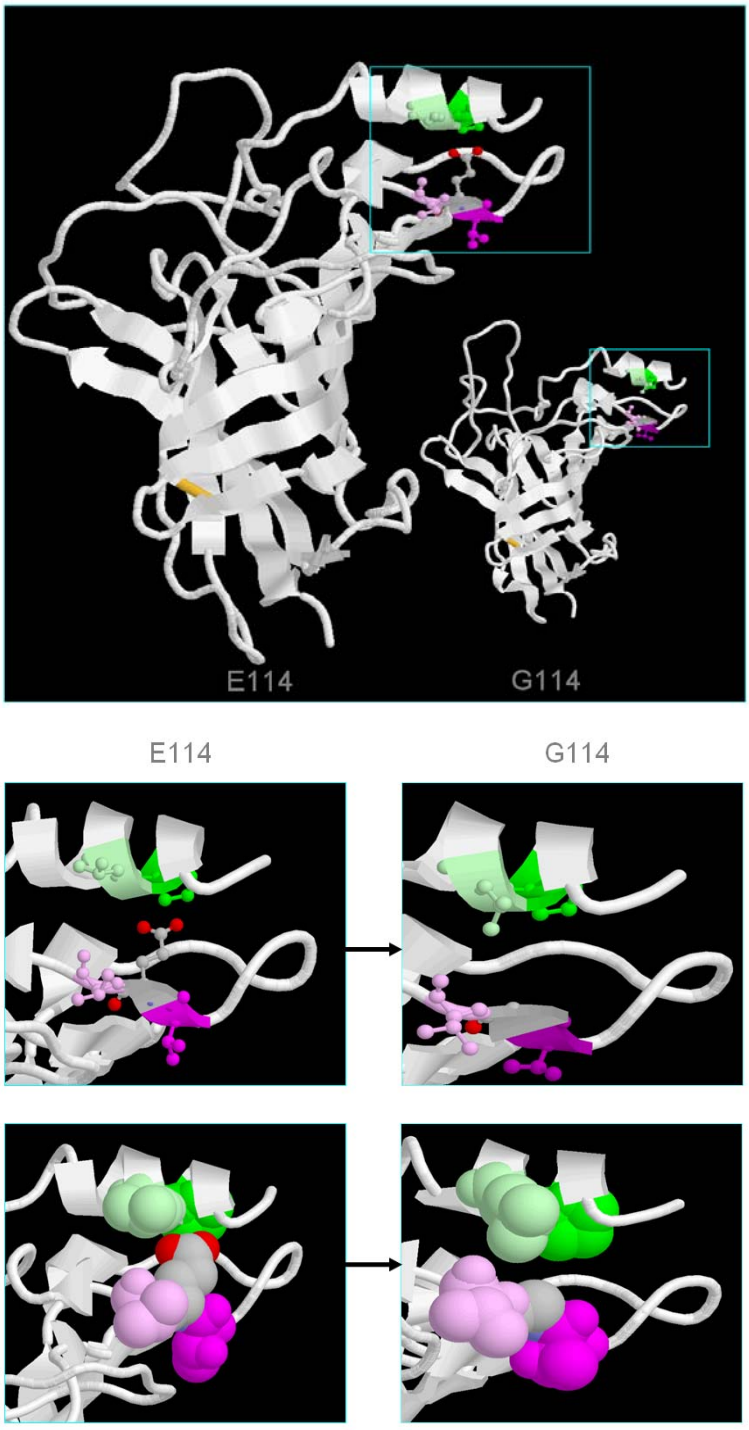

Figure 36: Model of the GluClα3B N-terminus carrying the E114G mutation
A) Cartoon model of the side view of a single GluClα3B subunit. Inset cartoon of model carrying the E114G mutation. The blue box represents the areas enlarged in 8B)
B) Cartoon model of the pentameric structure of the *wt* channel with ball and stick (top) and spacefill (bottom) illustrations of the residues including and contacting position 114. The pictures on the left are of a glutamic acid at residue 114 and the pictures of the right are of a glycine at position 114.

5.2.7 Model of GluClα3B V235A mutant.

Position 235 is found at the bottom of the β-sandwich in a highly conserved area of β10 the ninth β-strand of the sandwich. On the pentameric structure it is found on the outside facing edge and interacts primarily with residues on the final β11 strand. The most important of these residues is L256. The substitution of a valine to an alanine is a relatively minor substitution, whereas valine is hydrophobic and aliphatic its position at the heart of a β-strand indicates a more structural purpose and the substitution to alanine which is not particularly hydrophobic though neither is it polar. From the model pictures we can see there is little or no effect of the substitution on the surrounding amino acids.

Position	Residue	Representative colour
235	**Valine / Alanine**	**Natural grey**
234	Valine	Light blue
236	Threonine	Blue
254	Lysine	Pink
255	Leucine	Purple
256	Leucine	Red

Table 11. Table summarising the amino acids in contact with V235A in the GluClα3B subunit

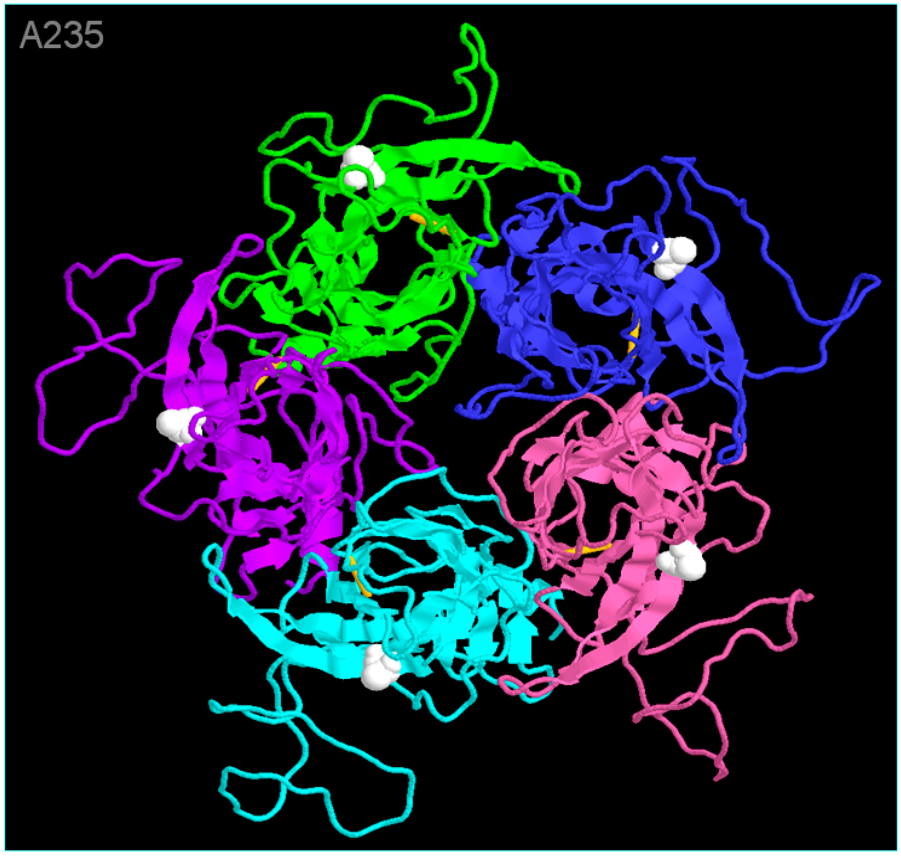

Figure 37: Model representation of the pentameric homomer of the V235A GluClα3B subunit.

The structure is shown as a cartoon representation with each subunit a different colour. The alanine at position 235 is shown as a spacefill molecule

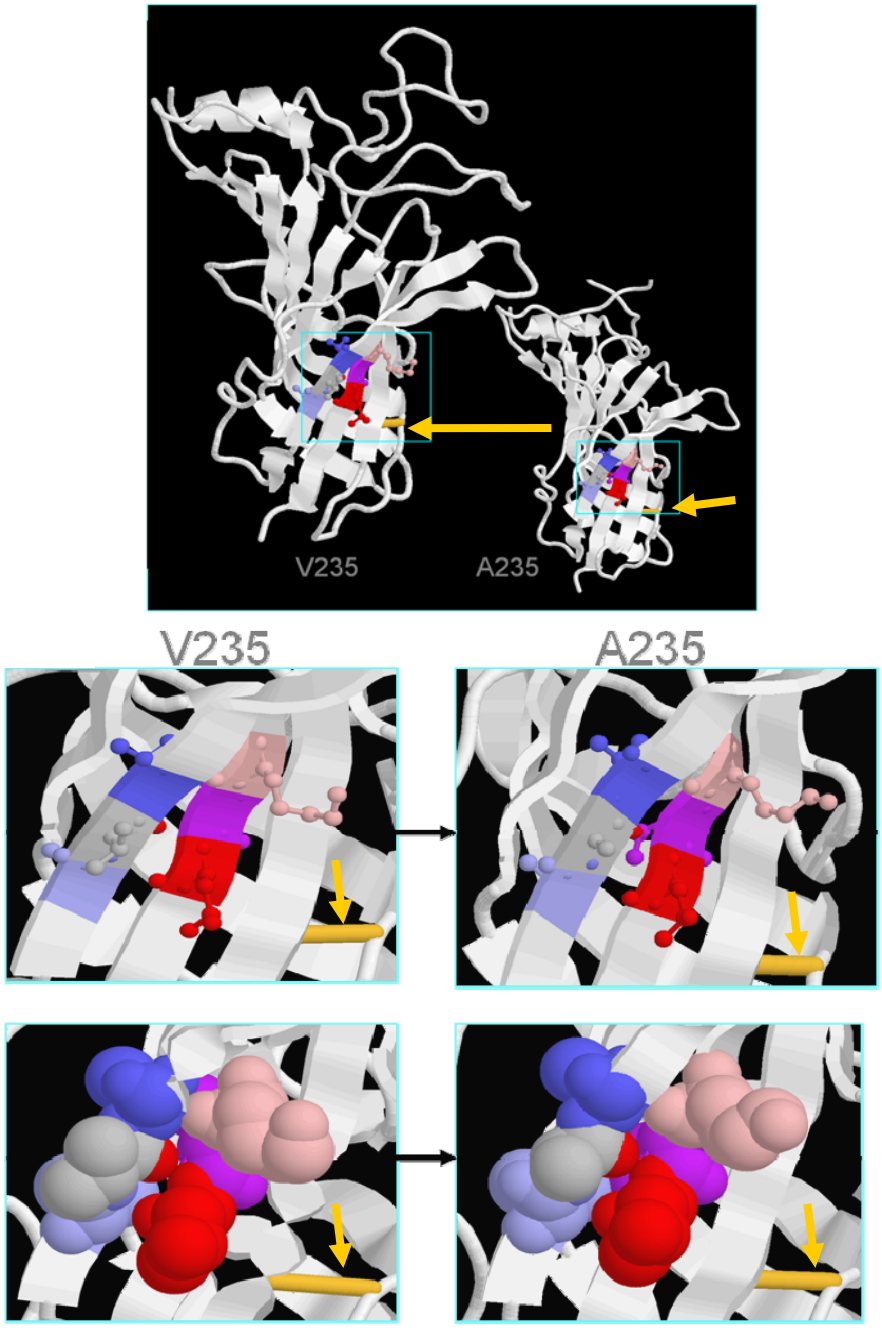

Figure 38: Model of the GluClα3B N-terminus carrying the V235A mutation
A) Cartoon model of a single GluClα3B subunit. Inset cartoon of model carrying the V235A mutation. The blue box represents the areas enlarged in 9B). Yellow arrows point to the position of the disulphide bridge.
B) Cartoon model of the pentameric structure of the *wt* channel with ball and stick (top) and spacefill (bottom) illustrations of the residues including and contacting position 235. The pictures on the left are of a valine at residue 235 and the pictures of the right are of an alanine at position 235.

5.2.8 Model of GluClα3B L256F, L256Y, L256W and L256V mutants

The leucine at position 256 is adjacent to a relatively large number of amino acids and in the pentameric structure is found in the centre of the outside face of the channel. The two residues that are most closely in association with the Leucine 256 are V235 and L193. In the *wt* channel the leucine appears to be neither attracted nor repulsed by any of its neighbours, which is understandable as they are all relatively un-reactive side-chains. Being hydrophobic, leucine prefers to be buried in protein hydrophobic cores. It also shows a preference for being within α-helices more so than in β-strands (Betts et al. 2003), neither of which condition is present in the *wt* strand.

The modelling of the substitution of leucine to phenylalanine results in an obvious interaction with the neighbouring polar amino acid asparagine at residue 191 in which an attraction seems to be occurring (see Figure 40). This phenomenon is also seen with the L256V and L245Y mutations (see Figure 41 and Figure 42), strangely the L256W has no apparent effect on the N191 residue.

Phenylalanine, tryptophan and tyrosine are all aromatic and hydrophobic whereas valine is not aromatic but is still hydrophobic.

The L256V mutation causes attraction of N191 and also a resulting change in orientation of the polar K254 residue, which is also seen in all the L256 mutants. There is no change in any interaction with the V235 residue, with the exception of a minor twisting due to the L256Y and L256W substitutions.

Table 12. Table summarising the amino acids in contact with L256 in the GluClα3B subunit

Position	Residue	Representative colour
256	**Leucine/ mutant**	**Natural grey**
254	Lysine	Pink
255	Leucine	Purple
257	Leucine	Red
235	Valine	Cyan
234	Valine	Light blue
236	Threonine	Blue
191	Asparagine	Green
192	Cysteine	Yellow
193	Leucine	Orange

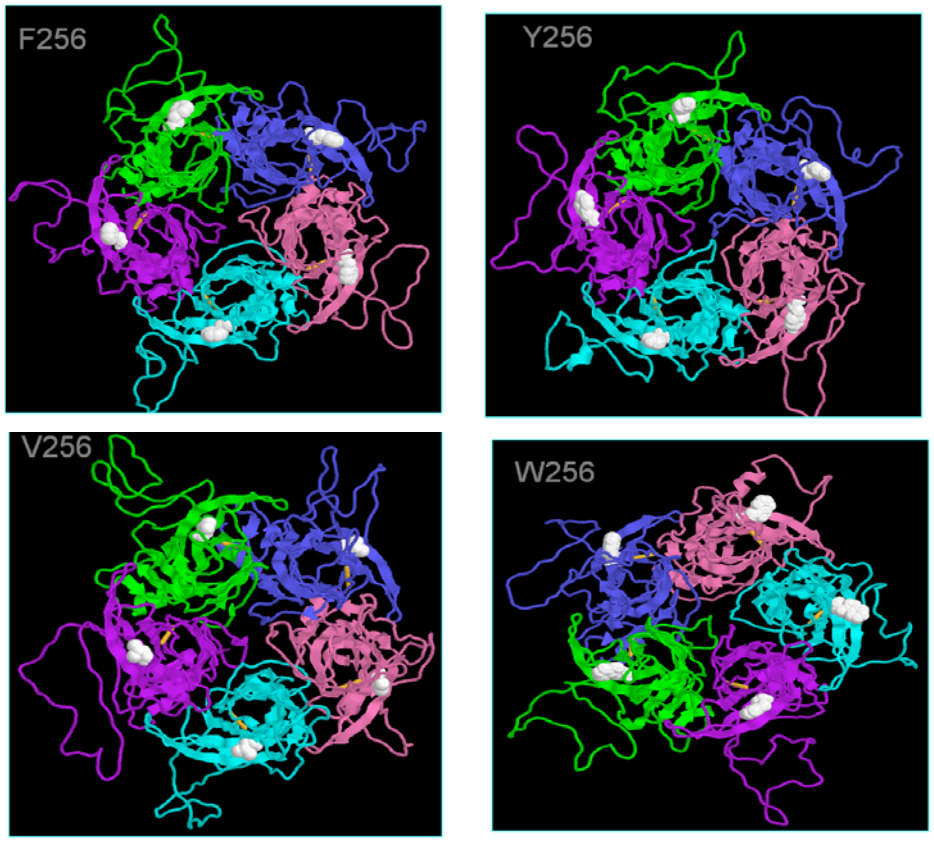

Figure 39: Model representation of the pentameric homomer of the L256 mutant GluClα3B subunits.
The structure is shown as a cartoon representation with each subunit a different colour. The residues at position 256 are shown as spacefill molecules.

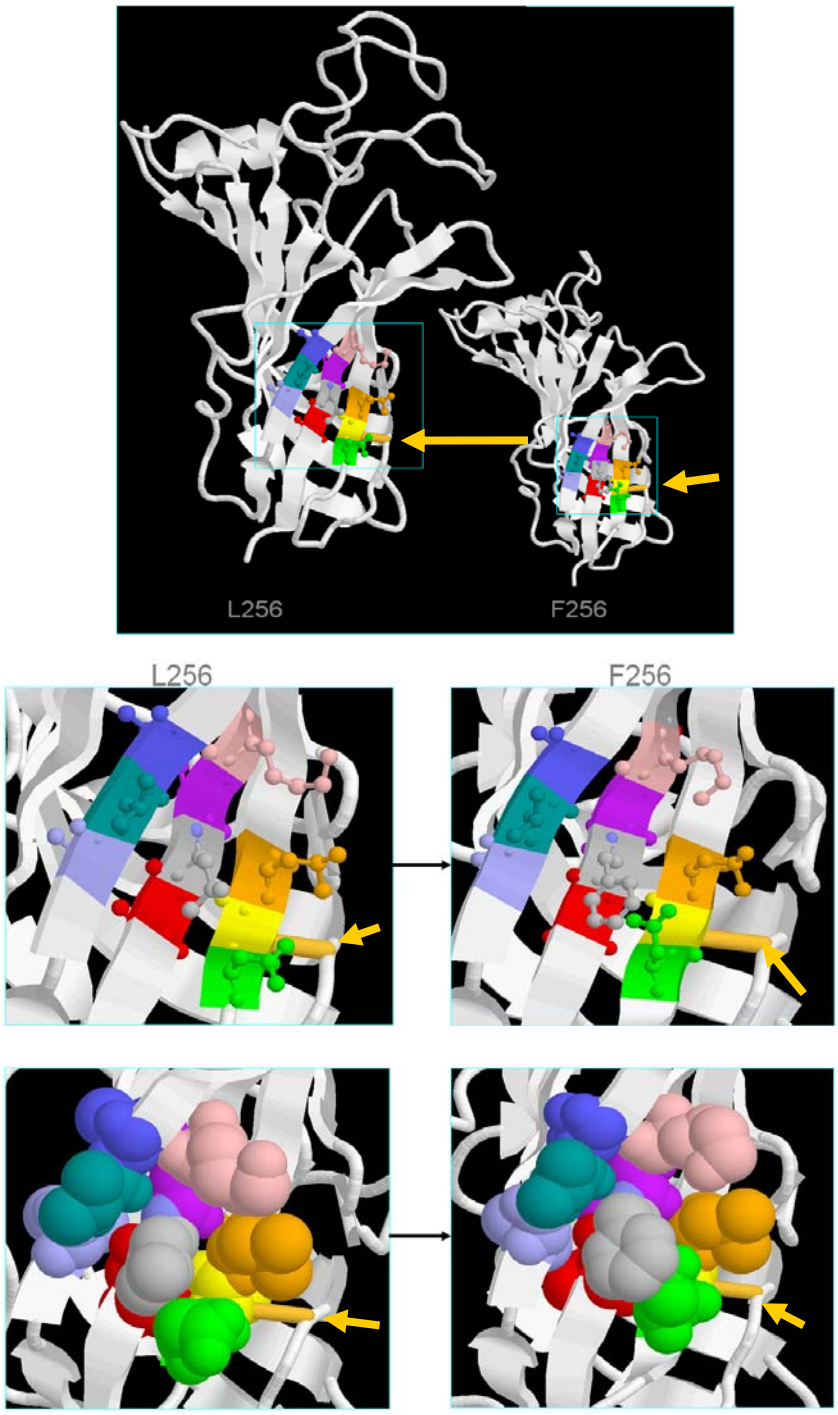

Figure 40: Model of the GluClα3B N-terminus carrying the L256F mutation
A) Cartoon model of the side view of a single GluClα3B subunit. Inset cartoon of model carrying the L256F mutation. The blue box represents the areas enlarged in 10B) Yellow arrows point to the position of the disulphide bridge
B) Cartoon model of the pentameric structure of the *wt* channel with ball and stick (top) and spacefill (bottom) illustrations of the residues including and contacting position 256. The pictures on the left are of a leucine acid at residue 256 and the pictures of the right are of a phenylalanine at position 256.

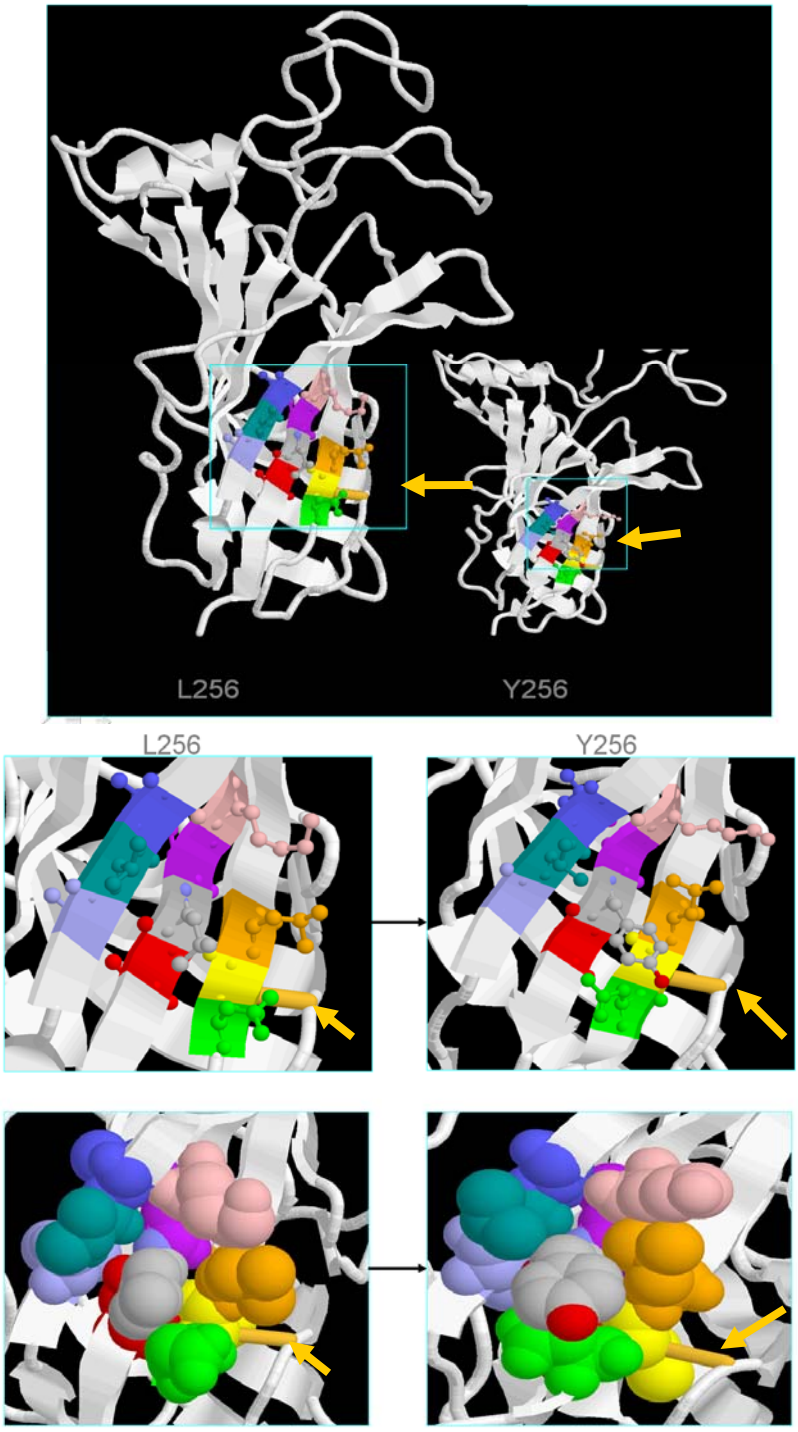

Figure 41: Model of the GluClα3B N-terminus carrying the L256Y mutation
A) Cartoon model of the side view of a single GluClα3B subunit. Inset cartoon of model carrying the L256Y mutation. The blue box represents the areas enlarged in 11B) Yellow arrows point to the position of the disulphide bridge
B) Cartoon model of the pentameric structure of the *wt* channel with ball and stick (top) and spacefill (bottom) illustrations of the residues including and contacting position 256. The pictures on the left are of a leucine acid at residue 256 and the pictures of the right are of a tyrosine at position 256.

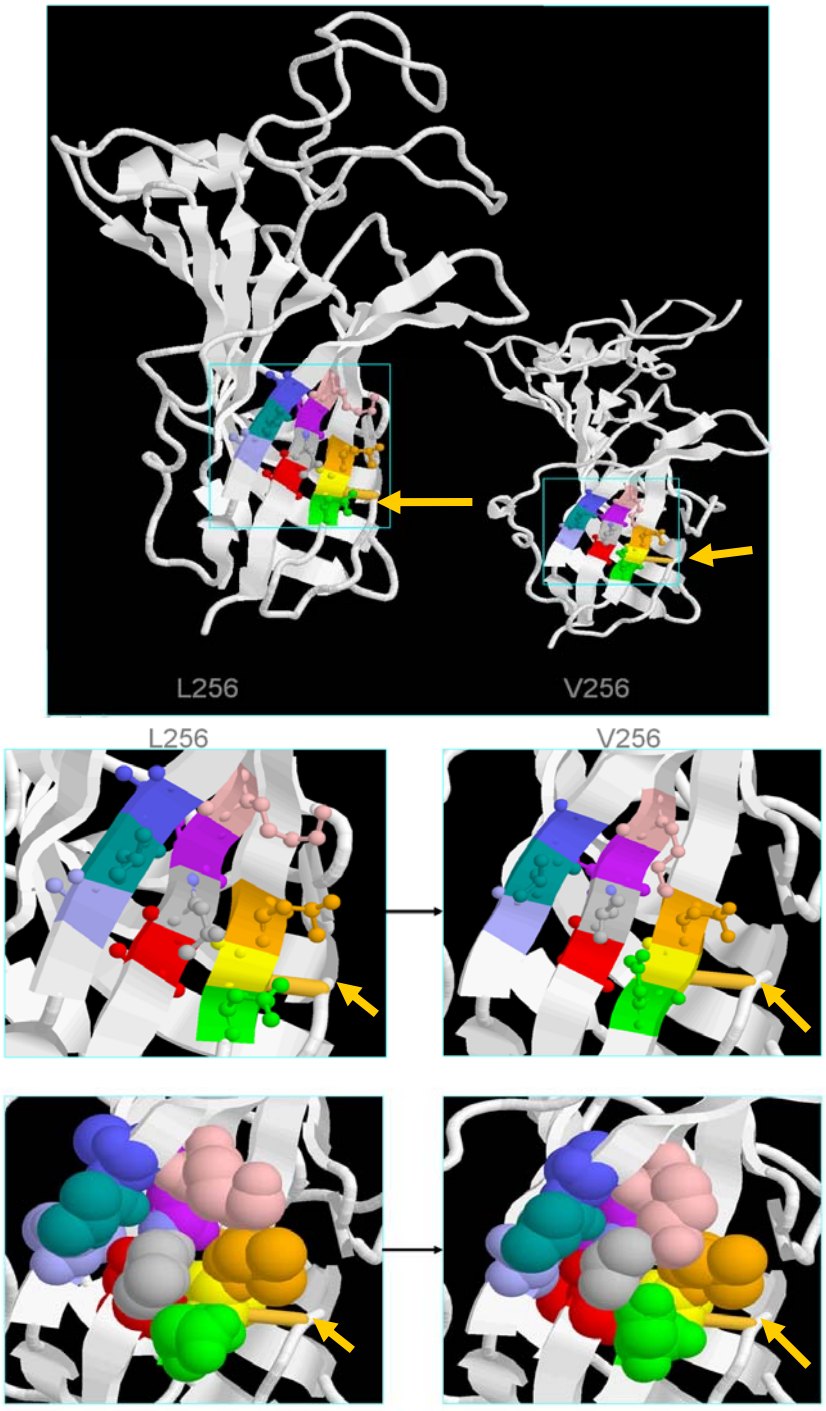

Figure 42: Model of the GluClα3B N-terminus carrying the L256V mutation
A) Cartoon model of the side view of a single GluClα3B subunit. Inset cartoon of model carrying the L256V mutation. The blue box represents the areas enlarged in 12B) Yellow arrows point to the position of the disulphide bridge
B) Cartoon model of the pentameric structure of the *wt* channel with ball and stick (top) and spacefill (bottom) illustrations of the residues including and contacting position 256. The pictures on the left are of a leucine acid at residue 256 and the pictures of the right are of a valine at position 256.

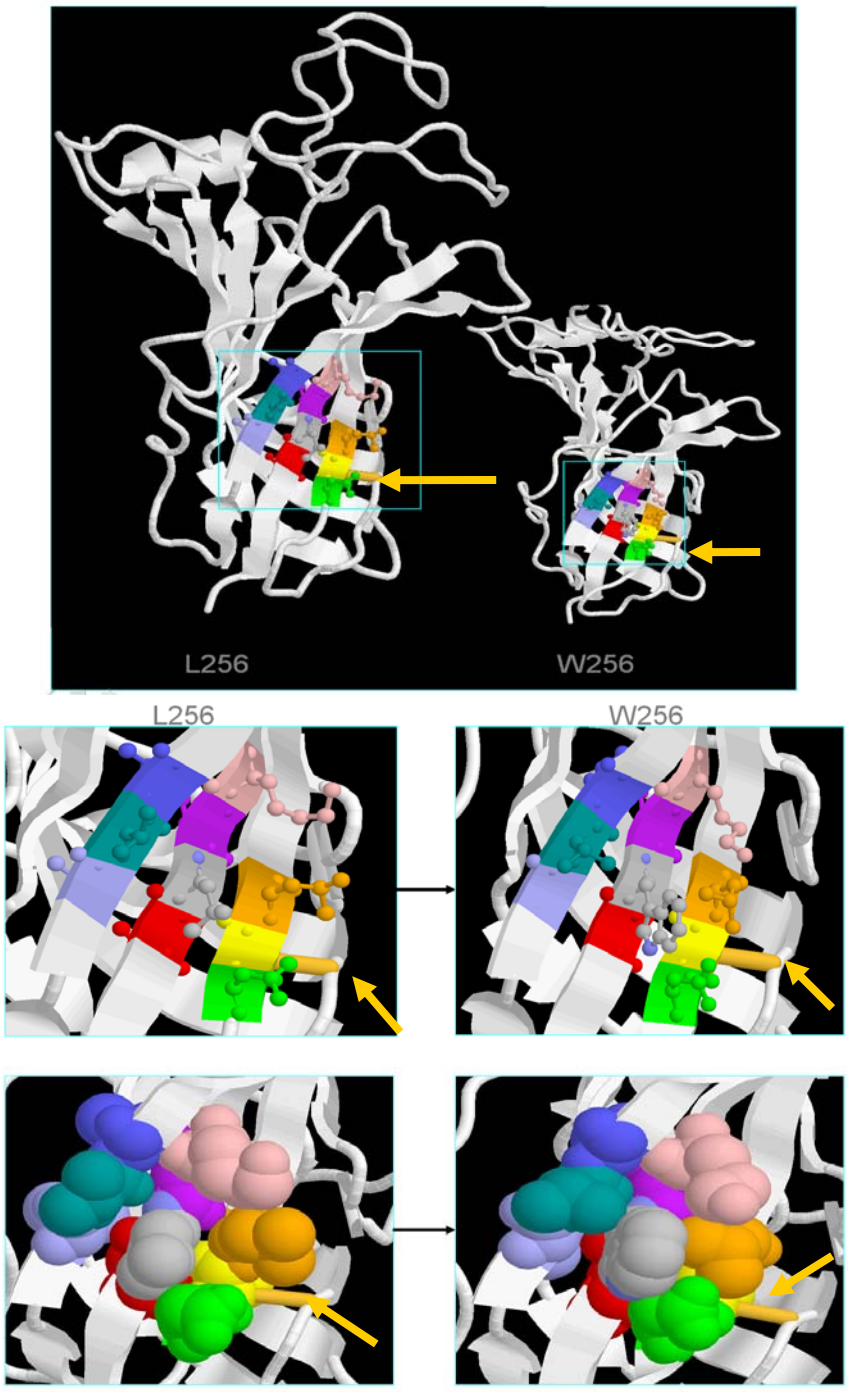

Figure 43: Model of the GluClα3B N-terminus carrying the L256W mutation
A) Cartoon model of the side view of a single GluClα3B subunit. Inset cartoon of model carrying the L256V mutation. The blue box represents the areas enlarged in 13B) Yellow arrows point to the position of the disulphide bridge
B) Cartoon model of the pentameric structure of the *wt* channel with ball and stick (top) and spacefill (bottom) illustrations of the residues including and contacting position 256. The pictures on the left are of a leucine acid at residue 256 and the pictures of the right are of a tryptophan at position 256.

5.3 Discussion

Comparative modeling is based on the observation that in protein families, structure is more conserved than sequence (Russell et al. 1997). Consequently, the unknown structure of a protein can be approximated “by comparison” to the known structure of another member of the “fold” family (Ernst et al. 2003).

The models created in this chapter can only be as accurate as their template allows them to be, and despite the production of higher resolution nAChR channels being published the highest alignment match against the GluClα3B subunit was the Acetylcholine-binding protein (AChBP), a soluble protein found in the snail *Lymnaea stagnalis* (Smit et al. 2001). It is produced and stored in glial cells, and released in an acetylcholine-dependent manner into the synaptic cleft, where it modulates synaptic transmission. A mature AChBP is 205- 210 residues long and forms a stable homopentamer. It aligns well, the GluClα3B subunit but also with the N-terminal domains of pentameric LGICs and lacks the transmembrane and intracellular domains present in the superfamily (Smit et al. 2001). Of all the LGIC AChBP is, understandably, most closely related to the α-subunits of the nAChRs (Brejc et al. 2001), which are more similar in length and have a considerably higher level of homology than that of the GluCls or any other LGIC. The AChBP structure, thus, in principle is a valid template and presently the only one available for modeling all other superfamily members, especially due to the fact that the newer crystal structures have a higher resolution they also have ACh bound to them (Ernst et al. 2003). It is very difficult to say how accurate models are when they have such a low level of homology to the template, just 17% identity between GluClα3B and the AChBP at first glance, although this increases to 30% when you discount the extra 60 amino acids present in the *H. contortus* sequence. Even mapping nAChRs onto the AChBP has its difficulties with homology, there have also been problems with modelling GABA receptors. In the $GABA_A$ receptor subunits there is an estimated 60–75% of amino acid residues possess structural equivalents in the modeling template AChBP, and like the GluClα3B most variation is found at beginnings and ends of the secondary structure motifs, through the lengths and conformations of loops, and in number, placement and length of shorter β-strands and helices (Brejc et al. 2001; Ernst et al. 2003). Therefore lengths of residues within secondary structures are more reliably modeled, than those at the ends.

Apart from the alignment issues, which can be overcome with careful manual observation of the alignment, some areas of the AChBP structure are probably anomalous within the LGIC family. For instance, L2 as well as L7 (the “cys-loop”) are located at the “bottom” (solvent exposed) surface in AChBP. In the receptors these regions are associated with the *trans*-membrane domain (Kash et al. 2003) and possibly with the membrane, certainly not exclusively with the aqueous surroundings as in AChBP. In these segments the AChBP structure thus is not an ideal template, which also is reflected by the lack of sequence conservation in L7 area (Brejc et al. 2001). The C-terminus of the AChBP corresponds to the C-terminal end of the receptor extracellular domain. It has been shown recently that comparative models of the extracellular domain can be combined with models of the transmembrane domain without difficulties (Trudell 2002; Kash et al. 2003). Thus, the C-end of the comparative models appears to be reliable (Ernst et al. 2003). Therefore it was important to ensure that all mutations carried out in the modeling experiment were carried in areas of not only reasonably high homology, but in areas that correspond to the secondary structure. All of the mutations investigated correspond to areas within β-strands, with mutations at position 69, 235 and 256 within the β sandwich and therefore supported by interactions between β-strands. Confidence is especially high in the information gathered from mutations in the C-terminal area such as those found at position 235 and 256.

The models generated of the GluClα3B subunit show a sensible level of visual similarity to the template and also to the other known LGIC structures (see Figure 43). Moreover the mathematical assessments carried out indicate that the protein folded in an energetically favourable way. The fact that the DOPE scores for the pentameric models are lower for the models gives a great deal of confidence to the final product. There are areas of the models that should not be fully trusted. As previously mentioned the GluClα3B subunit is 60 amino acids longer than the template resulting in areas of no homology. Although these areas have been folded mathematically, they still appeared less structured than the rest, as in evidence in all the pentameric figures. This area is obviously folded slightly differently in each subunit, and therefore should be dismissed as an area of study in modelling until a better template is produced.

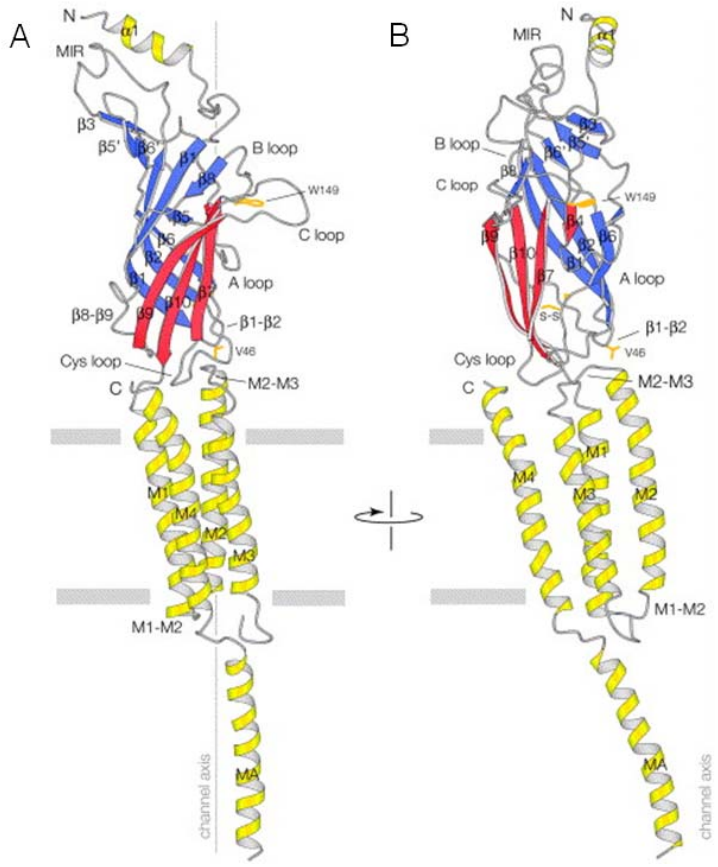

Figure 44: Diagram of nAChR subunit at 4 Å

Ribbon diagrams of a single subunit, viewed parallel with the membrane plane, in orientations such that the central axis of the pentamer (vertical line) is (a) at the back and (b) to the side. The α-helices are in yellow; the β-strands composing the β-sandwich are in blue (inner) and red (outer). Locations of the N and C termini, Trp149, V46, the Cys-loop disulphide bridge and the membrane (horizontal bars) are indicated. Part of the M3–M4 loop (connecting MA to M3) is missing (Unwin 2005)

Homology modelling of the GluClα3B mutants has proven interesting and useful. Of the mutants modelled, it was interesting to see that the L256F mutant and the V235A which were both observed, together in the same population of Ivermectin resistant *Cooperia oncophora* (Njue et al. 2004), are actually in close contact *in situ.* The L256F mutation is responsible for a three fold loss of sensitivity to glutamate in functional channels and a 6.5 fold decrease in sensitivity to IVM, and although the V235A mutation apparently had no effect alone on either response to glutamate or IVM, it may have an effect when both mutations are expressed together. It raises the question of what caused these mutations *in vivo*, although both mutations and

indeed, the E114G mutation that was also observed in the IVR *C. oncophora* were all due to single base mutations, and therefore it is reasonable to assume the probability of mutation is quite high, but the probability that two substitutions occurred in the sequence, that produced two amino acid substitutions that directly interact with one another is lower, but still well within the realms of possibility.

The mutations at position 256 illustrate the greatest conformational changes seen by any of the mutants. The L256 holds an important position within the structure of the β-sandwich. This position carries many neighbours including V235 as already discussed; it is also adjacent to C192 which holds one half of the disulphide bridge, one of the major structural properties of the ligand binding domain. Substitution of L256 to phenylalanine and tryptophan cause the greatest pharmacological changes of the channel, demonstrating a 6 fold decrease in sensitivity to IVM (and a 3-fold loss to glutamate in the case of L256F), this is not seen with the valine substitution and to a lesser extent with tyrosine. From observing the models there is no obvious reason for this, no strong interaction not present with valine or tyrosine. However it is clear to see that the larger the amino acid side chain the more sensitivity is lost, therefore it is reasonable to assume that steric hindrance may be to blame for altering the adjacent N191 and C192 residues and therefore altering the disulphide bridge. Although the 256 mutation is in an ideal area of the subunit for study i.e close to the reliable C-end of the extracellular domain, within secondary structure with close proximity to a disulphide bridge, we cannot rely of the modelling for showing individual atomic interactions, the template itself is only at a resolution of 2.7Å. Therefore in reality the small amino acid interactions may be inaccurate, but we can be confident of the positioning of the residues within the structure.

The V69E mutation which carries a change from a C-β branched, neutral, hydrophobic amino acid to a negatively charged polar molecule results in a loss of the start of the β2 which is the first β-strand of the β-sandwich. The change in mutation doesn't appear to have a significant change on the position of any surrounding residues but as previously discussed this may not be the case, but a genuine change is seen in *in vitro* experiments with the K_d of GluClα3B to IVM is more than doubled from 0.35 ± 0.10 nM to 0.8 ± 0.24 nM with the V69E substitution, this is not a big change, but it is possible that the loss of structural integrity of caused by the shortening of the β2-strand is enough to create a small effect on the binding ability of IVM.

Chapter 6: Final discussion

The aim of this research was to assess and characterize the pharmacology of the *H. contortus* GluClα3B subunit and investigate the effects of specific single amino acid substitutions on subunit pharmacology in respect to glutamate, the natural agonist, and the anthelmintic drug ivermectin. Prior to this study it was known that GluClα3B formed homomeric channels that responded to glutamate and IVM. It was also known that different mutations in the glutamate gated chloride channels of other nematode and insect species conferred a level of resistance to IVM. This study introduced these mutations and others into *H. contortus* GluClα3B cDNA which was expressed either in *Xenopus* oocytes for electrophysiological readings or COS-7 cells for ligand binding studies. The N-terminal domain of the GluClα3B was visualized by homology modeling using the related acetylcholine binding protein as a template in order to characterize the mutations and their effects on the channel further.

One mutation found in IVR *C. oncophora* L256F confers a 3-fold loss of sensitivity to glutamate and a 6.5 fold loss of sensitivity to IVM. This mutation is found in the C-terminal area of the extracellular region of the channel and, from homology modeling, we know it lies in close proximity and possibly interferes with another candidate mutation V235A, and the cysteine residue at position 192 which forms one side of the structurally significant disulphide bridge. Further introduction of different mutations at this position showed the larger the substituted amino acid, the greater the effect on IVM sensitivity, indicating that the effect of the mutation is caused by steric hindrance pushing the surrounding amino acids apart, including the C192 thus mediating the effect on channel activity. There is currently no available data to know whether this loss of sensitivity is sufficient to cause IVM resistance *in vivo.*

Another amino acid substitution (T300S) results in the prohibition of a functional channel in *Xenopus* oocytes, the reason for this currently unknown although it has been shown that the protein when produced in mammalian COS-7 cells is able to bind IVM with high affinity.

Although significant progress has been made in understanding the effects of the mutants illustrated here, no mutant that has been investigated causes complete IVM

resistance, therefore no significant answer to the problem of IVM resistance has been forthcoming. It appears that the cause of IVM resistance is not going to be as simple as in the case of BZ resistance, but screening of candidate mutations should, ideally, continue. Screening between IVS and IVR strains in the GluCl subunits of various nematodes such as *D. immitis, A. suum* and further study of *H. contortus* will, hopefully, unearth more polymorphisms that can be investigated and found to confer resistance. The creation of a homology model of the N-terminal region of the GluClα3B will allow a more targeted approach to designing mutations that may have an effect on ligand binding.

It is increasing likely that the cause of IVM resistance is multigenic. A combination of several factors such as reduced ivermectin sensitivity (like L256F) with actions by P-glycoproteins and other factors may be enough to confer resistance. Some P-glycoproteins and multidrug resistance proteins have been found to act as membrane transporters which pump drugs from the cell. It has been suggested that a disruption of the *mdrla* gene, which encodes a P-glycoprotein in mice, results in hypersensitivity to ivermectin. Some of the genes encoding members of the P-glycoprotein family are known to exist in nematodes. Some data suggests that a P-glycoprotein may play a role in ivermectin resistance in *H. contortus* (Xu et al. 1998). It is clear that in *C. elegans* the ML have multiple GluCl targets and so high level resistance requires mutations in multiple genes. This may explain why the avermectins have been relatively long lived effective antiparasitic drugs as a single mutation in one of the targets is not enough to confer resistance (Dent et al. 1997; Martin et al. 1998). However, there are some questions concerning the applicability of these very elegant *C. elegans* studies to parasitic species. It is unlikely that a reduction in ML sensitivity of > 4000 fold is necessary to cause clinical resistance and it may be that further studies on lower level resistance might yield better clues to its mechanism in parasites. Many of the *C. elegans* mutants are null, or functional nulls, and this complete loss of channel function has marked behavioral and other effects (Dent et al. 2000; Cook et al. 2006) that might make them too deleterious to allow parasites to survive in the wild. It is also interesting that the *C. elegans* screens have not identified a role for the P-glycoproteins (P-gp) in ML resistance, despite the evidence from parasites (Kerboeuf et al. 2003; von Samson-Himmelstjerna et al. 2005).

Understanding the molecular pharmacology of the GluCl is highly important because the GluCls are only found in invertebrates and therefore make an ideal broad spectrum drug target for insecticides and endectocides. An in-depth knowledge of how the channels function is essential for not only tracking and understanding resistance, but is also useful for modifying exsisting compounds and directing new drug research.

References

Adelsberger, H., Lepier, A., Dudel, J. (2000). "Activation of rat recombinant $\alpha_1\beta_2\gamma_{2s}$ $GABA_A$ receptor by the insecticide ivermectin." European Journal of Pharmacology **394**(2): 163-170.

Akabas, M. H., C. Kaufmann, et al. (1994). "Identification of acetylcholine receptor channel-lining residues in the entire M2 segment of the alpha subunit." Neuron **13**(4): 919-27.

Ali, A. and J. K. Nayar (1985). "Activity of an avermectin insecticide, Abamectin (MK-936), against mosquitoes and chironomid midges in the laboratory." J Am Mosq Control Assoc **1**(3): 384-6.

Altschul, S. F., T. L. Madden, et al. (1997). "Gapped BLAST and PSI-BLAST: a new generation of protein database search programs." Nucleic Acids Res **25**(17): 3389-402.

Altun, Z. F. and D. H. Hall (2005). Hermaphrodite anatomy. Handbook of C. elegans anatomy. WormAtlas.

Amoussou, P.-L., J. Ashurst, et al. (2004). Broadly based resistance to nematodes in the rice and potato crops of subsistence farmers Plant Sciences Research Programme Highlights & Impact Report. . **Crop Transformation**.

Arena, J. P., K. K. Liu, et al. (1991). "Avermectin-sensitive chloride currents induced by Caenorhabditis elegans RNA in Xenopus oocytes." Mol Pharmacol **40**(3): 368-74.

Arena, J. P., K. K. Liu, et al. (1995). "The mechanism of action of avermectins in Caenorhabditis elegans: correlation between activation of glutamate-sensitive chloride current, membrane binding, and biological activity." J Parasitol **81**(2): 286-94.

Arena, J. P., K. K. Liu, et al. (1992). "Expression of a glutamate-activated chloride current in Xenopus oocytes injected with Caenorhabditis elegans RNA: evidence for modulation by avermectin." Brain Res Mol Brain Res **15**(3-4): 339-48.

Aubry, M. L., P. Cowell, et al. (1970). "Aspects of the pharmacology of a new anthelmintic: pyrantel." Br J Pharmacol **38**(2): 332-44.

Avery, L. and H. R. Horvitz (1989). "Pharyngeal pumping continues after laser killing of the pharyngeal nervous system of C. elegans." Neuron **3**(4): 473-85.

Avery, L. and H. R. Horvitz (1990). "Effects of starvation and neuroactive drugs on feeding in Caenorhabditis elegans." J Exp Zool **253**(3): 263-70.

Awadzi, K., K. Y. Dadzie, et al. (1985). "The chemotherapy of onchocerciasis X. An assessment of four single dose treatment regimes of MK-933 (ivermectin) in human onchocerciasis." Ann Trop Med Parasitol **79**(1): 63-78.

Awapara, J. (1950). "Occurrence of free gamma-aminobutyric acid in brain and its formation from L-glutamic acid." Tex Rep Biol Med **8**(4): 443-7.

Awapara, J., A. J. Landua, et al. (1950). "Free gamma-aminobutyric acid in brain." J Biol Chem **187**(1): 35-9.

Bamber, B. A., A. A. Beg, et al. (1999). "The Caenorhabditis elegans unc-49 locus encodes multiple subunits of a heteromultimeric GABA receptor." J Neurosci **19**(13): 5348-59.

Bamber, B. A., J. E. Richmond, et al. (2005). "The composition of the GABA receptor at the Caenorhabditis elegans neuromuscular junction." Br J Pharmacol **144**(4): 502-9.

Bamber, B. A., R. E. Twyman, et al. (2003). "Pharmacological characterization of the homomeric and heteromeric UNC-49 GABA receptors in C. elegans." Br J Pharmacol **138**(5): 883-93.

Baron, S., R. C. Peake, et al. (1996). Section 4. Parasitology. Medical Microbiology. S. Baron, The University of Texas Medical Branch at Galveston

Bartos, M., D. Rayes, et al. (2006). "Molecular determinants of pyrantel selectivity in nicotinic receptors." Mol Pharmacol **70**(4): 1307-18.

Basanez, M. G., S. D. Pion, et al. (2006). "River blindness: a success story under threat?" PLoS Med **3**(9): e371.

Bauer, C., J. C. Merkt, et al. (1986). "Prevalence and control of benzimidazole-resistant small strongyles on German thoroughbred studs." Vet Parasitol **21**(3): 189-203.

Beckstein, O. and M. S. Sansom (2004). "The influence of geometry, surface character, and flexibility on the permeation of ions and water through biological pores." Phys Biol **1**(1-2): 42-52.

Berman, H. M., J. Westbrook, et al. (2000). "The Protein Data Bank." Nucleic Acids Res **28**(1): 235-42.

Betts, M. J. and R. B. Russell (2003). Amino acid properties and consequences of subsitutions.
. In Bioinformatics for Geneticists. M. R. Barnes and I. C. Gray. Wiley.

Beugnet, F., D. Kerboeuf, et al. (1996). "Use of free living stages to study the effects of thiabendazole, levamisole, pyrantel and ivermectin on the fine structure of Haemonchus contortus and Heligmosomoides polygyrus." Vet Parasitol **63**(1-2): 83-94.

Bird, A. F. and J. Bird (1991). The Structure of Nematodes. San Diego.

Blackhall, W. J., J. F. Pouliot, et al. (1998). "Haemonchus contortus: selection at a glutamate-gated chloride channel gene in ivermectin- and moxidectin-selected strains." Exp Parasitol **90**(1): 42-8.

Blaxter, M. (1998). "Caenorhabditis elegans is a nematode." Science **282**(5396): 2041-6.

Blaxter, M. L., A. P. Page, et al. (1992). "Nematode surface coats: actively evading immunity." Parasitol Today **8**(7): 243-7.

Brejc, K., W. J. van Dijk, et al. (2001). "Crystal structure of an ACh-binding protein reveals the ligand-binding domain of nicotinic receptors." Nature **411**(6835): 269-76.

Brimblecombe, R. W., R. R. Hunt, et al. (1969). "The synthesis and pharmacology of some 1,4,5,6-tetrahydropyrimidines." Br J Pharmacol **37**(2): 425-35.

Brisson, A. and P. N. Unwin (1984). "Tubular crystals of acetylcholine receptor." J Cell Biol **99**(4 Pt 1): 1202-11.

Bull, K., A. Cook, et al. (2007). "Effects of the novel anthelmintic emodepside on the locomotion, egg-laying behaviour and development of Caenorhabditis elegans." International Journal for Parasitology **37**(6): 627.

Campbell, W. C. (1981). "An introduction to the avermectins." N Z Vet J **29**(10): 174-8.

Campbell, W. C. and G. W. Benz (1984). "Ivermectin: a review of efficacy and safety." J Vet Pharmacol Ther **7**(1): 1-16.

Celie, P. H., S. E. van Rossum-Fikkert, et al. (2004). "Nicotine and carbamylcholine binding to nicotinic acetylcholine receptors as studied in AChBP crystal structures." Neuron **41**(6): 907-14.

Chabala, J. C., H. Mrozik, et al. (1980). "Ivermectin, a new broad-spectrum antiparasitic agent." J Med Chem **23**(10): 1134-6.

Chalfie, M. and J. White (1988). The Nervous System The Nematode *Caenorhabditis elegans*. W. B. Wood. New York, Cold Spring Harbour Laboratory Press**:** 337-391.

Chan, M. S., G. F. Medley, et al. (1994). "The evaluation of potential global morbidity attributable to intestinal nematode infections." Parasitology **109 (Pt 3)**: 373-87.

Cheeseman, C. L., N. S. Delany, et al. (2001). "High-affinity ivermectin binding to recombinant subunits of the Haemonchus contortus glutamate-gated chloride channel." Mol Biochem Parasitol **114**(2): 161-8.

Çirak, V. Y., E. Güleğen, et al. (2004). "Benzimidazole resistance in cyathostomin populations on horse farms in western Anatolia, Turkey." Parasitology Research **93**(5): 392.

Cleland, T. A. (1996). "Inhibitory glutamate receptor channels." Mol Neurobiol **13**(2): 97-136.

Conway, D. P. (1964). "Variance In The Effectiveness Of Thiabendazole Against Haemonchus Contortus In Sheep." Am J Vet Res **25**: 844-6.

Cook, A., N. Aptel, et al. (2006). "Caenorhabditis elegans ivermectin receptors regulate locomotor behaviour and are functional orthologues of Haemonchus contortus receptors." Molecular and Biochemical Parasitology **147**(1): 118-125.

Copley, R. R. and G. J. Barton (1994). "A Structural Analysis of Phosphate and Sulphate Binding Sites in Proteins : Estimation of Propensities for Binding and Conservation of Phosphate Binding Sites." Journal of Molecular Biology **242**(4): 321.

Corringer, P.-J., J.-L. Galzi, et al. (1995). "Identification of a New Component of the Agonist Binding Site of the Nicotinic [IMAGE]7 Homooligomeric Receptor." J. Biol. Chem. **270**(20): 11749-11752.

Corringer, P.-J., N. L. Novere, et al. (2000). "Nicotinic Receptors at the Amino Acid Level." Annual Review of Pharmacology and Toxicology **40**(1): 431-458.

Corry, B. (2004). "Theoretical conformation of the closed and open states of the acetylcholine receptor channel." Biochim Biophys Acta **1663**(1-2): 2-5.

Crompton, D. W. (1988). "The prevalence of Ascariasis." Parasitol Today **4**(6): 162-9.

Crompton, D. W. (1999). "How much human helminthiasis is there in the world?" J Parasitol **85**(3): 397-403.

Crompton, D. W. T. and M. C. Nesheim (2002). "Nutritional Impact of Intestinal Helminthiasis During the Human Life Cycle." Annual Review of Nutrition **22**(1): 35-59.

Culetto, E., H. A. Baylis, et al. (2004). "The Caenorhabditis elegans unc-63 Gene Encodes a Levamisole-sensitive Nicotinic Acetylcholine Receptor {alpha} Subunit." J. Biol. Chem. **279**(41): 42476-42483.

Cully, D. F., P. S. Paress, et al. (1996). "Identification of a Drosophila melanogaster glutamate-gated chloride channel sensitive to the antiparasitic agent avermectin." J Biol Chem **271**(33): 20187-91.

Cully, D. F., D. K. Vassilatis, et al. (1994). "Cloning of an avermectin-sensitive glutamate-gated chloride channel from Caenorhabditis elegans." Nature **371**(6499): 707-11.

Cully, D. F., D. K. Vassilatis, et al. (1994). "Cloning of an avermectin-sensitive glutamate-gated chloride channel
from Caenorhabditis elegans." Nature **371**(6499): 707.

Cully, D. F., Vassilatis, D.K., Liu, K.K., Paress, P., Van der Ploeg, L.H.T., Schaeffer, J.M., Arena, J.P. (1994). "Cloning of an avermectin-sensitive glutamate-gated chloride channel from Caenorhabditis elegans." Nature **371**: 707-711.

Cully, D. F., H. Wilkinson, et al. (1996). "Molecular biology and electrophysiology of glutamate-gated chloride channels of invertebrates." Parasitology **113 Suppl**: S191-200.

Dawson, G. R., Wafford, K.A., Smith, A., Marshall, G.R., Bayley, P.J., Schaeffer, J.M., Meinke, P.T., McKernan, R.M. (2000). "Anticonvulsant and adverse effects of avermectin analogs in mice are mediated through the $\gamma-$ aminobutyric $acid_A$ receptor." Journal of Pharmacology and Experimental Therapeutics **295**(3): 1051-1060.

de Silva, N., H. Guyatt, et al. (1997). "Anthelmintics. A comparative review of their clinical pharmacology." Drugs **53**(5): 769-88.

Del Castillo, J., W. C. De Mello, et al. (1967). "The Initiation of Action Potentials in the Somatic Musculature of Ascaris Lumbricoides." J Exp Biol **46**(2): 263-279.

Del Castillo, J., W. C. Demello, et al. (1963). "The Physiological Role Of Acetylcholine In The Neuromuscular System Of Ascaris Lumbricoides." Arch Int Physiol Biochim **71**: 741-57.

Del Castillo, J., W. C. Demello, et al. (1964). "Influence Of Some Ions On The Membrane Potential Of Ascaris Muscle." J Gen Physiol **48**: 129-40.

Delany, N. S., D. L. Laughton, et al. (1998). "Cloning and localisation of an avermectin receptor-related subunit from Haemonchus contortus." Mol Biochem Parasitol **97**(1-2): 177-87.

Dellisanti, C. D., Y. Yao, et al. (2007). "Crystal structure of the extracellular domain of nAChR [alpha]1 bound to [alpha]-bungarotoxin at 1.94 A resolution." Nat Neurosci **10**(8): 953.

Dent, J. A., M. W. Davis, et al. (1997). "avr-15 encodes a chloride channel subunit that mediates inhibitory glutamatergic neurotransmission and ivermectin sensitivity in Caenorhabditis elegans." Embo J **16**(19): 5867-79.

Dent, J. A., M. W. Davis, et al. (1997). "avr-15 encodes a chloride channel subunit that mediates inhibitory glutamatergic neurotransmission and ivermectin sensitivity in Caenorhabditis elegans." European Molecular Biology Organisation Journal **16**(19): 5867-5879.

Dent, J. A., M. M. Smith, et al. (2000). "The genetics of ivermectin resistance in Caenorhabditis elegans." Proc Natl Acad Sci U S A **97**(6): 2674-9.

Dent, J. A., M. M. Smith, et al. (2000). "The genetics of ivermectin resistance in Caenorhabditis elegans." Proceedings of the National Academy of Sciences of the United States of America **97**(6): 2674-2679.

Egerton, J. R., J. Birnbaum, et al. (1980). "22, 23--dihydroavermectin B1, a new broad-spectrum antiparasitic agent." Br Vet J **136**(1): 88-97.

Enos, A. and G. C. Coles (1990). "Effect of benzimidazole drugs on tubulin in benzimidazole resistant and susceptible strains of Caenorhabditis elegans." Int J Parasitol **20**(2): 161-7.

Ernst, M., D. Brauchart, et al. (2003). "Comparative modeling of GABAA receptors: limits, insights, future developments." Neuroscience **119**(4): 933.

Etter, A., D. F. Cully, et al. (1999). "Picrotoxin blockade of invertebrate glutamate-gated chloride channels: subunit dependence and evidence for binding within the pore." J. Neurochem **72**: 318–326.

Etter, A., D. F. Cully, et al. (1996). "An amino acid substitution in the pore region of a glutamate-gated chloride channel enables the coupling of ligand binding to channel gating." J Biol Chem **271**(27): 16035-9.

ffrench-Constant RH, Rocheleau TA, et al. (1993). "A point mutation in a Drosophila GABA receptor confers insecticide resistance." Nature **363**(449-451).

ffrench-Constant, R. H., T. A. Rocheleau, et al. (1993). "A point mutation in a Drosophila GABA receptor confers insecticide resistance." Nature **363**(6428): 449-51.

ffrench-Constant, R. H., T. A. Rocheleau, et al. (1993). "A point mutation in a Drosophila GABA receptor confers insecticide resistance." Nature **363**(6428): 449.

ffrench-Constant, R. H., J. C. Steichen, et al. (1993). "A single-amino acid substitution in a gamma-aminobutyric acid subtype A receptor locus is associated with cyclodiene insecticide resistance in Drosophila populations." Proc Natl Acad Sci U S A **90**(5): 1957-61.

Filippova, N., A. Sedelnikova, et al. (2000). "Regulation of recombinant gamma-aminobutyric acid (GABA)(A) and GABA(C) receptors by protein kinase C." Mol Pharmacol **57**(5): 847-56.

Fleming, J. T., M. D. Squire, et al. (1997). "Caenorhabditis elegans Levamisole Resistance Genes lev-1, unc-29, and unc-38 Encode Functional Nicotinic Acetylcholine Receptor Subunits." J. Neurosci. **17**(15): 5843-5857.

Forrester, S. G., F. F. Hamdan, et al. (1999). "Cloning, sequencing, and developmental expression levels of a novel glutamate-gated chloride channel homologue in the parasitic nematode Haemonchus contortus." Biochem Biophys Res Commun **254**(3): 529-34.

Forrester, S. G., R. K. Prichard, et al. (2002). "A glutamate-gated chloride channel subunit from Haemonchus contortus: expression in a mammalian cell line, ligand binding, and modulation of anthelmintic binding by glutamate." Biochem Pharmacol **63**(6): 1061-8.

Forrester, S. G., R. K. Prichard, et al. (2003). "Haemonchus contortus: HcGluCla expressed in Xenopus oocytes forms a glutamate-gated ion channel that is activated by ibotenate and the antiparasitic drug ivermectin." Mol Biochem Parasitol **129**(1): 115-21.

Francis, M. M., S. P. Evans, et al. (2005). "The Ror Receptor Tyrosine Kinase CAM-1 Is Required for ACR-16-Mediated Synaptic Transmission at the C. elegans Neuromuscular Junction." Neuron **46**(4): 581.

Franks, C. J., L. Holden-Dye, et al. (2006). "Anatomy, physiology and pharmacology of Caenorhabditis elegans pharynx: a model to define gene function in a simple neural system." Invert Neurosci **6**(3): 105-22.

Gally, C. and J. L. Bessereau (2003). "GABA is dispensable for the formation of junctional GABA receptor clusters in Caenorhabditis elegans." J Neurosci **23**(7): 2591-9.

Geary, T. G., S. M. Sims, et al. (1993). "Haemonchus contortus: ivermectin-induced paralysis of the pharynx." Exp Parasitol **77**(1): 88-96.

Georgi, J. R. and M. E. Georgi (1990). Parasitology for Veterinarians. Philadelphia, W.B. Saunders Company.

Georgiev, V. S. (2001). "Pharmacotherapy of ascariasis." Expert Opinion on Pharmacotherapy **2**(2): 223-239.

Ghisi, M., R. Kaminsky, et al. (2007). "Phenotyping and genotyping of Haemonchus contortus isolates reveals a new putative candidate mutation for benzimidazole resistance in nematodes." Veterinary Parasitology **144**(3-4): 313.

Gill, J. H. and E. Lacey (1998). "Avermectin/milbemycin resistance in trichostrongyloid nematodes." Int J Parasitol **28**(6): 863-77.

Gill, J. H., J. M. Redwin, et al. (1991). "Detection of resistance to ivermectin in Haemonchus contortus." Int J Parasitol **21**(7): 771-6.

Gill, J. H., J. M. Redwin, et al. (1995). "Avermectin inhibition of larval development in Haemonchus contortus--effects of ivermectin resistance." Int J Parasitol **25**(4): 463-70.

Giraudat, J., M. Dennis, et al. (1986). "Structure of the high-affinity binding site for noncompetitive blockers of the acetylcholine receptor: serine-262 of the delta subunit is labeled by [3H]chlorpromazine." Proc Natl Acad Sci U S A **83**(8): 2719-23.

Gisselmann, G., H. Pusch, et al. (2002). "Two cDNAs coding for histamine-gated ion channels in D. melanogaster." Nature Neuroscience **5**(1): 11-12.

Grant, W. (2000). "What is the real target for ivermectin resistance selection in Onchocerca volvulus?" Parasitol Today **16**(11): 458-9; discussion 501-2.

Grosman, C., F. N. Salamone, et al. (2000). "The extracellular linker of muscle acetylcholine receptor channels is a gating control element." J Gen Physiol **116**(3): 327-40.

Gubanov, N. M. (1951). "[Giant nematoda from the placenta of Cetacea; Placentonema gigantissima nov. gen., nov. sp.]." Dokl Akad Nauk SSSR **77**(6): 1123-5.

Guest, M., K. Bull, et al. (2007). "The calcium-activated potassium channel, SLO-1, is required for the action of the novel cyclo-octadepsipeptide anthelmintic, emodepside, in Caenorhabditis elegans." International Journal for Parasitology **37**(14): 1577.

Guilhon, J. (1966). "[Action of a imidazothiazole derivative (Tetramizole) on gastrointestinal Strongyloides in sheep]." Bull Acad Vet Fr **39**(7): 255-64.

Hall, D. H. and R. L. Russell (1991). "The posterior nervous system of the nematode Caenorhabditis elegans: serial reconstruction of identified neurons and complete pattern of synaptic interactions." J. Neurosci. **11**(1): 1-22.

Hamon, A., H. Le Corronc, et al. (1998). "BIDN, a bicyclic dinitrile convulsant, selectively blocks GABA-gated Cl- channels." Brain Res **780**(1): 20-6.

Harder, A. and G. von Samson-Himmelstjerna (2002). "Cyclooctadepsipeptides - a new class of anthelmintically active compounds." Parasitology Research **88**(6): 481.

Harrow, I. D. and K. A. F. Gration (1985). "Mode of action of the anthelmintics morantel, pyrantel and levamisole on muscle cell membrane of the nematode <I>Ascaris suum</I>." Pesticide Science **16**(6): 662-672.

Holden-Dye, L. and R. Walker (2007). Anthelmintic drugs. Wormbook. M. Chalfie.

Holden-Dye, L. and R. J. Walker (1988). "ZAPA, (Z)-3-[(aminoiminomethyl)thio]-2-propenoic acid hydrochloride, a potent agonist at GABA-receptors on the Ascaris muscle cell." Br J Pharmacol **95**(1): 3-5.

Holden-Dye, L. and R. J. Walker (1990). "Avermectin and avermectin derivatives are antagonists at the 4-aminobutyric acid (GABA) receptor on the somatic muscle cells of Ascaris; is this the site of anthelmintic action?" Parasitology **101 Pt 2**: 265-71.

Holland, C. V. and M. W. Kennedy (2002). The Geohelminths: Ascaris, Trichuris And Hookworm, .

Horoszok, L., V. Raymond, et al. (2001). "GLC-3: a novel fipronil and BIDN-sensitive, but picrotoxinin-insensitive, L-glutamate-gated chloride channel subunit from Caenorhabditis elegans." Br J Pharmacol **132**(6): 1247-54.

Horoszok, L., Raymond, V., Sattelle, D.B., Wolstenholme, A.J. (2001). "GLC-3: a novel fipronil and BIDN-sensitive, but picrotoxinin-insensitive, L-glutamate-gated chloride channel subunit from Caenorhabditis elegans." British Journal of Pharmacology **132**(5): 1247-1254.

Horton, J. (2003). "Human gastrointestinal helminth infections: are they now neglected diseases?" Trends in Parasitology **19**(11): 527.

Hosie, A. M., H. A. Baylis, et al. (1995). "Actions of the insecticide fipronil, on dieldrin-sensitive and- resistant GABA receptors of Drosophila melanogaster." Br J Pharmacol **115**(6): 909-12.

Hosie, A. M., Y. Shirai, et al. (1995). "Blocking actions of BIDN, a bicyclic dinitrile convulsant compound, on wild-type and dieldrin-resistant GABA receptor homo-oligomers of Drosophila melanogaster expressed in Xenopus oocytes." Brain Res **693**(1-2): 257-60.

Hucho, F. (1986). "The nicotinic acetylcholine receptor and its ion channel." Eur J Biochem **158**(2): 211-26.

Iovchev, M. I., P. Kodrov, et al. (2002). "Altered drug resistance and recovery from paralysis in *Drosophila melanogaster* with a deficient histamine-gated chloride channel." Journal of Neurogenetics **16**: 249-262.

J.A. Van Wyk, F. S. Malan, et al. (1997). " How long before resistance makes it impossible to control some field strains of *Haemonchus contortus* with any of the anthelmintics?" *Vet. Parasitol.* **70**: pp. 111-112.

Jackson, F., E. Jackson, et al. (1992). "Evidence of multiple anthelmintic resistance nematodes in a strain of Teladorsagia circumcincta (Ostertagia circumcincta) from goats in Scotland." Res. Vet. Sci(53): 371–374.

Jagannathan, S. (1998). Nematode Inhibitory Glutamate-Gated Chloride Ion Channel Receptors. Department of Biology and Biochemistry. Bath, University of Bath. **PhD**.

Jagannathan, S., D. L. Laughton, et al. (1999). "Ligand-gated chloride channel subunits encoded by the Haemonchus contortus and Ascaris suum orthologues of the Caenorhabditis elegans gbr-2 (avr-14) gene." Mol Biochem Parasitol **103**(2): 129-40.

Jasmer, D. P., C. Yao, et al. (2000). "Multiple lethal effects induced by a benzimidazole anthelmintic in the anterior intestine of the nematode Haemonchus contortus." Mol Biochem Parasitol **105**(1): 81-90.

Johnstone, C. (1998). Parasites and Parasitic Diseases of Domestic Animals University of Pennsylvania.

Jones, A. and D. Sattelle (2008). "The cys-loop ligand-gated ion channel gene superfamily of the nematode, Caenorhabditis elegans." Invertebrate Neuroscience **8**(1): 41.

Jones, A. K. and D. B. Sattelle (2004). "Functional genomics of the nicotinic acetylcholine receptor gene family of the nematode, <I>Caenorhabditis elegans</I>." BioEssays **26**(1): 39-49.

Kaminsky, R., P. Ducray, et al. (2008). "A new class of anthelmintics effective against drug-resistant nematodes." Nature **452**(7184): 176.

Kane, N. S., B. Hirschberg, et al. (2000). "Drug-resistant Drosophila indicate glutamate-gated chloride channels are targets for the antiparasitics nodulisporic acid and ivermectin." PNAS **97**(25): 13949-13954.

Kane, N. S., Hirschberg, B., Qian, S., Hunt, D., Thomas, B., Brochu, R., Ludmerer, S.W., Zheng, Y., Smith, M., Arena, J.P., Cohen, C.J., Schmatz, D., Warmke, J., Cully, D.F. (2000). "Drug-resistant *Drosophila* indicate glutamate-gated chloride channels are targets for the antiparasitics nodulosporic acid and ivermectin." Proceedings of the National Academy of Sciences USA **97**(25): 13949-13954.

Kash, T. L., A. Jenkins, et al. (2003). "Coupling of agonist binding to channel gating in the GABAA receptor." Nature **421**(6920): 272.

Kass, I. S., C. C. Wang, et al. (1980). "Avermectin B1a, a paralyzing anthelmintic that affects interneurons and inhibitory motoneurons in Ascaris." Proc Natl Acad Sci U S A **77**(10): 6211-5.

Keen, M. (1995). The problems and pitfalls of Radioligand binding. Signal Transduction Protocols. D. Kendall and S. Hill, Humana Press. **41**.

Kerboeuf, D., W. J. Blackhall, et al. (2003). "P-glycoprotein in helminths: function and perspectives for anthelmintic treatment and reversal of resistance." International Journal of Antimicrobial Agents **22**: 332-346.

Khakh, B. J., Procter, W.R., Dunwiddie, T.V., Labarca, C., Lester, H.A. (1999). "Allosteric control of gating and kinetics at $P2X_4$ receptor channels." Journal of Neuroscience **19**(17): 7289-7299.

Kimchi-Sarfaty, C., J. M. Oh, et al. (2007). "A "Silent" Polymorphism in the MDR1 Gene Changes Substrate Specificity." Science **315**(5811): 525-528.

Knight, D. H. (1987). "Heartworm infection." Vet Clin North Am Small Anim Pract **17**(6): 1463-518.

Korystov, Y. N., N. V. Ermakova, et al. (2004). "Avermectins inhibit multidrug resistance of tumor cells." European Journal of Pharmacology **493**(1-3): 57.

Krause, R. M., B. Buisson, et al. (1998). "Ivermectin: a positive allosteric effector of the alpha7 neuronal nicotinic acetylcholine receptor." Mol Pharmacol **53**(2): 283-94.

Krause, R. M., Buisson, B., Bertrand, S., Corringer, P.J., Galzi, J.L., Changeux, J.P., Bertrand, D. (1998). "Ivermectin: a positive allosteric effector of the $\alpha 7$ neuronal nicotinic acetylcholine receptor." Molecular Pharmacology **53**(2): 283-294.

Krishek, B. J., X. Xie, et al. (1994). "Regulation of GABAA receptor function by protein kinase C phosphorylation." Neuron **12**(5): 1081-95.

Kwa, M. S., J. G. Veenstra, et al. (1994). "Benzimidazole resistance in Haemonchus contortus is correlated with a conserved mutation at amino acid 200 in beta-tubulin isotype 1." Mol Biochem Parasitol **63**(2): 299-303.

Kyte, J. and R. F. Doolittle (1982). "A simple method for displaying the hydropathic character of a protein." Journal of Molecular Biology **157**(1): 105.

Labarca, C., M. W. Nowak, et al. (1995). "Channel gating governed symmetrically by conserved leucine residues in the M2 domain of nicotinic receptors." Nature **376**(6540): 514-6.

Lacey, E. (1990). "Mode of action of benzimidazoles." Parasitol Today **6**(4): 112-5.

Laskowski, R. A., D. S. Moss, et al. (1993). "Main-chain bond lengths and bond angles in protein structures." J Mol Biol **231**(4): 1049-67.

Laughton, D. L. (1993). Characterisation of nematode recepters. Department of Biology and Biochemistry. Bath, University of Bath. **PhD**

Laughton, D. L., G. G. Lunt, et al. (1997). "Alternative splicing of a Caenorhabditis elegans gene produces two novel inhibitory amino acid receptor subunits with identical ligand binding domains but different ion channels." Gene **201**(1-2): 119-25.

Laughton, D. L., G. G. Lunt, et al. (1997). "Reporter gene constructs suggest that the Caenorhabditis elegans avermectin receptor beta-subunit is expressed solely in the pharynx." J Exp Biol **200**(Pt 10): 1509-14.

Le Jambre, L. F., J. H. Gill, et al. (1995). "Characterisation of an avermectin resistant strain of Australian Haemonchus contortus." Int J Parasitol **25**(6): 691-8.

Lea, T. J. and P. N. R. Usherwood (1973). "Effect of ibotenic acid on chloride permeability of insect muscle-fibres." Comparative and General Pharmacology **4**(16): 351.

Leidenheimer, N. J., P. J. Whiting, et al. (1993). "Activation of calcium-phospholipid-dependent protein kinase enhances benzodiazepine and barbiturate potentiation of the GABAA receptor." J Neurochem **60**(5): 1972-5.

Lewis, J. A., C. H. Wu, et al. (1980). "The genetics of levamisole resistance in the nematode Caenorhabditis elegans." Genetics **95**(4): 905-28.

Lewis, J. A., C. H. Wu, et al. (1980). "Levamisole-resistant mutants of the nematode Caenorhabditis elegans appear to lack pharmacological acetylcholine receptors." Neuroscience **5**(6): 967-89.

Lilley, C. J., P. Devlin, et al. (1999). "Parasitic nematodes, proteinases and transgenic plants." Parasitol Today **15**(10): 414-7.

Lok, J. B., D. H. Knight, et al. (1995). "Studies of reproductive competence in male Dirofilaria immitis treated with milbemycin oxime." Trop Med Parasitol **46**(4): 235-40.

Lubega, G. W. and R. K. Prichard (1991). "Interaction of benzimidazole anthelmintics with Haemonchus contortus tubulin: binding affinity and anthelmintic efficacy." Exp Parasitol **73**(2): 203-13.

Lubega, G. W. and R. K. Prichard (1991). "Specific interaction of benzimidazole anthelmintics with tubulin from developing stages of thiabendazole-susceptible and -resistant Haemonchus contortus." Biochem Pharmacol **41**(1): 93-101.

Ludmerer, S. W., V. A. Warren, et al. (2002). "Ivermectin and nodulosporic acid receptors in *Drosophila melanogaster* contain both γ–aminobutyric acid-gated Rdl and glutamate-gated GluClα chloride channel subunits." Biochemistry **41**: 6548-6560.

Macdonald, R. L. (1995). "Ethanol, gamma-aminobutyrate type A receptors, and protein kinase C phosphorylation." Proc Natl Acad Sci U S A **92**(9): 3633-5.

Maingi, N., H. Bjorn, et al. (1996). "A survey of anthelmintic resistance in nematode parasites of goats in Denmark." Veterinary Parasitology **66**(1-2): 53.

Martin R, J. and P. Robertson A (2007). "Mode of action of levamisole and pyrantel, anthelmintic resistance, E153 and Q57." Parasitology **134**(8): 1093.

Martin, R. J., I. Murray, et al. (1998). "Anthelmintics and ion-channels: after a puncture, use a patch." International Journal for Parasitology **28**(6): 849-862.

Martin, R. J. and A. J. Pennington (1989). "A patch-clamp study of effects of dihydroavermectin on Ascaris muscle." Br J Pharmacol **98**(3): 747-56.

McCracken, R. O. and W. H. Stillwell (1991). "A possible biochemical mode of action for benzimidazole anthelmintics." Int J Parasitol **21**(1): 99-104.

McDonald, B. J., A. Amato, et al. (1998). "Adjacent phosphorylation sites on GABAA receptor beta subunits determine regulation by cAMP-dependent protein kinase." Nat Neurosci **1**(1): 23-8.

McDonald, B. J., H. J. Chung, et al. (2001). "Identification of protein kinase C phosphorylation sites within the AMPA receptor GluR2 subunit." Neuropharmacology **41**(6): 672-9.

McDonald, B. J. and S. J. Moss (1994). "Differential phosphorylation of intracellular domains of gamma-aminobutyric acid type A receptor subunits by calcium/calmodulin type 2-dependent protein kinase and cGMP-dependent protein kinase." J Biol Chem **269**(27): 18111-7.

McDonald, B. J. and S. J. Moss (1997). "Conserved phosphorylation of the intracellular domains of GABA(A) receptor beta2 and beta3 subunits by cAMP-dependent protein kinase, cGMP-dependent protein kinase protein kinase C and Ca2+/calmodulin type II-dependent protein kinase." Neuropharmacology **36**(10): 1377-85.

McHardy M. Smith, Vivien A. Warren, et al. (2000). "Nodulisporic acid opens insect glutamate-gated chloride channels: identification of a new high affinity modulator.

." Biochemistry.
39(18): 5543-54.

McIntire, S. L., E. Jorgensen, et al. (1993). "Genes required for GABA function in Caenorhabditis elegans." Nature **364**(6435): 334-7.

McIntire, S. L., E. Jorgensen, et al. (1993). "The GABAergic nervous system of Caenorhabditis elegans." Nature **364**(6435): 337-41.

McLeod, R. S. (1995). "Costs of major parasites to the Australian livestock industries." International Journal for Parasitology **25**(11): 1363.

Meeusen, E. N. (1999). "Immunology of helminth infections, with special reference to immunopathology." Vet Parasitol **84**(3-4): 259-73.

Mellanby, H. (1955). "The identification and estimation of acetylcholine in three parasitic nematodes (Ascaris lumbricoides, Litomosoides carinii, and the microfilariae of Dirofilaria repens)." Parasitology **45**(3-4): 287-94.

Miller, H. R. (1984). "The protective mucosal response against gastrointestinal nematodes in ruminants and laboratory animals." Vet Immunol Immunopathol **6**(1-2): 167-259.

Miller, H. R. (1996). "Prospects for the immunological control of ruminant gastrointestinal nematodes: natural immunity, can it be harnessed?" Int J Parasitol **26**(8-9): 801-11.

Miyazawa, A., Y. Fujiyoshi, et al. (1999). "Nicotinic acetylcholine receptor at 4.6 A resolution: transverse tunnels in the channel wall." J Mol Biol **288**(4): 765-86.

Miyazawa, A., Y. Fujiyoshi, et al. (2003). "Structure and gating mechanism of the acetylcholine receptor pore." Nature **423**(6943): 949-55.

Molento, M. B. and R. K. Prichard (1999). "Effects of the multidrug-resistance-reversing agents verapamil and CL 347,099 on the efficacy of ivermectin or moxidectin against unselected and drug-selected strains of Haemonchus contortus in jirds (Meriones unguiculatus)." Parasitol Res **85**(12): 1007-11.

Molyneux, D. H. and J. B. Davies (1997). "Onchocerciasis control: Moving towards the millennium." Parasitol Today **13**(11): 418-25.

Mongan, N. P., H. A. Baylis, et al. (1998). "An extensive and diverse gene family of nicotinic acetylcholine receptor alpha subunits in Caenorhabditis elegans." Receptors Channels. **6**(3): 213-28.

Mongan, N. P., A. K. Jones, et al. (2002). "Novel {alpha}7-like nicotinic acetylcholine receptor subunits in the nematode Caenorhabditis elegans." Protein Sci **11**(5): 1162-1171.

Moss, S. J., B. J. McDonald, et al. (1996). "Phosphorylation of the predicted major intracellular domains of the rat and chick neuronal nicotinic acetylcholine receptor alpha 7 subunit by cAMP-dependent protein kinase." Neuropharmacology **35**(8): 1023-8.

Mount, D. W. (2004). Bioinformatics: sequence and genome analysis, Cold Spring Harbor Laboratory Press.

Newton, S. E. and E. A. Munn (1999). "The development of vaccines against gastrointestinal nematode parasites, particularly Haemonchus contortus." Parasitol Today **15**(3): 116-22.

Njue, A. I., J. Hayashi, et al. (2004). "Mutations in the extracellular domains of glutamate-gated chloride channel 3 and subunits from ivermectin-resistant Cooperia oncophora affect agonist sensitivity." Journal of Neurochemistry **89**(5): 1137-1147.

Njue, A. I., J. Hayashi, et al. (2004). "Mutations in the extracellular domains of glutamate-gated chloride channel alpha3 and beta subunits from ivermectin-resistant Cooperia oncophora affect agonist sensitivity." J Neurochem **89**(5): 1137-47.

Njue, A. I. and R. K. Prichard (2004). "Genetic variability of glutamate-gated chloride channel genes in ivermectin-susceptible and -resistant strains of Cooperia oncophora." Parasitology **129**(Pt 6): 741-51.

Olsen, R. W. and T. M. DeLorey (1999). GABA and Glycine. Basic Neurochemistry: Molecular, Cellular and Medical Aspects. G. J. Siegel, B. W. Agranoff, R. W. Albers, S. K. Fisher and M. D. Uhler. Philadelphia, Lippincott,Williams & Wilkins.

Ortells, M. O. and G. G. Lunt (1995). "Evolutionary history of the ligand-gated ion-channel superfamily of receptors." Trends Neurosci **18**(3): 121-7.

Osei-Atweneboana, M. Y., J. K. L. Eng, et al. (2007). "Prevalence and intensity of Onchocerca volvulus infection and efficacy of ivermectin in endemic communities in Ghana: a two-phase epidemiological study." The Lancet **369**(9578): 2021.

Paiement, J., R. K. Prichard, et al. (1999). "Haemonchus contortus: characterization of a glutamate binding site in unselected and ivermectin-selected larvae and adults." Exp Parasitol **92**(1): 32-9.

Pawlowski, Z. S., G. A. Schad, et al. (1991). Hookworm infection and Anemia World Health Orginisation. Geneva, Switzerland 96 p.

Pemberton, D. J., C. J. Franks, et al. (2001). "Characterization of glutamate-gated chloride channels in the pharynx of wild-type and mutant Caenorhabditis elegans delineates the role of the subunit GluCl-alpha2 in the function of the native receptor." Mol Pharmacol **59**(5): 1037-43.

Peng, W., X. Zhou, et al. (1998). "Ascariasis in China." Adv Parasitol **41**: 109-48.

Porter, N. M., R. E. Twyman, et al. (1990). "Cyclic AMP-dependent protein kinase decreases GABAA receptor current in mouse spinal neurons." Neuron **5**(6): 789-96.

Portillo, V., S. Jagannathan, et al. (2003). "Distribution of glutamate-gated chloride channel subunits in the parasitic nematode Haemonchus contortus." J Comp Neurol **462**(2): 213-22.

Prichard, R. (2001). "Genetic variability following selection of Haemonchus contortus with anthelmintics." Trends in Parasitology **17**(9): 445.

Prichard R, K. and A. Roulet (2007). "ABC transporters and Beta-tubulin in macrocyclic lactone resistance: prospects for marker development." Parasitology **134**(8): 1123.

Prichard, R. K. (2007). "Markers for benzimidazole resistance in human parasitic nematodes?" Parasitology **134**(8): 1087.

Rand, J. B. (2007). Acetylcholine Acetylcholine T. C. e. R. Community.

Rand, J. B. and M. L. Nonet (1997). Synaptic Transmission. C. elegans II D. Riddle, T. Blumenthal, B. Meyer and J. Priess, Cold Spring Harbor Press 611-644.

Ranganathan, R., S. C. Cannon, et al. (2000). "MOD-1 is a serotonin-gated chloride channel that modulates locomotory behaviour in C. elegans." Nature **408**(6811): 470-5.

Rauh, J. J., E. Benner, et al. (1997). "Effects of [3H]-BIDN, a novel bicyclic dinitrile radioligand for GABA-gated chloride channels of insects and vertebrates." Br J Pharmacol **121**(7): 1496-505.

Rayes, D., M. J. De Rosa, et al. (2004). "Molecular basis of the differential sensitivity of nematode and mammalian muscle to the anthelmintic agent levamisole." J Biol Chem **279**(35): 36372-81.

Raymond, V., N. P. Mongan, et al. (2000). "Anthelmintic actions on homomer-forming nicotinic acetylcholine receptor subunits: chicken [alpha]7 and ACR-16 from the nematode Caenorhabditis elegans." Neuroscience **101**(3): 785-791.

Reynoldson, J. A., J. M. Behnke, et al. (1997). "Failure of pyrantel in treatment of human hookworm infections (Ancylostoma duodenale) in the Kimberley region of North West Australia." Acta Tropica **68**(3): 301.

Richmond, J. E. and E. M. Jorgensen (1999). "One GABA and two acetylcholine receptors function at the C. elegans neuromuscular junction." Nat Neurosci **2**(9): 791.

Riddle, D., T. Blumenthal, et al. (1997). Introduction to C. elegans. C. elegans II. D. Riddle, T. Blumenthal, B. Meyer and J. Priess, Cold Spring Harbor Press.

Roberts, E. and S. Frankel (1950). "gamma-Aminobutyric acid in brain: its formation from glutamic acid." J Biol Chem **187**(1): 55-63.

Robinson, M. W., N. McFerran, et al. (2004). "A possible model of benzimidazole binding to [beta]-tubulin disclosed by invoking an inter-domain movement." Journal of Molecular Graphics and Modelling **23**(3): 275.

Russell, R. B., M. A. S. Saqi, et al. (1997). "Recognition of analogous and homologous protein folds: analysis of sequence and structure conservation." Journal of Molecular Biology **269**(3): 423.

Sacko, M., D. De Clercq, et al. (1999). "Comparison of the efficacy of mebendazole, albendazole and pyrantel in treatment of human hookworm infections in the Southern Region of Mali, West Africa." Transactions of the Royal Society of Tropical Medicine and Hygiene **93**(2): 195.

Sali, A. and T. L. Blundell (1993). "Comparative protein modelling by satisfaction of spatial restraints." J Mol Biol **234**(3): 779-815.

Sangster, N. C., S. C. Bannan, et al. (1999). "Haemonchus contortus: Sequence Heterogeneity of Internucleotide Binding Domains from P-Glycoproteinsand an Association with Avermectin/Milbemycin Resistance." Experimental Parasitology **91**(3): 250.

Sangster, N. C., C. W. Davis, et al. (1991). "Effects of cholinergic drugs on longitudinal contraction in levamisole-susceptible and -resistant Haemonchus contortus." Int J Parasitol **21**(6): 689-95.

Sangster, N. C. and R. J. Dobson (2002). Anthelmintic resistance. The Biology of Nematodes. D. L. Lee. London and New York, Taylor and Francis**:** 531-567.

Schaeffer, J. M. and H. W. Haines (1989). "Avermectin binding in Caenorhabditis elegans. A two-state model for the avermectin binding site." Biochem Pharmacol **38**(14): 2329-38.

Schaeffer, J. M., J. H. Stiffey, et al. (1989). "A chemiluminescent assay for measuring avermectin binding sites." Anal Biochem **177**(2): 291-5.

Schnyder, M., P. R. Torgerson, et al. (2005). "Multiple anthelmintic resistance in Haemonchus contortus isolated from South African Boer goats in Switzerland." Veterinary Parasitology **128**(3-4): 285.

Schofield, P. R., M. G. Darlison, et al. (1987). "Sequence and functional expression of the GABAA receptor shows a ligand-gated receptor super-family." Nature **328**(6127): 221.

Shan, Q., Haddrill, J.L., Lynch, J.W. (2001). "Ivermectin, an unconventional agonist of the glycine receptor chloride channel." Journal of Biological Chemistry **276**(16): 12556-12564.

Silvestre, A. and J. Cabaret (2002). "Mutation in position 167 of isotype 1 [beta]-tubulin gene of Trichostrongylid nematodes: role in benzimidazole resistance?" Molecular and Biochemical Parasitology **120**(2): 297.

Sine, S. M. (2002). "The nicotinic receptor ligand binding domain." J Neurobiol **53**(4): 431-46.

Singh, R. N. and J. E. Sulston (1978). "Some observations on molting in *C. elegans*." Nematologica **24**: 63-71.

Sixma, T. K. (2007). "Nicotinic receptor structure emerging slowly." Nat Neurosci **10**(8): 937.

Smit, A. B., N. I. Syed, et al. (2001). "A glia-derived acetylcholine-binding protein that modulates synaptic transmission." Nature **411**(6835): 261.

Smyth , J. (1994). Introduction to animal parasitology.

Song, M. and R. O. Messing (2005). "Protein kinase C regulation of GABAA receptors." Cell Mol Life Sci **62**(2): 119-27.

Sulston, J. E. and J. G. White (1988). The nematode Caenorhabditis elegans, Cold Spring Harbor Laboratory, Cold Spring Harbor, New York.

Touroutine, D., R. M. Fox, et al. (2005). "acr-16 Encodes an Essential Subunit of the Levamisole-resistant Nicotinic Receptor at the Caenorhabditis elegans Neuromuscular Junction." J. Biol. Chem. **280**(29): 27013-27021.

Toyoshima, C. and N. Unwin (1990). "Three-dimensional structure of the acetylcholine receptor by cryoelectron microscopy and helical image reconstruction." J Cell Biol **111**(6 Pt 1): 2623-35.

Trudell, J. R. (2002). "Unique assignment of inter-subunit association in GABAA [alpha]1[beta]3[gamma]2 receptors determined by molecular modeling." Biochimica et Biophysica Acta (BBA) - Biomembranes **1565**(1): 91.

Turton, J. A. (1969). "Anthelmintic action of levamisole injection in cattle." Vet Rec **85**(9): 264-5.

Unwin, N. (1995). "Acetylcholine receptor channel imaged in the open state." Nature **373**(6509): 37-43.

Unwin, N. (2002). "Structure of the acetylcholine-gated channel." Novartis Found Symp **245**: 5-15; discussion 15-21, 165-8.

Unwin, N. (2003). "Structure and action of the nicotinic acetylcholine receptor explored by electron microscopy." FEBS Lett **555**(1): 91-5.

Unwin, N. (2005). "Refined structure of the nicotinic acetylcholine receptor at 4A resolution." J Mol Biol **346**(4): 967-89.

Varady, M., A. Konigova, et al. (2000). "Benzimidazole resistance in equine cyathostomes in Slovakia." Veterinary Parasitology **94**(1-2): 67.

Vassilatis, D. K., J. P. Arena, et al. (1997). "Genetic and biochemical evidence for a novel avermectin-sensitive chloride channel in Caenorhabditis elegans. Isolation and characterization." J Biol Chem **272**(52): 33167-74.

Vassilatis, D. K., J. P. Arena, et al. (1997). "Genetic and biochemical evidence for a novel avermectin sensitive chloride channel in *C. elegans* isolation and characterisation." Journal of Biological Chemistry **272**(52): 33167-33174.

Vassilatis, D. K., K. O. Elliston, et al. (1997). "Evolutionary relationship of the ligand-gated ion channels and the avermectin-sensitive, glutamate-gated chloride channels." J Mol Evol **44**(5): 501-8.

Vercruysse, J. and R. S. Rew (2002). Macrocylic Lactones in Antiparasitic Therapy, CABI Publishing.

von Samson-Himmelstjerna, G. and W. Blackhall (2005). "Will technology provide solutions for drug resistance in veterinary helminths?" Veterinary Parasitology **132**(3-4): 223-239.

Von Samson-Himmelstjerna, G., J. Blackhall W, et al. (2007). "Single nucleotide polymorphism (SNP) markers for benzimidazole resistance in veterinary nematodes." Parasitology **134**(8): 1077.

Wafford, K. A., P. Whiting, et al. (1992). "Functional modulation of cloned GABAA receptors expressed in Xenopus oocytes." Adv Biochem Psychopharmacol **47**: 75-9.

Wafford, K. A. and P. J. Whiting (1992). "Ethanol potentiation of GABAA receptors requires phosphorylation of the alternatively spliced variant of the gamma 2 subunit." FEBS Lett **313**(2): 113-7.

Wang, Z.-W., O. Saifee, et al. (2001). "SLO-1 Potassium Channels Control Quantal Content of Neurotransmitter Release at the C. elegans Neuromuscular Junction." Neuron **32**(5): 867.

Wei, L., G. Wei, et al. (2005). "Synthesis of new, potent avermectin-like insecticidal agents." Carbohydr Res **340**(9): 1583-90.

Wharton, D. A. (1986). A Functional Biology of Nematodes

White, J. G., E. Southgate, et al. (1986). "The structure of the nervous system of the nematode C. elegans." Philosophical Transactions of the Royal Society of London- Series B: Biological Sciences **314**: 1- 340.

WHO. (2000). "Fact sheet 102: Lymphatic filariasis " Fact sheets, from http://www.who.int/mediacentre/factsheets/fs102/en/index.html.

Williamson, S. M., T. K. Walsh, et al. (2007). "The cys-loop ligand-gated ion channel gene family of Brugia malayi and Trichinella spiralis: a comparison with Caenorhabditis elegans." Invert Neurosci.

Willson, J., K. Amliwala, et al. (2004). "Latrotoxin Receptor Signaling Engages the UNC-13-Dependent Vesicle-Priming Pathway in C. elegans." Current Biology **14**(15): 1374.

Wirtherle, N., T. Schnieder, et al. (2004). "Prevalence of benzimidazole resistance on horse farms in Germany." Vet Rec **154**(2): 39-41.

Witty, M. J. (1999). "Current strategies in the search for novel antiparasitic agents." Int J Parasitol **29**(1): 95-103; discussion 113-4.

Xu, M., M. Molento, et al. (1998). "Ivermectin resistance in nematodes may be caused by alteration of P-glycoprotein homolog." Molecular and Biochemical Parasitology **91**(2): 327.

Yates, D. M., V. Portillo, et al. (2003). "The avermectin receptors of Haemonchus contortus and Caenorhabditis elegans." International Journal for Parasitology **33**(11): 1183-1193.

Yates, D. M., V. Portillo, et al. (2003). "The avermectin receptors of Haemonchus contortus and Caenorhabditis elegans." Int J Parasitol **33**(11): 1183-93.

Yates, D. M. and A. J. Wolstenholme (2004). "An ivermectin-sensitive glutamate-gated chloride channel subunit from Dirofilaria immitis." Int J Parasitol **34**(9): 1075-81.

Yue, C., G. Coles, et al. (2003). "Multiresistant nematodes on a Devon farm." The Veterinary Record **153**(19): 604.

Zhao, X. L., V. L. Salgado, et al. (2004). "Kinetic and pharmacological characterization of desensitizing and non-desensitizing glutamate-gated chloride channels in cockroach neurons." Neurotoxicology **25**(6): 967-980.

Zheng, Y., B. Hirschberg, et al. (2002). "Identification of Two Novel Drosophila melanogaster Histamine-gated Chloride Channel Subunits Expressed in the Eye." J. Biol. Chem. **277**(3): 2000-2005.

Zheng, Y., B. Hirschberg, et al. (2002). "Identification of two novel Drosophila melanogaster histamine-gated chloride channel subunits expressed in the eye." J Biol Chem **277**(3): 2000-5.

Zhong, W., J. P. Gallivan, et al. (1998). "From ab initio quantum mechanics to molecular neurobiology: a cation-pi binding site in the nicotinic receptor." Proc Natl Acad Sci U S A **95**(21): 12088-93.

7: Appendices

7.1 Appendix 1. Map of vector pcDNA3.1

Map of mammalian expression vector pcDNA3.1+ (supplied by Invitrogen)

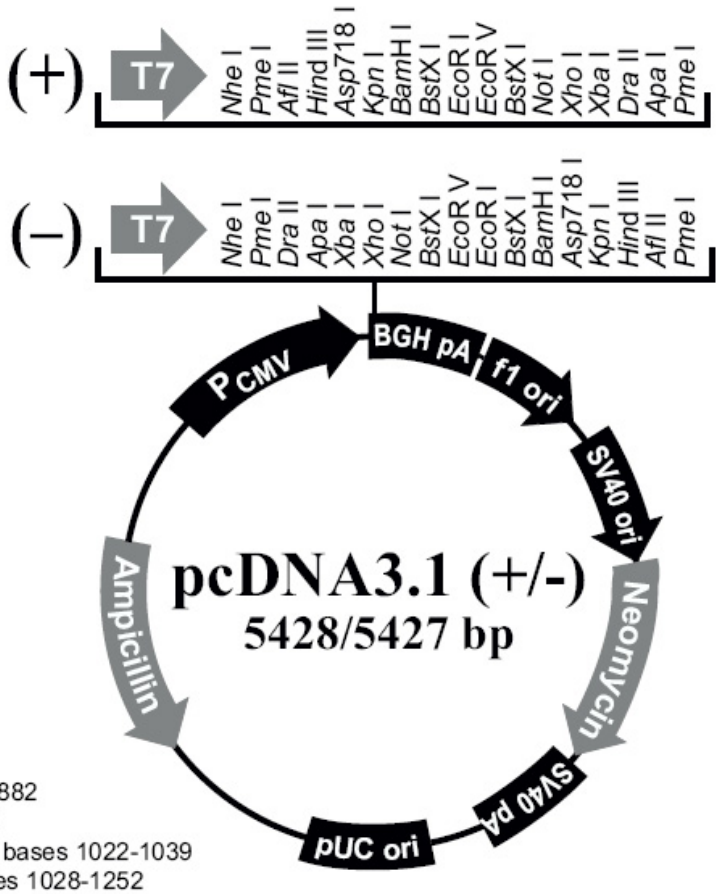

Comments for pcDNA3.1 (+)
5428 nucleotides

CMV promoter: bases 232-819
T7 promoter/priming site: bases 863-882
Multiple cloning site: bases 895-1010
pcDNA3.1/BGH reverse priming site: bases 1022-1039
BGH polyadenylation sequence: bases 1028-1252
f1 origin: bases 1298-1726
SV40 early promoter and origin: bases 1731-2074
Neomycin resistance gene (ORF): bases 2136-2930
SV40 early polyadenylation signal: bases 3104-3234
pUC origin: bases 3617-4287 (complementary strand)
Ampicillin resistance gene (*bla*): bases 4432-5428 (complementary strand)
ORF: bases 4432-5292 (complementary strand)
Ribosome binding site: bases 5300-5304 (complementary strand)
bla promoter (P3): bases 5327-5333 (complementary strand)

7.2 Appendix 2. Primers used for site directed mutagenesis

GluCl α3 mutant	Nucleotide change	Primers
T300S	ACA to TCA	F-5’ TCTCTGGGTGTCACGTCACTGCTCACAATGAC-3’ R-5’ GTCATTGTGAGCAGTGACGTGACACCCAGAGA-3’
E114G	GAG to GGG	F-5’ CGAATCCACGGGGGTGCCGCCGTT-3’ R-5’ AACGGCACCCCCGTGGATTCG-3’
V235A	GTT to GCT	F-5’ CGAATTCGAAGATGTCGCCACCAAGTACTGCACC-3’ R-5’ GGTGCAGTACTTGGTGGCGACATCTTGCCATTCG-3’
L256F	CTC to TTC	F-5’ GCTCGGGTCAAACTTTTCTTGCGAAGAGAGTACA-3’ R-5’ TGTACTCTCTTCGCAAGAAAAGTTTGACCCGAGC-3’
L256W	CTC to TGG	F-5' GTGCTCGGGTCAAACTTTGGTTGCGAAGAGAGTACAG 3' R-5' CTGTACTCTCTTCGCAACCAAAGTTTGACCCGAGCAC 3'
L256V	CTC to GTC	F-5' CTCTCTTCGCAAGACAAGTTTGACCCGAG 3' R-5' CTCGGGTCAAACTTGTCTTGCGAAGAGAG 3'
L256Y	CTC to TAC	F-5' GTGCTCGGGTCAAACTTTACTTGCGAAGAGAGTAC 3' R-5' GTACTCTCTTCGCAAGTAAAGTTTGACCCGAGCAC 3'
V69E	GTG to GAG	F-5’ GGTCCTGTGCTGGAGACGGTAAACATC 3' R-5’ GATGTTTACCGTCTCCAGCACAGGACC 3'
A308S	GCA to TCA	F-5’ GCTCACAATGACAACTCAGTCAAGCGGTATCAACTCC 3’ R-5' GGAGTTGATACCGCTTGACTGAGTTGTCATTGTGAGC 3'
P316S	CCA to TCA	F-5' GTATCAACTCCAAACTCTCACCTGTCTCTTACATC 3' R-5' GATGTAAGAGACAGGTGAGAGTTTGGAGTTGATAC 3
S295T	TCT to ACT	F-5’ CCAGCTCGAGTGACTCTGGGTGTCACG 3’ R-5’ CGTGACACCCAGAGTCACTCGAGCTGG 3’
T362A	ACG to GCG	F-5’ GGAGAAAAAGAAGAAACGCGTCTGGACGACTG 3’ R-5' CAGTCGTCCAGACGCGTTTCTTCTTTTTCTCC 3

7.3 Appendix 3. Modeller 9v2- procedure and scripts

Example: Modelling of GluClα3B using 1I9B.pdb as a template

GluClα3B amino acid sequence must be put in PIR format file, with the extension .ali it must be in a plain text format.

All modeller command files are written in python programming language and carry the .py file extension

```
>P1;GluCla3B
sequence:GluCla3B:::::::0.00: 0.00
MRNSVPLATRIGPMLALICTVSTIMSAVEAKRKLKEQEIIQRILNNYDWRVRPRGL
NASWPDTGGPVLVTVNIYLRSISKIDDVNMEYSAHFTFREEWVDARLAYGRFED
ESTEVPPFVVLATSENADQSQQIWMPDTFFQNEKEARRHLIDKPNVLIRIHKDGS
ILYSVRLSLVLSCPMSLEFYPLDRQNCLIDLASYAYTTQDIKYEWKEQNPVQQKD
GLRQSLPSFELQDVVTKYCTSKTNTGEYSCARVKLLLRREYSY*
```

File: GluCla3B.ali

Aligning the query and template sequences using the following 'align2d.py' command. Words highlighted can be modified on a case by case basis

```
from modeller import *

env = environ()
aln = alignment(env)
mdl = model(env, file='1I9B', model_segment=('FIRST:A','LAST:A'))
aln.append_model(mdl, align_codes='1I9BA', atom_files='1I9B.pdb')
aln.append(file='GluCla3B.ali', align_codes='GluCla3B')
aln.align2d()
aln.write(file='GluCla3B-1I9BA.ali', alignment_format='PIR')
aln.write(file='GluCla3B-1I9BA.pap', alignment_format='PAP')
```

File: align2d.py

The alignment will be written out in two formats, PIR and PAP. The PIR format is used in subsequent model building stages, while the PAP file is easy to examine and inspect visually.

Once a target template alignment is constructed, MODELLER calculates a 3D model of the target completely automatically, using its automodel class. The following script

will generate a number of models based on the template and the alignment in file 'GluCla3B-1I9BA.ali' (file ‘model-single.py)

```
from modeller import *
from modeller.automodel import *

env = environ()
a = automodel(env, alnfile='GluCla3B-1I9BA.ali',
              knowns='1I9BA', sequence='GluCla3B')
                     assess_methods=(assess.DOPE, assess.GA341))
a.starting_model = 1
a.ending_model = 50
a.make()
```

File: model-single.py

The highlighted areas can be changed depending on the query, template and the required number of models generated

The output files from the “model-single.py” command are

- ‘model-single.log’ which reports warnings, errors and other useful information including input restraints and preliminary DOPE and objective function scores.
- ‘GluCla3B. B000000x.pdb’ files which are the models generated by the program. Pdb files can be viewed with many different programs including raswin and chime.

Once a final model has been selected based on its objective function and DOPE scores it can be evaluated a second time using the ‘evaluate-model.py’ command. It is also a good idea to evaluate the template and compare the results directly using the evaluate-template.py command.

```
from modeller import *
from modeller.scripts import complete_pdb

log.verbose()    # request verbose output
env = environ()
env.libs.topology.read(file='$(LIB)/top_heav.lib') # read topology
env.libs.parameters.read(file='$(LIB)/par.lib') # read parameters

# read model file
mdl = complete_pdb(env, 'GluCla3B.B000023.pdb')

# Assess with DOPE:
s = selection(mdl)   # all atom selection
s.assess_dope(output='ENERGY_PROFILE NO_REPORT', file='GluCla3B.profile',
              normalize_profile=True, smoothing_window=15)
```

File: evaluate-model.py

```
from modeller import *
from modeller.scripts import complete_pdb

log.verbose()    # request verbose output
env = environ()
env.libs.topology.read(file='$(LIB)/top_heav.lib') # read topology
env.libs.parameters.read(file='$(LIB)/par.lib') # read parameters

# read model file
mdl = complete_pdb(env, '1I9BA.pdb')

# Assess with DOPE:
s = selection(mdl)   # all atom selection
s.assess_dope(output='ENERGY_PROFILE NO_REPORT', file='1I9B.profile',
              normalize_profile=True, smoothing_window=15)
```

evaluate-template.py

Highlighted words can be changed for different pdb files that require evaluation
The output files are carry the .profile extension and report DOPE and objective function scores a reasonable model will have similar values to the template